UNIVERSITEIT VAN PRETORIA
UNIVERSITY OF PRETORIA
YUNIBESITHI YA PRETORIA

EXPERIMENTAL COMPARISON OF ACTIVE SEISMIC SURFACE WAVE TESTS ON SHALLOW AND DEEP BEDROCK SITES

MOSITO NTAOTE

A dissertation submitted in partial fulfilment of the requirements for the degree of

MASTER OF ENGINEERING (GEOTECHNICAL ENGINEERING)

In the

FACULTY OF ENGINEERING

UNIVERSITY OF PRETORIA

July 2022

DISSERTATION SUMMARY

EXPERIMENTAL COMPARISON OF ACTIVE SEISMIC SURFACE WAVE TESTS ON SHALLOW AND DEEP BEDROCK SITES

MOSITO NTAOTE

Supervisor: Professor G. Heymann

Department: Civil Engineering

University: University of Pretoria

Degree: Master of Engineering (Geotechnical Engineering)

SUMMARY

Active seismic surface wave tests are seismic tests for which the signal is generated by artificial sources as opposed to passive tests where the signal is generated by natural source. Active tests are widely used around the world due to among other factors their non- intrusive nature. However, the use of these tests in different parts of the world is based on availability and experience. Practitioners do not always consider the technical abilities of a test relative to others, but they rather select the test based solely on the availability of that tests in that specific region. Thus, few unbiased technical comparisons of these tests have been done to date.

This study investigated the comparison of three active seismic surface wave tests, spectral analysis of surface waves (SASW) test, multi-channel analysis of surface waves (MASW) test, and the continuous surface wave (CSW) test. The objective was to compare these three tests in terms of repeatability (reliability), susceptibility to near field effects, and maximum and minimum investigation depth. The tests were carried out in the field on shallow and deep bedrock sites.

Midpoint SASW configuration was used with source offsets ranging from 1 m, 2 m, 4 m, 8 m, 16 m and 32 m. As there is currently no standard configuration for conducting MASW tests, MASW tests were performed using two different array configurations of 24 geophones spaced at 1 m and 2 m respectively. The source offsets used for the 1 m geophone spacing were as follows: 1 m, 2 m, 4 m,

8 m and 16 m and for the 2 m geophone spacing the offsets were set up as follows: 2 m, 4 m, 8 m, 16 m, and 32 m. CSW tests were performed using five geophones spaced at 1 m and the source offsets used were 1 m, 2 m and 4 m. 2.2 kg, 6.3 kg and 9.2 kg sledgehammers were used as energy sources for the SASW and MASW tests whereas high and low frequency shakers were used as energy sources for the CSW tests. The geophones used to detect the signal of propagating Raleigh waves were 4.5 Hz natural frequency and a PASI GEA 24 (24 bit) seismograph was used to log the signals.

After the evaluation and analysis of the shallow bedrock results, all the tests were found to be repeatable (reliable) though the repeatability of CSW was better than that of SASW and MASW. MASW was found to be more prone to near field effects with the configuration of 1 m geophone spacing being affected more than the 2 m geophones spacing configuration. SASW was the second most affected and hence CSW was the least affected. Furthermore, SASW was able to sample deeper and shallower than both MASW and CSW. MASW was second best for sampling deeper and CSW was the second best for sampling shallower.

At the deep bedrock site, the repeatability of the tests was better than on the shallow bedrock site however, the repeatability of MASW and CSW was better than that of SASW. With regards to near field effects, MASW test with 1 m geophones spacing configuration was affected the most, followed by SASW, then CSW. CSW was also affected by multiple modes (far field) effect. MASW test with 2 m geophones spacing configuration was affected the least. Lastly, SASW was able to sample deeper, followed by MASW and then CSW. However, SASW and MASW were able to sample to virtually the same minimum depth which was in turn shallower than that achieved by the CSW test.

DECLARATION

I, the undersigned hereby declare that:

- I understand what plagiarism is and I am aware of the University's policy in this regard;
- The work contained in this thesis is my own original work;
- I did not refer to work of current or previous students, lecture notes, handbooks or any other study material without proper referencing;
- Where other people's work has been used this has been properly acknowledged and referenced;
- I have not allowed anyone to copy any part of my thesis;
- I have not previously in its entirety or in part submitted this thesis at any university for a degree.

Signature of student: 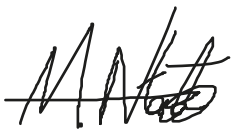

Name of student: **Mosito Ntaote**

Student number: **15302084**

Date: **July 2022**

ACKNOWLEDGEMENTS

I wish to express my sincere appreciation to the following organisations and persons who made this project dissertation possible:

a) Prof G Heymann for his guidance and encouragement during the course of the study.

b) Islam Mohammed my colleague for encouragement and vital discussions and offering of his car which made our travelling and carrying of equipment much easier during the study.

c) Engineering 4.0 laboratory staff for their support and assistance with the use of heavy laboratory machinery.

d) My mother, sister and my friends for their support and enhancement of my wellbeing during the study

TABLE OF CONTENTS

LIST OF TABLES

LIST OF FIGURES

LIST OF SYMBOLS

λ	Raleigh wavelength
ν	Poisson's ratio
Δϕ	Phase difference
γ^2	Coherence value between signal traces
f	Frequency
FFT	Fast Fourier Transform
G_{11}	Auto power spectrum for receiver 1
G_{22}	Auto power spectrum for receiver 2
G_{12}	Cross power spectrum for 2 receivers
P wave	Compression wave
S wave	Shear wave
R wave	Raleigh wave
L wave	Love wave
V_p	Compression wave velocity
V_s	Shear wave velocity
V_r	Raleigh wave velocity
CSW1m	CSW performed with the source at 1 m offset
CSW2m	CSW performed with the source at 2 m offset
CSW4m	CSW performed with the source at 4 m offset
MASW1m	MASW performed with 1 m geophones spacing
MASW2m	MASW performed with 2 m geophones spacing

Different MASW tests were named as MASW(geophone spacing)(source offset)(sledgehammer size) i.e MASW test performed at particular geophone spacing and source offset using a specific sledgehammer size e.g MASW1m2m2.2kg for MASW performed at 1 m geophones spacing and 2 m source offset using 2.2 kg sledgehammer.

MASW2m4m6.3kg for MASW performed at 2 m geophones spacing and 4 m source offset using a 6.3 kg sledgehammer.

1 INTRODUCTION

1.1 Background

Characterization of the subsurface geomaterials is of utmost importance in Geotechnical Engineering. This can be accomplished by determining subsurface soil design parameters using seismic methods, laboratory and in situ tests. These parameters can be utilized in dynamic problems such as site response evaluation, liquefaction potential evaluation, earthquake Engineering and foundations of vibrating machines (Strobbia, 2003). However, seismic methods are mainly focused on the determination of soil stiffness which can be used to ensure that sufficient margin of safety is maintained in the design of geotechnical structures such as excavations and tunnels, as the soil stiffness enables ground movements both during and after construction to be predicted (Matthews et al., 1996).

Seismic methods are in-situ geophysical measurements aimed at determining ground stiffness as mentioned above. These can be intrusive and non-intrusive. The seismic surface wave method is non-intrusive whereas intrusive methods require a drilled borehole or insertion of a probe into the soil. Non-intrusive tests rely on the detection of elastic waves, particularly Raleigh waves, and can be conducted with all the instrumentation placed on the ground surface (Foti, 2000 and Stokoe et al., 2004). Seismic methods can further be divided into two more categories, active and passive types and they differ by means of the signal source. Active tests use a signal that is generated artificially by means of sledge hammer, a drop weight or a fixed or variable frequency shaker. For passive tests, the signal source is natural and is mainly due to many different causes like wind, sea wave motion, vibrations from structures and car traffic (Bignardi, 2011).

Although active seismic surface wave methods (non-intrusive) are affected by some degree of uncertainty, they nevertheless have gained popularity worldwide and are widely used in Geotechnical Engineering. This is mainly due to the fact that they do not require drilling and hence they are also not associated with any potential environmental hazards associated with drilling. Also, since they do not require sampling, no sample disturbance occurs hence they can characterise hard-to-sample deposits or soils. They can also cover large areas of land quickly and economically during testing. With these methods, ground variability in terms of stiffness can be assessed and this process can in turn be used for evaluation of ground improvement schemes. Unlike other seismic methods, surface wave methods are capable of detecting soft layers beneath stiffer layers or even soft layers sandwiched between two stiff layers. Lastly, the practitioner has control over the signal source during testing (Matthews et al., 1996; Foti, 2000 and Stokoe et al., 2004).

The three most widely used seismic surface wave tests are spectral analysis of surface waves (SASW), Multi-channel analysis of surface waves (MASW), and the Continuous surface wave (CSW) method. The advantages and limitations of each of these tests are well known from literature. However, few direct comparisons of these tests have been reported. In cases where such comparisons have been made tests were not performed with the same equipment, time sampling parameters, array configurations (spatial sampling range) and not even on sites of the same geological nature. Thus, the research objective is to compare the performance of these three tests as objectively as possible.

1.2 Problem definition

Active seismic surface wave tests have evolved to a mature state today and the most widely used active seismic surface wave tests include the spectral analysis of surface waves (SASW), Multi-channel analysis of surface waves (MASW) and the Continuous surface wave (CSW) method. The popularity of these tests differs throughout the world and the practitioners typically prefer a particular test due to its availability in that region rather than the consideration of its technical abilities. The SASW method is mostly used in the USA, Asia and Europe, MASW method is widely used in North and South America, Europe and some Asian countries, whereas the CSW method is actively used in the United Kingdom, South Africa, Australia and some Asian countries (Stokoe et al., 2004). No scientific comparison of the three tests have been found in the literature. Therefore, unbiased and rigorous comparison of these tests is required in order to enable engineers to know the merits of each test relative to the others.

1.3 Objectives of the study

At present three seismic surface wave tests are commonly used in industry: SASW, MASW and CSW. However, there are conflicting views regarding which one of these tests is superior. Thus, the objective of this study is to determine which of these three seismic surface wave tests performs the best.

1.4 Scope of the study

The scope of the study is summarised as follows.

- The performance of the three non-intrusive seismic surface wave tests (SASW, MASW and CSW) were compared. The tests were compared with regard to:
    i. Repeatability

ii. Susceptibility of the test to near field effects
iii. Depth of measurement

- All the experimental work was field based, hence comparison using numerical methods will not form part of the study.
- The experiments were conducted on profiles with different bedrock depths at University of Pretoria Engineering 4 site and at the Wind Africa project site in Free state.
- Other seismic tests such as passive wave tests and borehole seismic tests did not form part of the scope of the study.
- The study was limited to sledge hammers, low and high frequency vibrator (shakers) as seismic sources.

1.5 Methodology

SASW, MASW, and CSW field tests were conducted on shallow bedrock (Engineering 4.0) and deep bedrock (Wind Africa) sites. The tests were performed with respect to the same centre line so as to ensure the same sampling range in space. 2.2 kg, 6.3 kg and 9.2 kg sledgehammers striking a circular (185 mm diameter and 30 mm thick) plate were used for SASW and MASW tests, whereas low and high frequency shakers were used for the CSW test. Traditional 2 receiver SASW with common midpoint configuration was employed. As there is currently no standard for MASW configuration, two sets of MASW tests were performed, one with 1 m geophone spacing (MASW1m) and the other 2 m geophones spacing (MASW2m), and 24 geophones were used in both configurations. CSW on the other hand was conducted using 5 geophones spaced at 1 m.

Furthermore, multiple source offsets were used for each of the tests for the assessment of the influence of near field effects for each test. SASW was performed with the offsets of 1 m, 2 m, 4 m, 8 m, 16 m, and 32 m as defined by the pioneer of SASW, Prof Kenneth Stokoe of the University of Texas. To maintain consistency, MASW with 1 m geophone spacing was performed at offsets of 1 m, 2 m, 4 m, 8 m and 16 m whereas 2 m, 4 m, 8 m, 16 m and 32 m source offsets were used for MASW executed with 2 m geophone spacing. On the other hand, CSW was carried out with source offsets of 1 m, 2 m, and 4 m. Thus, it is evident that for each of these three tests the source offsets were increased in a similar pattern as the offset was doubled each time.

.

SASW and CSW data were analysed using Python codes developed for this study by the author whereas Geopsy software was used for the analysis of MASW data. The analysed results were presented in the form of dispersion curves to achieve the objectives of the study. The same procedures were followed on the two sites tested to allow comparison of the three tests for both shallow and deep bedrock sites.

1.6 Organisation of the dissertation

The dissertation consists of the following chapters and appendices:

- Chapter 1 serves as an introduction to the dissertation and gives brief details of what can be expected in the study.
- Chapter 2 provides technical information of the main aspects of the study acquired from literature.
- Chapter 3 discusses the research methodology used to develop a rational experimental plan for SASW, MASW and CSW, which includes, the selection of equipment, spatial configuration of data acquisition devices and determination of time sampling parameters.
- Chapter 4 presents field results as well as their analysis and discussion
- Chapter 5 provides the conclusions and recommendations of the study.
- Chapter 6 gives a list of references from the literature.
- Appendix A, B, C, D, and E follow at the end of the report.

2 LITERATURE REVIEW

2.1 Introduction

This chapter gives historical background on both the theoretical and technical aspects related to this study. The literature review covers the following fields:

- Background on stress waves;
- Seismic equipment;
- Overview of active seismic surface wave methods;
- Technical aspects of active seismic methods
- Limitation of active seismic surface wave methods;
- Noise and its interaction with seismic records, and
- Layout parameters for active tests
- Seismic data processing techniques
- Inversion process
- Comparison of seismic tests

2.2 Background on seismic stress waves

When the ground is disturbed either artificially or naturally, different types of waves propagate in different ways in the ground. These include body waves and surfaces, whereby body waves propagate as spherical fronts from the source of disturbance, whilst surface waves propagate only along the ground (Stokoe et al., 2004 and Clayton et el.,1982).

2.2.1 Body waves

They are of two different types, which are Compression wave (P wave) and Shear wave (S wave). For P wave the ground motion is parallel to the direction of wave of propagation whereas S wave's direction propagation is perpendicular to ground motion (Stokoe et al., 2004 and Clayton et el.,1982). Figure 2.1 and Figure 2.2 show these two propagation modes.

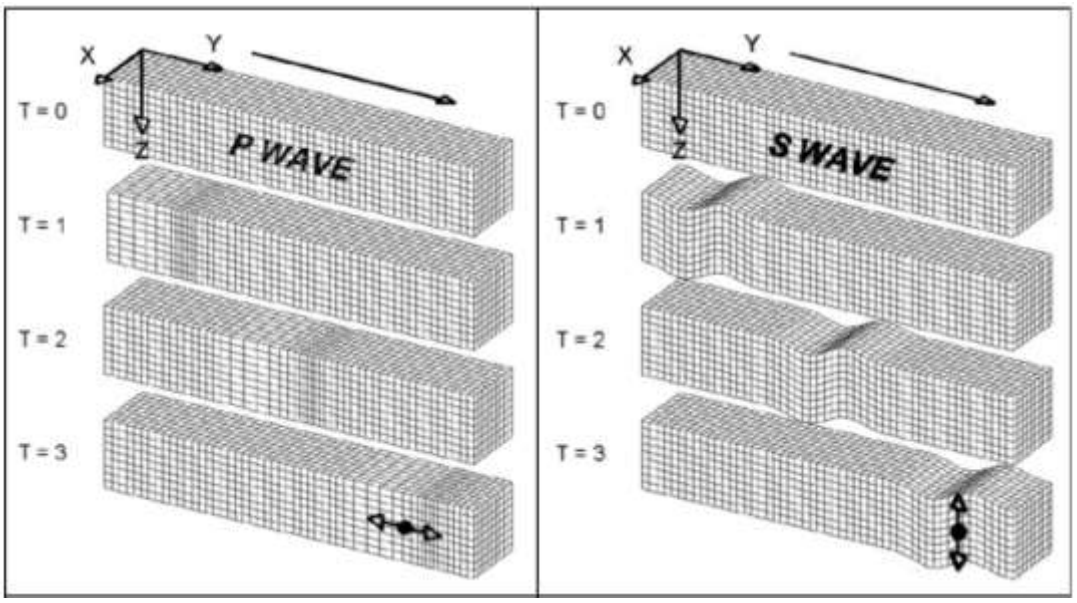

Figure 2.1: Propagation modes for body waves (Strobbia, 2003)

P waves travel faster than any other type of induced wave. S wave on the other hand can only attain maximum velocity which amounts to 70 % of P wave velocity (V_p) when they propagate within the same medium (Clayton et el.,1982). Equation 2.1 and Equation 2.2 show the calculation of V_p and S wave velocity (V_s) respectively whereas Equation 2.3 shows the relationship between of V_p and V_s for a homogeneous and isotropic material (Stokoe et al.,2004).

$$V_p = \sqrt{\frac{M}{\rho}} = \sqrt{\frac{B+\frac{4G}{3}}{\rho}} = \sqrt{\frac{E(1-\nu)}{\rho(1+\nu)(1-2\nu)}} \quad 2.1$$

$$V_s = \sqrt{\frac{G}{\rho}} \quad 2.2$$

$$V_p = V_s\sqrt{\frac{1-\nu}{0.5-\nu}} \quad 2.3$$

Where:

M = Constrained modulus

ρ = Mass density

B = Bulk modulus

G = Shear modulus

E = Young's modulus

ν = Poisson's ratio

Furthermore, S wave has two degrees of freedom unlike P wave which has one. S wave also takes two forms SH and SV which are its components parallel and perpendicular to the surface of the ground respectively. It is also worth mentioning that P wave travels through the soil particles and fluid in their pore spaces whereas S waves only travel through soil skeleton because fluid has no shear resistance (Clayton et el., 1982).

2.2.2 Surface waves

Surface waves are of two different types, Love wave (L wave) and Raleigh wave (R wave). The ground motion for L wave is parallel and perpendicular to the direction of wave propagation. However, since only a small fraction of the induced energy is transmitted as L wave then these wave has not been used extensively in seismic investigations (Stokoe et al., 2004 and Heymann 2007).

For propagating R wave, the ground motion is a combination of vertical (shear) and horizontal (compression) motion following a retrograde elliptical path in a vertical plane parallel to the direction of propagation (Stokoe et al., 2004, Clayton et el.,1982 and Heymann, 2007). This phenomenon can be seen in Figure 2.2.

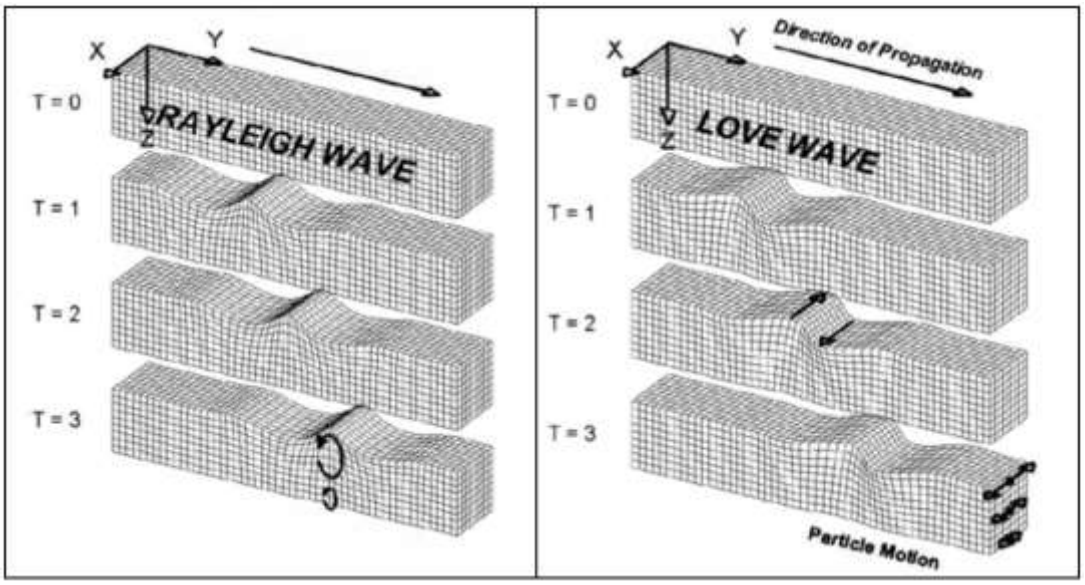

Figure 2.2: Propagation modes for surface waves (Strobbia, 2003)

Two thirds of energy produced into the ground is converted to R waves whereas the remaining one third is converted into all other wave types. R waves attenuate slowly at the rate of $\frac{1}{\sqrt{r}}$ where r is the distance from the source of ground disturbance (Heymann, 2007). According to Clayton et el.(1982), the velocity of R wave travels slower than P and S waves and its velocity depends on wave length and the thickness of the surface layer. Equation 2.4 shows an implicit definition of R wave velocity (V_r) in terms of V_p and V_s whereas Equation 2.5 shows the approximation of V_r in terms of V_s and ν Stokoe et al. (2004) and Heymann (2007).

$$[2 - (\frac{V_r}{V_s})^2]^2 - 4[1 - (\frac{V_r}{V_p})^2]^{\frac{1}{2}}[1 - (\frac{V_r}{V_s})^2]^{\frac{1}{2}} = 0 \qquad 2.4$$

$$V_r \cong \frac{0.874+1.11\nu}{1+\nu} V_s \qquad 2.5$$

2.3 Seismic equipment

2.3.1 Sources

A source is any equipment that produces energy into the ground through vibration or impact hence giving rise to seismic waves. The source can be either impulsive or vibratory both of which produce high-amplitude waves without generating a large amount of coherent-noise. For surface wave testing, two key parameters for the selection of the

source are considered, which are energy and frequency content. This is to ensure that it yields waves with adequate energy to give sufficient signal-to-noise ratio (SNR) over the frequency range of interest and offset range. Other important aspects that are looked at in the selection of the appropriate source are cost, source repeatability, cycle time between shots, environmental damage and safety requirements (Foti et al., 2014). Table 2.1 shows different types of sources used in seismic testing.

Table 2.1: Types of energy source for active seismic testing, adapted from Zahari (2014)

Source Type	On Land	On water
Impact	1. Sledge Hammer 2. Drop weight 3. Accelerated weight	
Impulsive	1. Dynamite 2. Airgun 3. Detonating cord 4. Shotgun 5. Borehole Sparker	1. Water gun 2. Steam gun 3. Gas gun
Vibrator	1. Vibroseis 2. Vibrator Plate 3. Raleigh wave generator	1. Multipulse 2. GeoChirp

2.3.1.1 Impact and impulsive sources

Impulsive sources produce energy into the ground by a short pulse of pressure. They can be of mechanical type (such as sledgehammer, weight drop or piezoelectric in holes) or chemical explosives which includes explosives, blasting caps and seismic guns. Amongst the different types of impulsive sources, the most widely used impact source is the sledgehammer, due to its low cost of purchase and operation and also because with sledgehammers site preparation is not essential and environmental damage is negligible (Foti et al., 2014).

A sledgehammer produces surface waves by striking the metal or plastic plate placed on the ground surface or even by striking the ground surface directly. The plates in this case serve to increase the frequency of the induced signal, however, on stiff surfaces such as a rock, high frequency waves can be generated (more than 1000 Hz) without the metal plate. Small sledgehammers are utilized to acquire high frequency (small wavelength dispersion data) due to its limited input energy in the low frequency range ($f < 8Hz$) which then makes them effective only for small array lengths, typically 50 - 100 m. This therefore

renders sledgehammers suitable for characterization of shallow subsurface materials only (Foti et al., 2014 and Foti et al., 2018). Figure 2.3 shows typical sledgehammers used in seismic testing.

Figure 2.3: Typical sledgehammers used for active seismic tests (Mothkuri, 2014)

For sampling at great depths, typically 30 m or more, where the sledgehammer is not able to sample, other portable impulsive sources such as weight drop, and the accelerated weight drop can be used. It consists of a mass (few kilograms to numbers of tons) that is raised to a height of more than a meter to tens of meters using a winch or piston as shown in Figure 2.4. The mass is then dropped (accelerated) to the metallic base plate on ground surface to increase the frequency content (Foti et al., 2014).

Figure 2.4: Tripod with 50 kg drop weight (Groenewold, 2016)

Other types of impulsive sources such as seismic guns which input the energy by firing cartridges into the shallow hole dug into the ground can be used. However, seismic guns are not widely used as they require an experienced operator and as the operation itself can induce noise and disturbance. Likewise, explosives were used in the past whereby the charge was placed in a shallow hole in the ground and ignited. However, explosives are now prohibited in many areas as the generated vibrations from the detonated charge can cause damage to structures and underground structures such as water pipelines. Also, the need to drill a hole causes the rate of operation to be slow and hence the test in general to be expensive (Foti et al., 2014).

2.3.1.2 Vibrating sources

Rather than producing short pulse signals with the impulsive sources, vibrating (controlled or swept) sources can be used to produce longer controlled signals. The smallest vibratory sources are portable electromechanical shakers that weigh at most 100 kg and are capable of transmitting a force of up to 0.5 kN. The largest are track-mounted vibroseis weighing tens of tons and it can deliver a force up to 400 kN. The mechanical structure of vibrators consists of a base plate held against the ground by a hold down mass which can be the

weight of the machine or even the vehicle. It also consists of the actuator that imposes the movement to a reaction mass resulting in a force that is then transferred to the base plate, hence into the ground (Foti et al., 2014). In Figure 2.5 is a typical vibratory source.

Figure 2.5: Typical CSW vibratory source (Hunter and Crow, 2015)

The optimum performance of a vibrator is dependent on its rated frequency spectrum and its optimum force is limited by a number of factors in this bandwidth. In the low frequency range, the force or energy is limited by the peak-to-peak stroke of the reaction mass whereas in the high frequency range the limiting factors are the servo-valve bandwidth and the flexibility of the base plate particularly for hydraulic vibrators (Foti et al., 2014).

With vibratory sources, various signal types can be used which can be sweep, chirp and monochromatic signals. Sweep signals are non-stationary function that takes the general form as shown in Equation 2.6. If the input frequency is in the flat band of the receiver response curve, the amplitude of the sweep signal at different frequencies depends on the source and site response. In addition, this type of signal is mostly applicable in reflection surveys and has the advantage of covering the whole frequency spectrum of interest in a single signal (Strobbia, 2003 and Foti et al., 2014).

$$A = A(t)\sin(2\pi f(t) + \phi) \qquad 2.6$$

Where:

A = Amplitude

f = Frequency

ϕ = Phase

Sweep can be referred to as upsweep if frequency increases with time or down-sweep if the frequency decreases with time (Foti et al., 2014). Furthermore, if the frequency is a linear function of time, sweep is referred to as linear sweep, whereas logarithmic and quadratic sweeps are mostly used for effectively sampling low frequencies when frequency is logarithmic and quadratic functions of time respectively (Strobbia, 2003). The linear, logarithmic and quadratic dependence of frequency on time are shown in Equation 2.7, Equation 2.8 and Equation 2.9 respectively.

$$f(t) = f_o + ct \quad 2.7$$

$$f(t) = f_o + 10^{bt} \quad 2.8$$

$$f(t) = f_o + bt^2 \quad 2.9$$

Monochromatic signals possess constant amplitude for the whole time of record and the SNR for this signal improves with the length of the record. Thus, if the ambient noise sources are random the signal length will play the same role as stacking to enhance the signal power hence yielding better signal quality. SNR for this signal can be furthermore improved by internal stacking which involves evenly partitioning a single trace into segments as shown in Figure 2.6. The signals in these segments are perfectly in phase, hence the signal strength can be increased with their summation (Strobbia, 2003).

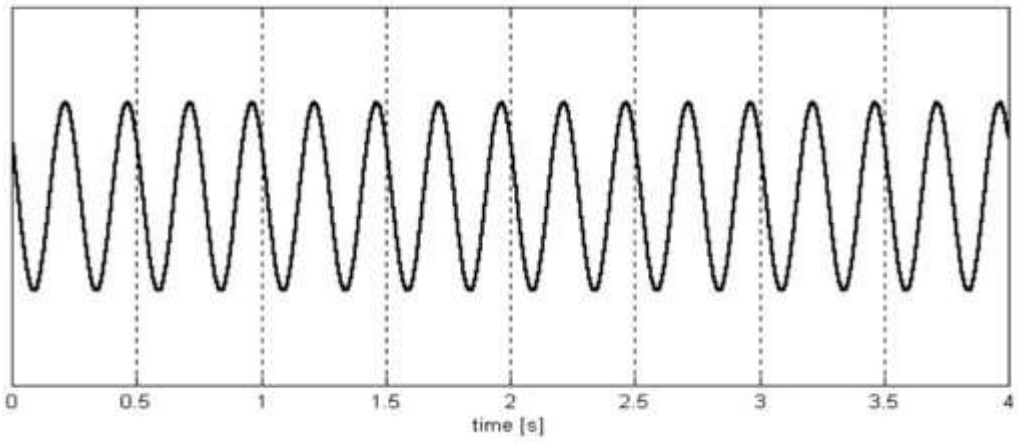

Figure 2.6: Monochromatic signal divided into portions of equal periods (Strobbia, 2003)

2.3.2 Receivers

Receivers are the first components of the series of recording devices to detect Raleigh waves. They convert ground motion (surface waves) into electric signal that is transferred to data logging devices. The type of receivers mostly used for shallow engineering tests are velocimeters known as Geophones. These are also utilized in passive surveys to record low frequencies, and these are called low-frequency geophones (Seismometers). Where the frequency of interest is high such as in pavement testing, the receivers used are accelerometers which can operate up to frequencies of a few kHz (Foti et al., 2014 and Foti, 2005).

According to Hwang (2014) there are three major requirements for receivers in seismic testing and these are as listed.

- The receiver must have a meaningful output over the frequency band required on site;
- Phase difference between receivers must be within certain limits often taken as 2 % of one cycle (360°), and
- Temperature of the geophone surface should be below roughly 95°F to preclude detrimental effects on its performance.

2.3.2.1 Geophones

Geophones are electrodynamic velocity transducers that consist of a moving coil suspended by a spring that is surrounded by a magnetic field induced by the magnet secured to the casing. As the soil vibrates, the base of the geophone oscillates in the vertical direction causing the relative movement between magnet and the coil and the inertia force on the suspended mass. The relative movement generates voltage in the coil which is known to be proportional to the velocity of motion. The circuit of the geophones also has a shunt resistor that eliminates the undesirable vibrational energy so as to damp the spring movement that can possibly swamp the recorded data. Damping is incorporated so that the geophone response is uniform over the desired frequency band with damping factors ranging from 0.6 to 0.7 (Foti, 2000; Foti, 2005 and Foti et al., 2014). A typical geophone is depicted in Figure 2.7.

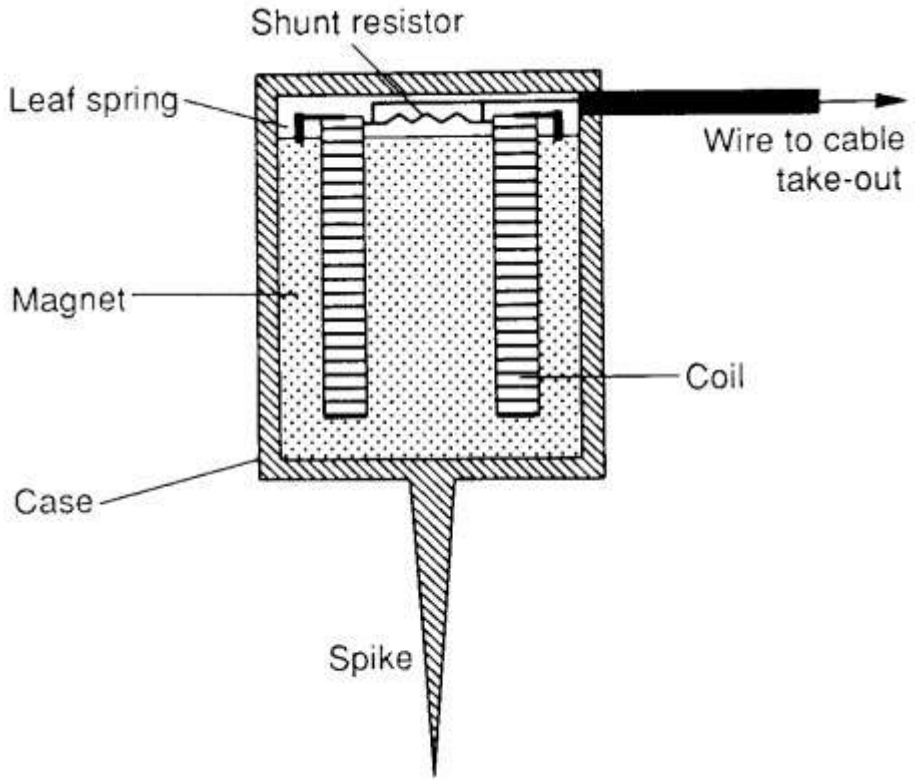

Figure 2.7: The structure of a geophone (Foti, 2000)

Geophones are typically categorized considering their resonance frequency or natural frequency which is the frequency below which the geophone response rapidly attenuates to zero. This frequency is important as it describes the minimum usable frequency of the

geophone. Thus, low natural frequency geophones (1 Hz or 2 Hz) can be used for sampling at great depths, however due to them being expensive and susceptible to environmental conditions, a compromise is often done by using 4.5 Hz geophones (Foti, 2000). Also, the geophone natural period of vibration is calculated with use the of Equation 2.10 below.

$$T_o = 2\pi\sqrt{\frac{m}{k}} \qquad 2.10$$

Where k is the spring constant and m the suspended mass.

2.3.2.2 Accelerometers and MEMS

Accelerometers are mainly used in applications where high frequency response is required, such as in pavement testing. They can be piezometric or piezoresistive whereby the former group depends on piezoceramic (zirkonate titanate) or single-crystal (mainly quartz) piezoelectric elements to produce voltage. The latter group of accelerometers is used for shock applications.

MEMS (microelectromechanical sensors) are sensors with high sensitivity, dynamic range and low noise. They are capable of recording frequencies that are virtually zero hence they are also eligible for recording gravity. They are also able to give a wide range of frequencies with precise amplitudes. They consist of a mobile proof mass attached on a mechanical suspension (such as polysilicon spring) to a reference frame. Fixed to the frame are the two plates in between which the mass with radial fingers is positioned. Acceleration causes the deflection of the mass from the centre position in different directions. Thus, the relative positions of the fingers and the plates generate the changes in differential capacitance that is then measured electronically with the use of modulation or demodulation techniques (Foti et al., 2014). A typical accelerometer is shown in Figure 2.8.

Figure 2.8: Typical accelerometer (Lin, 2007)

2.3.3 Data logging devices

The most common recording devices used by researchers are spectrum analysers and seismographs and they are as described below.

2.3.3.1 Spectrum analyser

Spectral analyser is a data recording device that is commonly used in surface wave surveys. It acquires a signal in the time domain from the receivers, the signal is then passed through a high grain amplifier where it is digitized and saved. The data is then converted to frequency domain after which the phase shift between signals at each geophone and the coherence of the cross-correlated signals can be ascertained. The data is considered reliable if the coherence of at least 0.9 is displayed, otherwise the data must be discarded. The merit of the device is that it enables the preliminary assessment of field data as it is capable of yielding dispersion data during acquisition on site (Matthews et al., 1996).

2.3.3.2 Seismograph

Seismograph is a data recording device commonly referred to as multi-channel recorder as it is used with at least twelve receivers. This device only measures data in the time domain, however, the data must first be transferred to a computer so as to convert data to the frequency domain so that phase difference between signals can be determined. This is a drawback of a seismograph relative to a spectrum analyser as the data quality cannot be evaluated on-site (Matthews et al., 1996).

2.3.3.3 Microcomputer

A Microcomputer can also be used in conjunction with an analogue-to-digital converter and memory card. It may also use a low pass filter that precludes distortions during data acquisition. Fourier transform software can be used in conjunction with the microcomputer so that the experimental dispersion curve can be determined whilst on site (Matthews et al., 1996).

2.4 Overview of active seismic methods

2.4.1 SASW method

SASW dates back to 1984 and was developed by Stokoe and Nazarian (Hebeler and Rix, 2001). It is a non-intrusive test that measures the frequency dependent velocity of the propagating surface waves that can in turn be used to determine the shear wave velocity of the site. It uses active sources that can range from sledgehammers, drop weights, accelerated weight systems or even harmonic sources. The frequency content and the wavelength of the produced wave is dictated by the shape and size of the source with a light source producing high frequency (short wavelength) waves whereas heavy sources produce low frequency (long wavelength) waves. The induced surface wave is detected by two or more geophones placed on the ground co-linearly with the source (Hunter and Crow, 2015).

SASW uses different configurations based on two methods known as the cross power method and the transfer function method. The experimental configurations used for the cross power method are common source and common midpoint configurations. For common source configuration, equal spacing between the source and the first receiver and between the first and the second receiver is used. Like the name implies, the source position is kept the same whereas the receiver spacing is then doubled for successive tests to acquire the data over a range of frequencies. For common midpoint configuration both the spacing between the source and the first receiver and the spacing between the first and second receiver is kept equal. However, now both the source and the receivers are moved by doubling the spacings for successive tests with the centreline maintained at the same position. For this setup the ground is excited by the source from both sides of the centreline of the array of receivers (Hebeler and Rix, 2001).

The soil is impacted on both sites of the centreline to generate forward and reverse profiles that can be averaged to avoid the effects of lateral heterogeneity and phase difference

between receivers and coherent noise (Alexander, 1992; Gucunski and Woods, 1992 and Foti et al., 2014). Measurements are done by using a number of source-receiver spacing sets usually at least six sets (Stokoe et al., 2004). The measurements are started with short spacing and light sources to measure high frequency waves and for large spacings large and heavy sources are used to generate low frequency waves (Bertel, 2006 and Foti al., 2014). Figure 2.9 shows common source and common midpoint configurations.

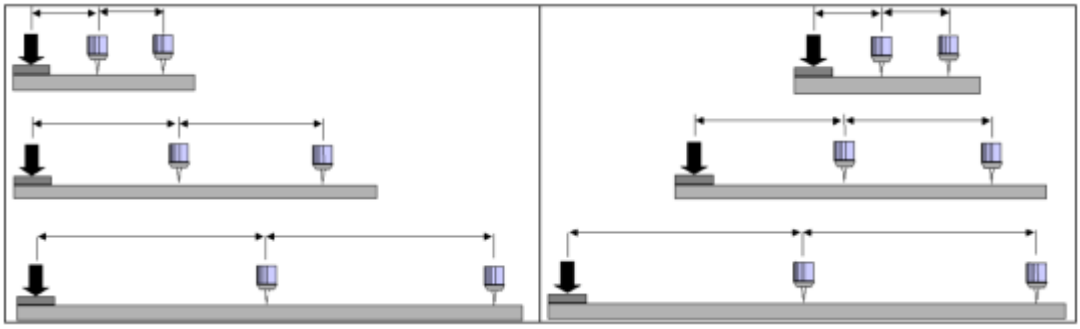

Figure 2.9: SASW common source (left) and common midpoint (right) configurations (Strobbia, 2003)

In the transfer function method, two receivers are deployed with one used as reference placed on the ground or on the harmonic source. The measurements are done by moving the second receiver in order to acquire data over a range of frequencies. The transfer function between the receivers is calculated and employed to yield the dispersion curve. Despite the drawback of the transfer function method of not being able to identify the individual Raleigh wave modes, it is nevertheless better for attenuation estimates. Also, the common first receiver position enables the material damping to be separated from the configuration of the measuring array (Hebeler and Rix, 2001).

2.4.2 MASW method

MASW is an array-based test whose inception was in the late 1990's and was developed to overcome some of the weaknesses of the SASW testing method (Park et al., 1998). It is used to measure indirectly the shear wave velocity profile of the topmost soil layers of a site. According to Groenewold (2016), MASW uses an array of geophones typically ranging from 6 to 48 and set up with equal spacings hence covering the whole range of different distances over which the required wavelengths of various sizes can be collected. For profiling to within 10 m of the subsurface 16 lb (7 kg) sledgehammer hitting a metal

plate and placed co-linear to the receiver array is typically used. For deeper testing, a heavy source such as a drop weight, or accelerated mass is adequate (Hunter and Crow, 2015). In Figure 2.10 the schematic representation of MASW is shown.

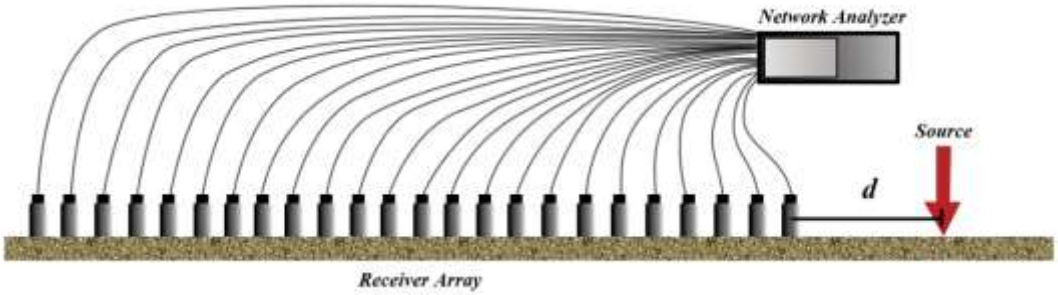

Figure 2.10: MASW test setup (McCaskill, 2014)

In addition, in practice the MASW test is performed at different source offsets to mitigate the effect of higher mode surface waves. Also, the source can be equipped with trigger if stacking of the records to improve SNR is essential in the field. However, it must be borne in mind that small prevalent errors in triggering times can also deteriorate the quality of the data hence sometimes negating this practice (Hunter and Crow, 2015).

2.4.3 CSW method

The Continuous Surface wave test is a non-intrusive geophysical technique employed for determination of the sub-surface shear wave velocity profile (Bouazza and Kavazanjian, 2000). It makes use of Raleigh waves induced by a mechanical, servo-hydraulic or electronic-magnetic vibrator placed on the ground to generate continuous sinusoidal waves at various controlled frequencies. During the test, Raleigh waves propagate away from the vibrator and are detected by co-linear low frequency (2 Hz) geophones that can typically range from 4 to 6. In Figure 2.11 is shown the schematic diagram of CSW test. The use of a vibrator in CSW is one of the factors that makes CSW highly attractive as the frequency can be controlled and varied hence yielding a reliable profile of phase velocity versus wavelength from which the soil stiffness profile can be evaluated (Clayton et al., 2012).

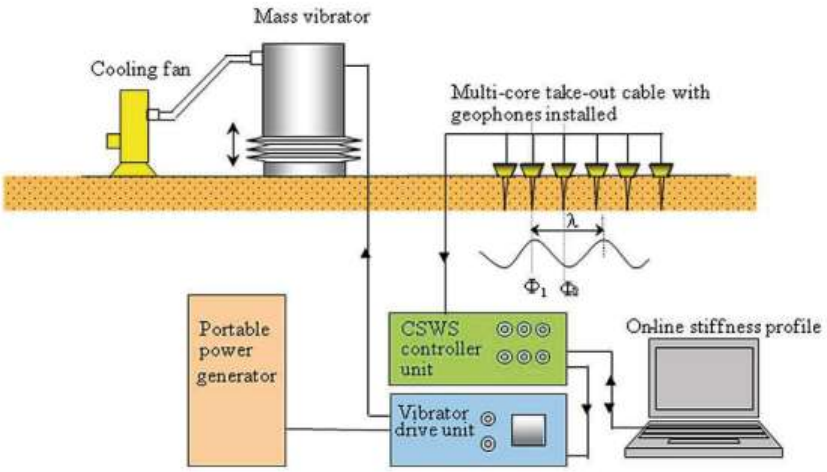

Figure 2.11: Schematic diagram for CSW test set-up (Aung and Leong, 2012)

The fewer Geophones required for the CSW test makes it suitable for being performed in confined spaces and less vulnerable to heterogeneity of the ground. It is also a relatively low cost and non-intrusive test that can also be used on contaminated lands. It is capable of sampling at very shallow depths hence suitable for linear and shallow foundation projects such as pipelines and highways. In addition, it can also be utilized in situations where other direct methods like penetration testing are not viable such as in highly weathered and fractured sites and where large rock fragments (boulders) prevail (Clayton et al., 2012).

2.5 Technical aspects of active seismic methods

In Table 2.2 and Table 2.3 give key features that describe each of active seismic surface wave tests and advantages and disadvantages of these tests respectively as discussed by Stokoe et al. (2004).

Table 2.2: Key features of different active seismic tests

Surface-Wave Method	Key Features
SASW method	• phase velocities from phase differences • two to four receivers typically used • superposed-mode phase velocity (apparent phase velocity) • global property over receiver-spread area • shear-wave velocity profile from the apparent phase velocities • comprehensive forward modeling or inversion analysis • impulsive source, swept-sine source, or random vibration source
f-k spectrum method	• phase velocities from frequency-wave number spectrum • multiple receivers (e.g. 128, 256, etc. receivers) • fundamental and higher-mode phase velocities • global property over receiver-spread area • shear-wave velocity profile from fundamental and higher modes • impulsive source
MASW method	• limited number of receivers (usually 24 receivers) • fundamental and higher-mode phase velocities • walk-away measurement • same measurement configuration as common-midpoint reflection survey • global property over receiver-spread area • shear-wave velocity profile from the fundamental mode • impulsive source or swept-sine source
CSW method	• phase velocity from the average phase-angle slope over receiver-spread area • four to six receivers used • superposed-mode phase velocity (apparent velocity) • global property over receiver-spread area • shear-wave velocity profile from the apparent velocities • steady-state harmonic source

Table 2.3: Advantages and disadvantages of active seismic tests

Surface-Wave Method	Advantages	Disadvantages
SASW method	• good sampling of shallow material • more sensitive measurements for layer stiffness contrast, using apparent velocity inversion analysis	• multiple measurements using different source-receiver configurations are required • expertise required for phase unwrapping and forward modeling
f-k method	•dispersion curves separated for fundamental and higher modes • body-wave effect extracted •dispersion curve global to the receiver-spread area	• aliasing problem in wave number domain • inaccurate mode separation in case of poor resolution in f-k spectrum • large number of traces required for good resolution in wave-number domain • limitation due to topographic constraint and instrumentation capability • long measurement time
MASW method	• mode separation of surface waves	• aliasing problem in wave-number domain • use of the fundamental mode only in inversion analysis
CSW method	• the effects of local anomalies minimized with the use of average phase-angle slope • no expertise required to calculate phase velocity • reliable measurements with controlled source	• dedicated inversion analysis required but not used • near-field effects included • exploration depth limited • frequency-content of vibrator is limited

2.6 Limitations of active seismic surface wave methods

Active seismic surface wave tests suffer from a number of limitations which can in turn affect the quality of the measured data. Section 2.6.1 gives the limitation of SASW as was discussed by Hunter and Crow (2015) and Lin et al. (2017). Section 2.6.2 describes MASW limitation by Hunter and Crow (2015). Lastly section 2.6.3 describes CSW limitations given by Clayton et al. (2012) and Hunter and Crow (2015).

2.6.1 SASW limitations

- The frequency content of the impact source can limit the desired depth of investigation;
- SASW is not capable of distinguishing between multiple modes hence resulting in apparent dispersion comprising a combination of different modes;
- Site geological conditions and topography can limit the test in terms of space, also vertical discontinuities can reflect the waves hence resulting in inaccurate results;
- The quality (resolution) of the surface wave velocity deteriorates with depth, and
- Conventional analysis of SASW suffers from phase un-wrapping errors and inefficient data filtering and synthesis.

2.6.2 MASW limitations

- MASW test assumes no lateral heterogeneity in the tested medium;
- It is not capable of acquiring data in areas where the depth to bedrock changes across the site or overburden geology varies laterally;
- It can only be performed on level ground as variation in the site topography alter the propagation fashion of surface waves;
- The presence of higher modes can lead to difficulty in interpretation of the dispersion curve hence leading to poor shear wave velocity profile;
- If the bedrock happens to be very close to the ground surface the conventional MASW test underestimate the shear wave velocity of the bedrock, and
- For sites where near-surface materials exhibiting V_s < 200 m/s are abundant it is difficult for the conventional MASW test to accurately measure shear wave velocity profile down to 30 m depth. Thus, this will require generation of low frequency surface waves (less than 2 Hz) of which generation and measurements of such low frequency waves can be complicated with conventional MASW equipment.

2.6.3 CSW limitations

- It is capable of good resolution of the shear wave velocity, however, the resolution decreases with depth;
- The energy produced by the vibratory sources decreases greatly for frequencies close to the minimum operating frequency of the source;
- Poor quality data can be produced if the frequency of ambient noise is in the same range of the frequencies for which the vibrator is operated, and
- The desired profiling depth is limited by the rated frequency spectrum of the vibrator.
- Complex ground profiles can influence the propagation mode of Raleigh waves hence complicating data interpretation.

2.7 Noise

In seismic testing, part of the recorded data is not perfectly pure as part of the signal is being distorted by environmental conditions as well as testing operations themselves. This distorted data is scientifically known as noise and does not convey any significant information about the signal properties except that it decreases the accuracy of the test results. Noise can be classified into two categories which are coherent and incoherent noise.

2.7.1 Coherent noise

It is considered as the deterministic events that form part of the subsurface propagation phenomenon but yield data that cannot reliably be explained by the assumed subsoil model and cause differences between the model and true Earth response. Coherent noise is caused by the interaction between the test equipment and the tested subsoil, and it can be classified into two, being non-surface wave events and non-compliant surface waves. Non-surface wave events comprise body waves from direct, refracted and reflected paths in the subsurface and air blasts which are acoustic waves that propagate in air as the result of the source stroke. Non-compliant surface waves involve the surface energy that does not propagate according to the assumed model due to spatial configuration of the test (Strobbia, 2003 and Foti et al., 2014).

2.7.2 Incoherent noise

It is often referred to as ambient noise meaning it is induced by random environmental effects. It is superimposed onto the signal hence leading to uncertainty in estimating the properties of the acquired data. This type of noise is the result of background vibrations at

the site induced by natural and human activities such as traffic, vibrating and moving machines, wind and movements of the ground water. This can also be as result of some imperfections within the recording system itself or electric or electronic noise in receivers and cables. Incoherent noise can be mitigated by increasing the SNR which can be accomplished in two ways, which is either by reducing the level of noise or by increasing the intensity of the signal.

Noise level can be reduced by ensuring that meticulous procedures are followed during testing. This can be done by adhering to a number of requirements for seismic testing, one which is to record ground vibrations on site without activating the seismic source. This helps in understanding the nature and level of incoherent noise which then gives guide as to which type of source can be used and during which time of the day the tests can be done. This means if the ambient noise is high then strong seismic sources must be employed, likewise data can be acquired during the quite times especially at night when the human noise is at a minimum. Minimising incoherent noise can also be achieved by careful use and ground coupling of the receivers.

Signal level can be increased by using a more powerful seismic source or by combining different sources for different frequency bandwidths. Alternatively, vertical stacking of synchronized repetitions of the tests must be exercised as this increases the SNR by the square root of the number of repetitions (Foti et al., 2014).

2.7.2.1 Near and far field effects

Unlike passive tests where waves are generated by distant sources, active tests use sources that are positioned very close to the receivers hence resulting in the so called near field effects. According to Yoon and Rix (2009) near field is the region where the assumption of plane Raleigh waves is not valid and the near field effects are the adverse effects associated with the invalid assumption, hence impacting seismic records. These effects include the cylindrically propagation of Raleigh waves together with coupled interactions of spherically spreading Body and Shear waves.

Near field effects can further be explained as a lump of three components firstly being “model compatibility” which is the effect resulting from modelling a cylindrically propagating Raleigh wave as a plane wave in the near field. The second effect is “near-field body wave effects” which is due to due the Body waves with mode of propagation different from that of Raleigh waves. Lastly is the phenomenon of “far-field body wave effects” which is the interference due to superimposed Body waves that yield multiple

modes that cannot be differentiated by traditional data processing methods (Zywicki and Rix, 2005).

In their work on numeral simulations of near field effects on Multi-channel method on unsaturated conditions (Poisson ratio (ν = 0.3)), Yoon and Rix (2009) concluded that (1) near field effects lead to underestimation of dispersion values; (2) Near field effects are dominant in irregular soils and less so in homogeneous and regular soil profiles; (3) An increased number of receivers mitigate the strength of near field effects in irregular soil profiles; and (4) To limit the error in Raleigh wave velocity (V_r) to within 15 % the Normalized centre array distance (NAC) must be greater than 1, whereas for errors less than 5 % NAC must be greater than 2. They defined NAC and normalized Raleigh wave velocity (NRV) as portrayed in Equation 2.11 and Equation 2.12 respectively and Figure 2.12 also depicts NAC.

$$NAC = \frac{\bar{x}}{\lambda_R} = \frac{\frac{1}{M}\sum_{m=1}^{M} x_m}{\lambda_R} = \frac{(\frac{1}{M}\sum_{m=1}^{M} x_m)f}{V_R} \quad 2.11$$

$$NRV = \frac{V_R}{V_{R,plane}} \quad 2.12$$

Where $\bar{x}$ is mean distance of all the receivers in an array relative to the source, λ_R= wavelength of the Raleigh wave, M = total number of receivers in the array x_m= distance of the mth receiver relative to the source, V_R = measured Raleigh wave velocity at frequency f and $V_{R,plane}$ = plane Raleigh wave at the same frequency.

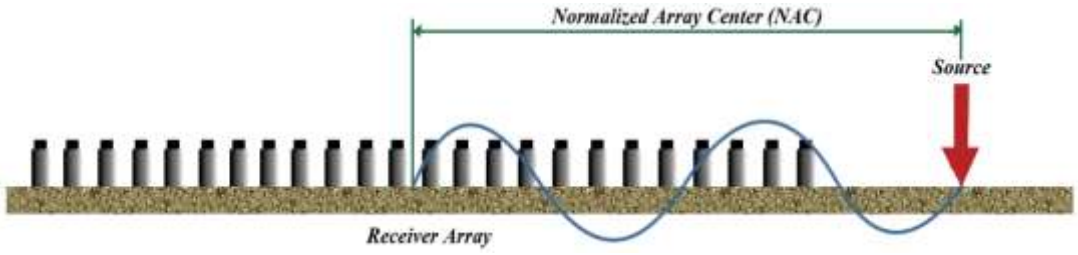

Figure 2.12: Representation of normalized centre array (NAC) for a 24 receiver array (McCaskill, 2014)

Near field effects decrease with distance from the active source, as with distance the Raleigh wave front will have had sufficient time to develop into a plane wave. Also, the body waves amplitude will have substantially diminished relative to Raleigh wave

amplitude (Yoon and Rix, 2009). This is because Body wave amplitude follow a geometric damping law of $\frac{1}{r^2}$ whereas Raleigh wave amplitude follow a geometric damping law of $\frac{1}{\sqrt{r}}$ where "r" is the radial distance from the source to the wave front (Heisey et al., 1981; Heymann, 2007 and Hwang, 2014). Furthermore, plane wave array-processing techniques such as Spatiospectral Correlation Matrix, Steering Vector and Conventional Plane Wave Beamformer have been found to reduce the severity of many of near field effects although they still cannot model cylindrically propagating Raleigh wave hence leading to biased velocity estimates. However, the Cylindrical Beamformer processing technique takes care of the cylindrical spreading nature of Raleigh waves as it utilizes the correct cylindrical wave field model hence leading to improved estimates of phase velocity (Zywicki and Rix, 2005).

2.7.2.2 Air blast

Air blast is the coherent effect resulting from the sound produced by seismic source shot that spreads into the atmosphere as a pressure wave and often also interfering with the ground and hence detected by seismic receivers. Its frequency is high with the velocity being virtually that of sound propagating in air defined by Equation 2.13. Air blast can be problematic in seismic testing as its velocity superimposes onto the induced Raleigh waves velocity making it difficult for a velocity filter to separate them.

$$v_{air} = 331.3\sqrt{1 + \frac{T}{273.15}}\ [m/s] \qquad 2.13$$

Where T is the temperature.

Air blast is apparent in time off-set and it is often recognised in frequency wave number (f - k) spectrum as a linear event with uniform velocity and low attenuation extending to higher frequency (Strobbia, 2003 and Foti et al., 2014). Figure 2.13 below portrays a seismogram in disturbed state due to air blast.

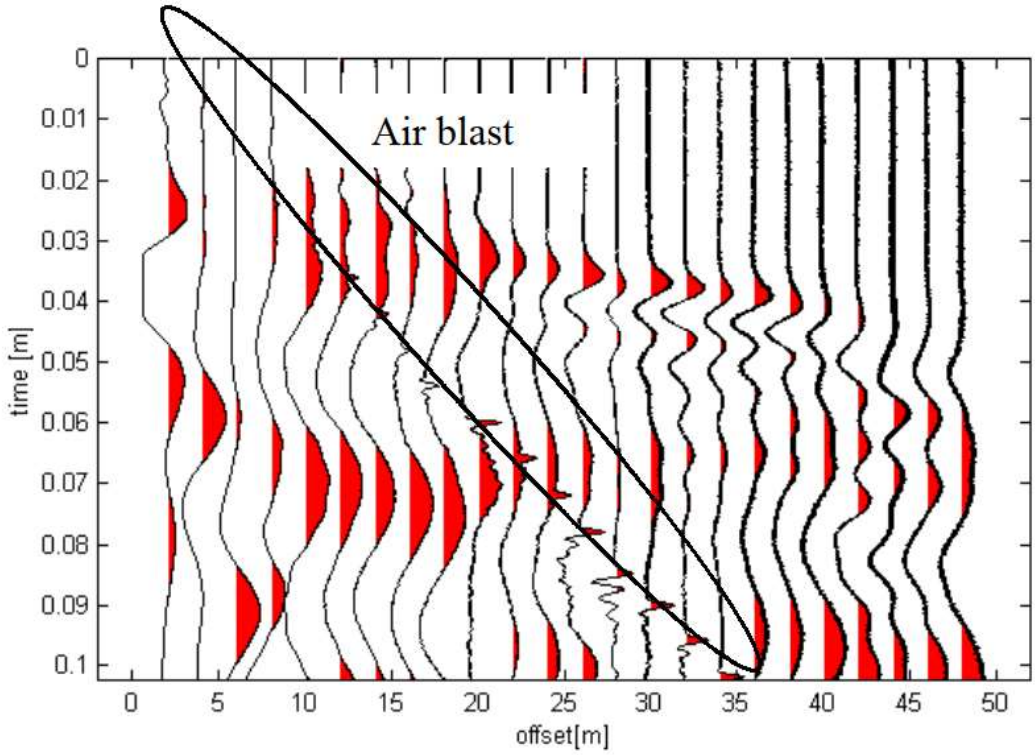

Figure 2.13: Seismogram contaminated by air blast (Strobbia, 2003)

2.7.2.3 Lateral variations

Lateral variation refers to sideways heterogeneity of the subsoil. However, in surface wave measurements the propagation is assumed to be laterally homogeneous, linear in time and phase offsets as this is in line with the 1D Earth model used for inversion. The results of lateral variations are considered as coherent noise as its presence yields data that cannot be interpreted precisely. Thus, it is important to select test sites that are not prone to effects of lateral variations such as lithological boundaries and soil layers tilted from the horizontal (dipping layers). In addition, caution must be given to the array length as it is a critical parameter as far as the consequences of lateral variations are concerned as the longer array length is likely to be affected by lateral variations (Foti et al., 2014).

Subsequent to data acquisition, the identification of lateral variations is a necessary step. The first method that can be deployed to detect lateral variation is the use of conjugate end-off acquisition and comparison of the two acquired dispersion curves. If the two dispersion curves show a significant difference, then there is good chance for the presence of lateral variations (Strobbia, 2003). A typical example of two dispersion curves showing the existence of lateral variations is shown in Figure 2.14.

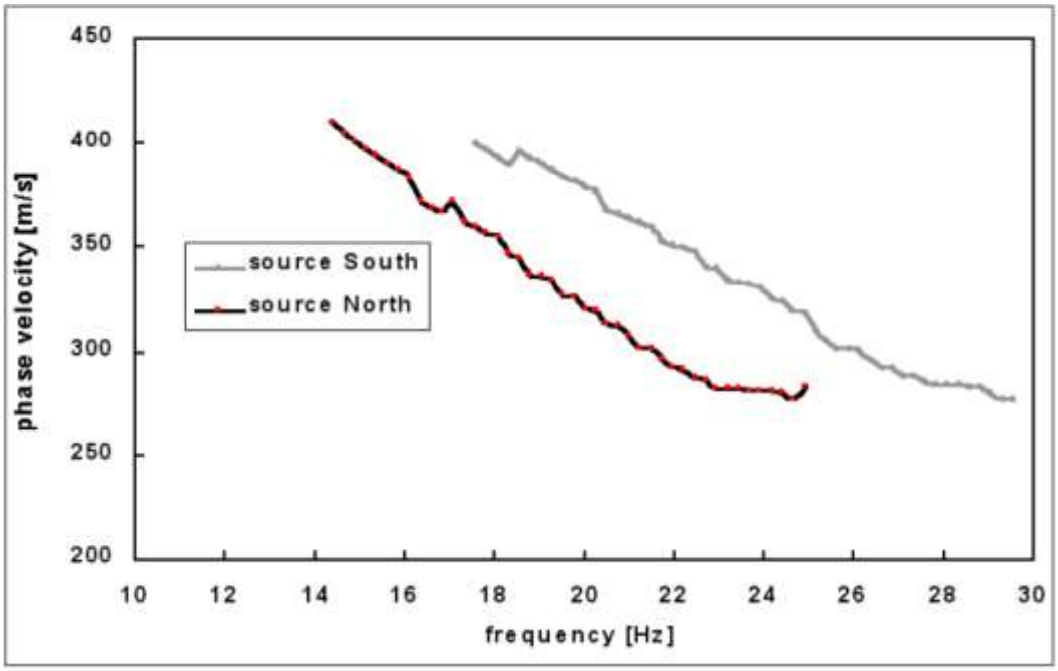

Figure 2.14: Two different dispersion curves revealing the presence of lateral variations (Strobbia, 2003)

Lateral variations can also be recognized with the use of a local phase difference processing technique between traces while keeping the frequency fixed. Then the linearity of generated phase difference-offset graphs is used to indicate the presence or absence of lateral variations. A fairly linear difference-offset graph shown in Figure 2.15 indicates the absence of lateral variations whereas the nonlinear graph shown in Figure 2.16 exhibit the existence of lateral variations. Lateral variations can also be identified by comparison of the data from different portions of the array length (Foti et al., 2014).

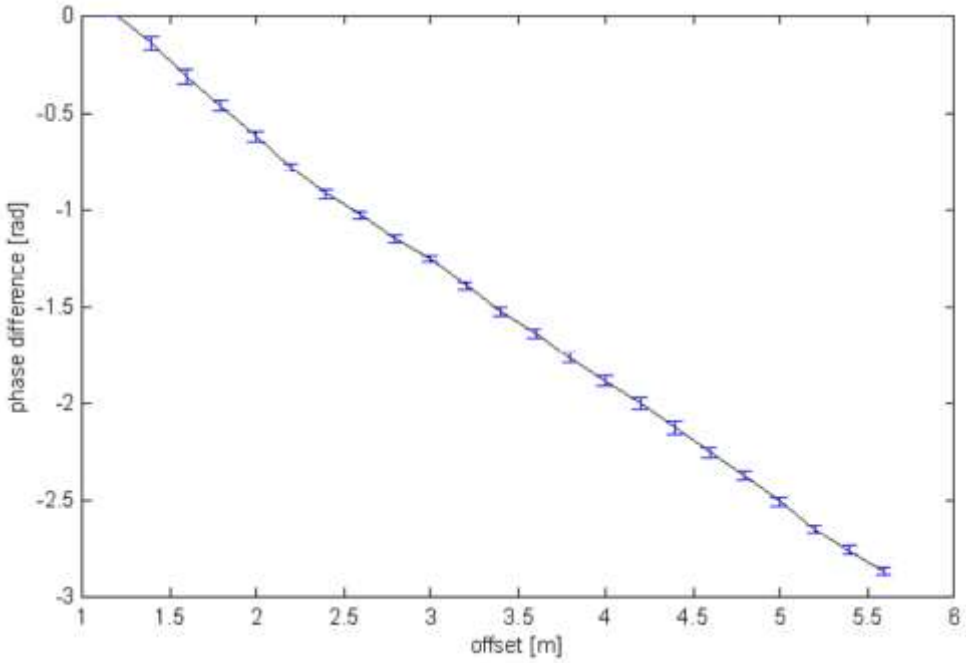

Figure 2.15: Linear phase difference-offset graphs justifying the absence of lateral variations (Strobbia, 2003)

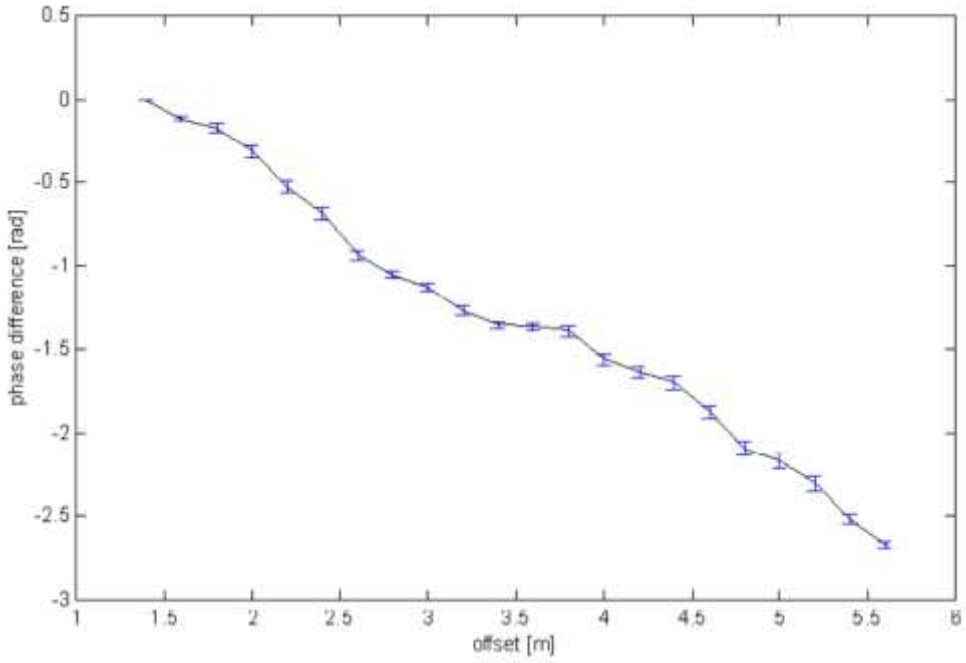

Figure 2.16: Nonlinear phase difference-offset graphs indicating the presence of lateral variations (Strobbia, 2003)

2.7.2.4 Higher Modes

Seismic data often exhibit multiple modes which include first (fundamental) mode and higher modes. These higher modes can convey important information about the profile and their phase velocity is dependent on the subsurface properties and they can be theoretically simulated and inverted. Seismic data acquisition should be in such a manner that these higher modes can be identified as the joint inversion of the fundamental and higher modes improves the reliability of the final result because higher modes represent additional independent information. Higher modes are rendered coherent noise by poor acquisition, processing or inversion techniques that misinterpret them, hence multi offset acquisition is ideal for satisfactorily identifying higher modes (Strobbia, 2003 and Foti et al., 2018).

2.8 Layout parameters for active seismic tests

2.8.1 Acquisition layout for active tests

The spatial configuration of the active seismic surface wave test is designed based on the aim of the test which can be the desired investigation depth and the resolution for shallow layers (Strobbia, 2003). This is governed by the three key parameters which are the receiver spacing (Δx), array length (L) and the source offset (d). Each of these parameters is designed to play a specific role during data acquisition. On the contrary as from Foti et al. (2014) the acquisition layout should also be designed to take into consideration geological issues that can include lateral variations and topographic changes as well as underground utilities such as foundations or buried pipes.

2.8.1.1 SASW layout parameters

In SASW the receiver spacing is not constant as the receivers need to be moved apart during the test to sample different wavelengths. A number of factors influence the selection of a set of receivers spacings, and this can be the desired investigation depth, shear wave velocity (V_s) of the site, attenuation properties of the site and wavelengths range of interest. Thus, Heisey et al. (1981) suggested an upper bound for receiver spacing of 2 to 3 times the wavelength to be sampled. This upper bound is set to assure that the wave energy of a certain wavelength does not attenuate excessively, and it is determined when the coherence value (γ^2) is virtually unity. Likewise, the lower bound for receiver spacing suggested by Heisey et al. (1981) is one third the wavelength to be sampled, and this is governed by the sensitivity of the instruments to measure phase shift between signals. Furthermore, the proposed source offset is in the range of 1 to 2 times the wavelength to be measured.

According to Bertel (2006) the receiver spacing can attain a minimum value of 1 to 3 times the minimum wavelength to be measured. On the other hand, the spacing can be as large as half the maximum wavelength to be sampled, which is in other words the depth to be profiled. The range of receiver spacing of one third to two times the wavelength to be measured has also been suggested by (Svensson and Möller, 2001) with the source offset in the same range.

2.8.1.2 MASW layout parameters

MASW is an array based seismic test that requires transformation of the wave field in both the time and spatial domains. Therefore, the receiver spacing should be designed in order to reliably sample short wavelengths associated with higher frequency waves that attenuate over a short distance. If it is designed based on the minimum wavelength expected in the signal which depends on the source and the velocity structure of the site, then a receiver spacing of 0.5 m to 4 m is recommended. On the contrary the array length, although it is dependent on the receiver spacing and the number of available receivers, should be adequate to sample long wavelengths and it must be greater than the anticipated maximum wavelength. In terms of the desired investigation depth the array length must be 2 to 3 times the desired depth. The source offset, which is the distance between the source and the nearest receiver, is designed to avoid near field effects while at the same time preserving the nature of high frequency waves that can attenuated significantly over a short distance. The recommended range of source offset is 3 m to 5 m times the receiver spacing for sources with good signal to noise ratio (Foti et al., 2018).

Furthermore, Park et al. (2002) suggests a minimum source to the nearest receiver distance of 10 m in order to give the propagating wave a sufficient distance for its non-planar components to attenuate. This can then allow a pure plane Raleigh wavelength of roughly 60 m to be captured. In addition, as the body waves and higher modes tend to dominate over the fundamental mode at far offsets (distance from the source to the furthest receiver) and higher frequencies, an empirical criterion for maximum receiver spread length of 100 m is recommended. Table 2.4 gives detailed information regarding MASW acquisition layout with the assumption that a sledgehammer heavier than 4.5 kg (10 lb) and a 24-bit recording instrument are used.

Table 2.4: Optimum MASW spatial geometric parameters (Park et al., 2002)

Receiver (Hz)	Max. Depth (m)	Minimum Offset (m)	Maximum Offset (m)	Receiver Spacing (m)
4.5	50	10	100	1
10	30	10	100	1
40	15	10	100	1

According to Foti et al. (2014) the receiver spacing can be as small as the minimum wavelength, however the receiver spacing in the range of 1 m to 5 m is suggested for soil characterization. Also, provided that the MASW source is capable of producing adequate signal to noise ratio the recommended array lengths can be in the range of 20 to 100 m. The source off-set parameter depends on the wavelength hence it ranges from 0.5 to 1 times the wavelength.

2.8.1.3 CSW layout parameters

Hunter and Crow (2015) suggested that a receiver spacing in the range of 0.5 to 1.25 m can be used. Joh et al. (2011) proposed the general criterion that the source offset should be 1 to 3 times the receiver spacing.

2.8.2 Active tests time sampling parameters

Time sampling parameters consists of five components being, time window, sampling rate (sampling frequency), Nyquist frequency, input frequency, and pre-trigger time. The time window is the time interval required to acquire the whole record of surface wave train. The sampling rate is the rate at which the records are taken, in other words the resolution in time domain. The Nyquist frequency is half logging frequency which is the reciprocal of the sampling rate, and the pre-trigger time is the time required to have signals centred in the time window enabling the deployment of hamming windows to preclude leakage during signal processing. The input frequency is the frequency range of the source in which wave records are taken and it should be greater than the resonant frequency of the geophones as the response of the geophones below this frequency becomes poor (Foti, 2005).

Foti et al. (2018) suggested that a time window of 2 s is sufficient for most testing arrays but should be longer if tests are done on softs sediments. A sampling rate of 2 ms which corresponds to a logging frequency of 500 Hz and Nyquist frequency of 250 Hz. They further recommended a pre-trigger time of 0.1 to 0.2 seconds. Likewise, Foti (2005) also commended a sampling rate of 2 ms. However, he emphasised that as the time window is

influenced by the frequency range of the signal in the frequency domain, the time window should be greater than 1 s. He further recommended a typical input frequency range of 5 to 100 Hz for geo-engineering applications.

2.8.3 Signal quality control

To acquire good quality data, good practice must be exercised on site and this includes.

- Properly working equipment must be deployed, particularly the receivers
- Geophones must be coupled and set flush to the ground with spikes, and few centimetres of the topmost soil profile or even thick grass must sometimes be removed to improve coupling. If testing is done on a hard surface, coupling must be enhanced by using a base plate, likewise if tests are conducted during bad weather conditions, the receivers must be covered against rain drops or droplets (Strobbia, 2003 and Foti et al., 2018).
- The time window must be long enough to record the whole surface wave train to avoid overestimation of phase velocities (V_s) due to the seismograms that can be truncated in time as a result of loss of a portion of low energy if the time wind is short (Strobbia, 2003).
- Ambient noise records must be taken to understand the nature and level of incoherent noise as this can enable one to know the appropriate sources to be deployed in order to improve the signal to noise ratio (SNR). Also, the receivers must be quantified so that traces with SNR less than 10 dB can be removed. SNR can be quantified from Equation 2.14 below (Foti et al., 2014 and Foti et al., 2018).

$$SNR[dB] = 20\log_{10}\frac{S}{N} \qquad 2.14$$

Where S is the signal power and N is the noise power

2.9 Seismic data processing techniques

A primary goal of seismic data analysis is to convert the recorded ground motions to a dispersion relation, which is a set of points that represent the trend followed by the Raleigh wave phase velocity as the frequency varies. For SASW and CSW this is achieved through the phase difference techniques whereas MASW uses array analysis techniques. These data processing techniques are described in the subsequent sections below.

2.9.1 SASW phase difference technique

In a traditional two sensor SASW test, time-series data collected during the experiment is first converted from the time domain to the frequency domain using the Fast Fourier Transform (FFT) algorithm. The phase difference of the cross-power spectrum between the two receivers is calculated using Equation 2.15 and plotted against the frequency to yield the "wrapped phase plot". If necessary, part of the data from the wrapped phase plot is eliminated (masked out) to circumvent the near field effects and regions of low signal coherence as explained in the subsequent paragraphs (McCaskill, 2014 and Groenewold, 2016).

After part of the data is masked out, "phase unwrapping" is done to produce the relation between frequency and unwrapped phase angle. With the unwrapped phase difference at a specific frequency, the propagating wavelength can be calculated using Equation 2.16. Equation 2.17 can further be employed for calculating the Raleigh wave velocity which is then plotted against frequency to yield the experimental dispersion curve for a particular receiver spacing. This process is repeated for different receiver spacings to generate dispersion curves that will be combined to a single composite dispersion curve also known as "field dispersion curve" that represents the geotechnical site (Strobbia, 2003; Hebeler and Rix, 2001 and McCaskill, 2014).

$$\Delta\phi_{wrapped}(f) = \tan^{-1}\left(\frac{Im(G_{12})}{Re(G_{12})}\right) \quad 2.15$$

$$\lambda = \frac{2\pi\Delta x}{\Delta\phi_{unwrapped}(f)} \quad 2.16$$

$$V_r = \lambda f \quad 2.17$$

Raleigh wave velocity can also be represented in terms of the wave number (k) as shown in Equation 2.18 below

$$V_r = \frac{2\pi f}{k} \quad 2.18$$

Where:

λ = wavelength

Δx = Receiver spacing

k..... = $\frac{\Delta\phi_{unwrapped}(f)}{\Delta x}$

$\Delta\phi_{wrapped}$ = Wrapped phase difference

$\Delta\phi_{unwrapped}$ = Unwrapped phase difference

f = Frequency

G_{12} = Cross power spectrum

V_r = Raleigh wave velocity

As mentioned in the preceding paragraphs, coherence(γ^2) is a parameter used to discern the quality of the signal as a function of frequency. It is an indicator of the extent by which the input signal at receiver 1 is linearly correlated to the output signal at receiver 2. Coherence values range between 0 and 1, and hence the values of 0.9 and above are indicative of good quality date. However, its values can degrade as a result of wave attenuation, interference of body waves, spatial variability, and elevated noise levels (Heisey et al., 1981 and Hebeler and Rix, 2001). The coherence of two signals can be calculated from auto and cross power spectra equations (Strobbia, 2003)

$$G_{11} = Y_1(f)\overline{Y_1(f)} \quad 2.19$$

$$G_{22} = Y_2(f)\overline{Y_2(f)} \quad 2.20$$

$$G_{12} = Y_1(f)\overline{Y_2(f)} \quad 2.21$$

$$\gamma_{12}^2 = \frac{G_{12}\overline{G_{12}}}{G_{11}G_{22}} \quad 2.22$$

Where G_{11} and G_{22} are auto power spectra for Receiver 1 and 2 respectively, G_{12} is the cross power spectrum for Receiver 1 and 2, γ_{12}^2 is the coherence between two receivers. $Y_1(f)$ and $Y_2(f)$ are Fast Fourier transformed signals on Receiver 1 and 2 respectively and $\overline{Y_1(f)}$ and $\overline{Y_2(f)}$ are the complex conjugates of $Y_1(f)$ and $Y_2(f)$ respectively.

2.9.2 CSW phase difference technique

During CSW testing, vertical ground motions are induced as the vibrator vibrates at a particular frequency. The motion is detected by geophones that are placed in a line that is co-linear with the vibrator and are also positioned at known distances apart. The signal that is recorded by the geophones is digitized and recorded with respect to time (time-domain). The data is then treated using the Fast Fourier Transform (FFT) to covert the signal into a plot of phase angle at each receiver against the distance of each receiver relative to the first receiver (Phase- distance plot) and this can be seen in Figure 2.17 below. The reciprocal of the gradient of Phase-distance plot is utilized in Equation 2.23 to determine the wavelength of the Raleigh wave, and Equation 2.24 is then used to determine the Raleigh wave phase velocity (Bouazza and Kavazanjian, 2000).

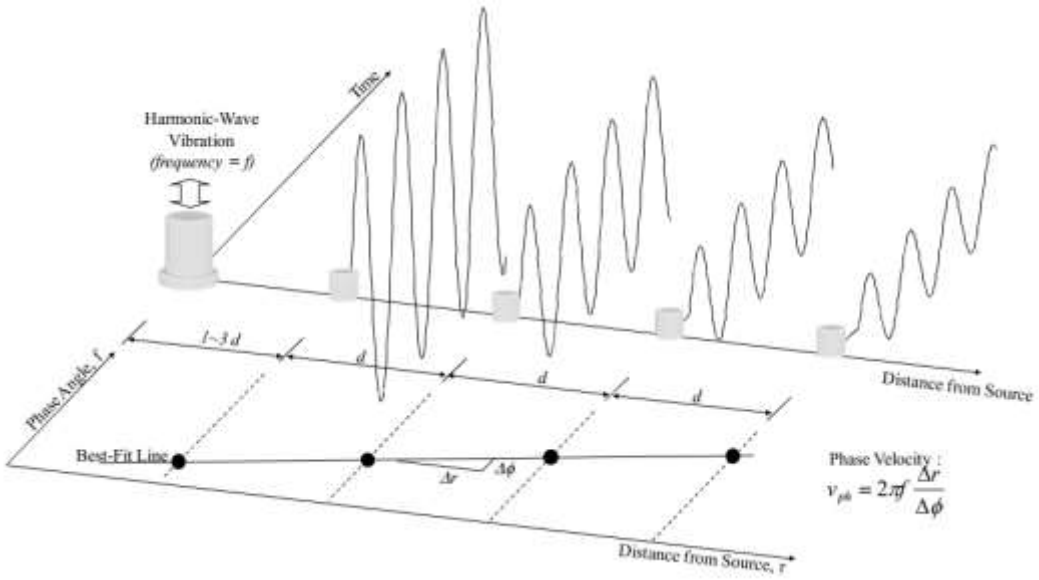

Figure 2.17: CSW unwrapped phase-distance plot (Joh et al., 2011)

$$\lambda = 2\pi \frac{\Delta x}{\Delta \phi} \qquad 2.23$$

Where λ is the wavelength of the Raleigh wave and $\frac{\Delta x}{\Delta \phi}$ is the reciprocal of the gradient of the phase-distance graph.

$$V_r = f\lambda \qquad 2.24$$

Where V_r and f are the velocity and the frequency of the Raleigh wave, respectively.

The phase angle(ϕ) at each receiver is calculated by Equation 2.25, which uses Fourier transformed signal z comprising a Real (Re(z)) and Imaginary (Im(z)) component of the geophone response (Heymann, 2007)

$$\phi = \tan^{-1}\left(\frac{Im(z)}{Re(z)}\right) \quad 2.25$$

This process is repeated by varying the frequency of the vibrator for which each frequency will result in a specific Raleigh wave velocity, hence the dispersion curve can be generated.

2.9.3 MASW array analysis technique

The dispersion curves in MASW are acquired after the raw field data is processed by array processing techniques (Transform-base methods). These techniques include Frequency-wavenumber (f-k) or 2-D Fourier transform, the Frequency-slowness transform, Phase-shift (plane wave beamform), the Cylindrical beamformer transform. These methods transform time series surface wave data from space-time domain into a different domain. Furthermore, all of these methods assume planar Raleigh wave except cylindrical beamformer which considers the cylindrical wave form (McCaskill, 2014; Olafsdottir et al., 2017).

Frequency-wavenumber transform uses the Fast Fourier Transform (FFT) algorithm to convert time series data for all the geophones into frequency domain. The wavefields corresponding to the frequencies found with the first FFT are converted from space domain to wavenumber domain by applying the second FFT. “F-P transform is a combination of slant-stack transformation of receiver time histories and the sum of power spectra of transformed traces for each frequency”. Phase-shift transform is a combination of the slant-stack and f-k methods (McCaskill, 2014).

2.10 Inversion process

Inversion is the last step of surface wave analyses. It consists of estimation of the parameters of a layered earth model from the dispersion curve of a site. This process is represented in Figure 2.18. The inversion process is nonlinear, mathematically ill-posed, mix-determined and it is also affected by non-uniqueness of the solution since different models can give equally good fit to the experimental data. Inversion is also associated with

uncertainty as the results can vary due to different layer-models used by different practitioners (Strobbia, 2003 and Foti et al., 2018).

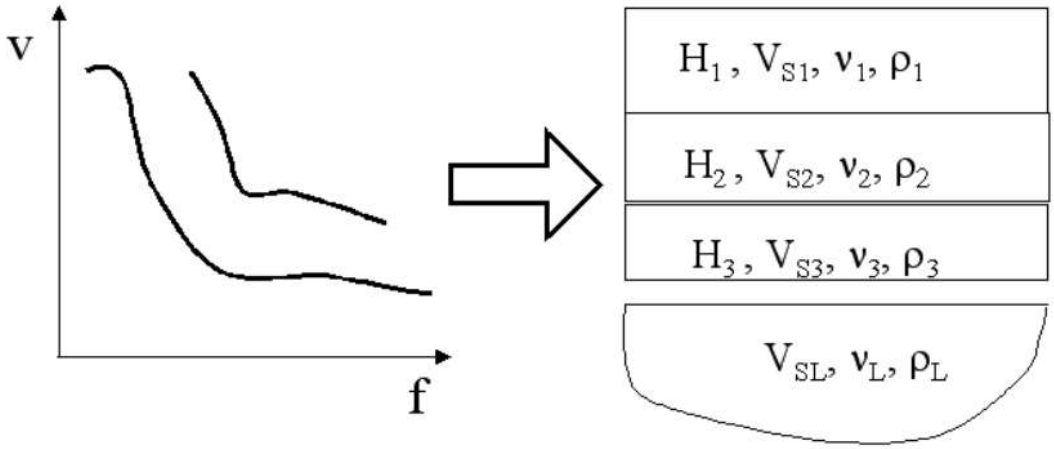

Figure 2.18: Inversion technique of surface wave methods (Strobbia, 2003)

In an inversion process, the subsurface is modelled as a vertical stack of homogeneous and isotropic linear elastic layers. Four parameters define each layer i.e thickness (excluding half space), mass density (ρ), Poisson's ratio (ν) and shear wave velocity (V_s). It is noteworthy that inversion solution is sensitive to layer thickness and V_s hence care must be given to these two parameters. However, for ν and ρ can remain fixed in the model since they have less influence (Strobbia, 2003 and Foti et al., 2018).

The number of layers must not be too many so as to avoid over-parameterization that can lead into unreliable model due to inadequate information to satisfy inversion. On the other hand, the number of layers must be sufficient to reproduce variation with depth (Foti et al., 2018). Furthermore, when modelling the parameters, values for saturated and unsaturated soils must be distinguished properly as failure to this may result in errors that can yield unrealistic V_s model. Also, reasonable estimation of water table for a site is essentially for the successful inversion process (Strobbia, 2003 and Foti et al., 2018).

Since inversion is non-linear process there are two inversion search categories that can perform inversion in a non-linear way. These are local and global search categories, and they search for the sets of parameters that best resemble the ground characteristics. The local search algorithm is a trial and error approach that aims at minimising the value of misfit function by an iterative process that starts from initial assumed model. Figure 2.19 show the solution of the local search method. It can be seen that part "a" represents initial

(green) and final (red) models, part “b” represent misfit as a function of the number of iterations and part “c” represents comparison of the experimental data (blue) with the response of initial (green) and final (red) models (Foti et al., 2018).

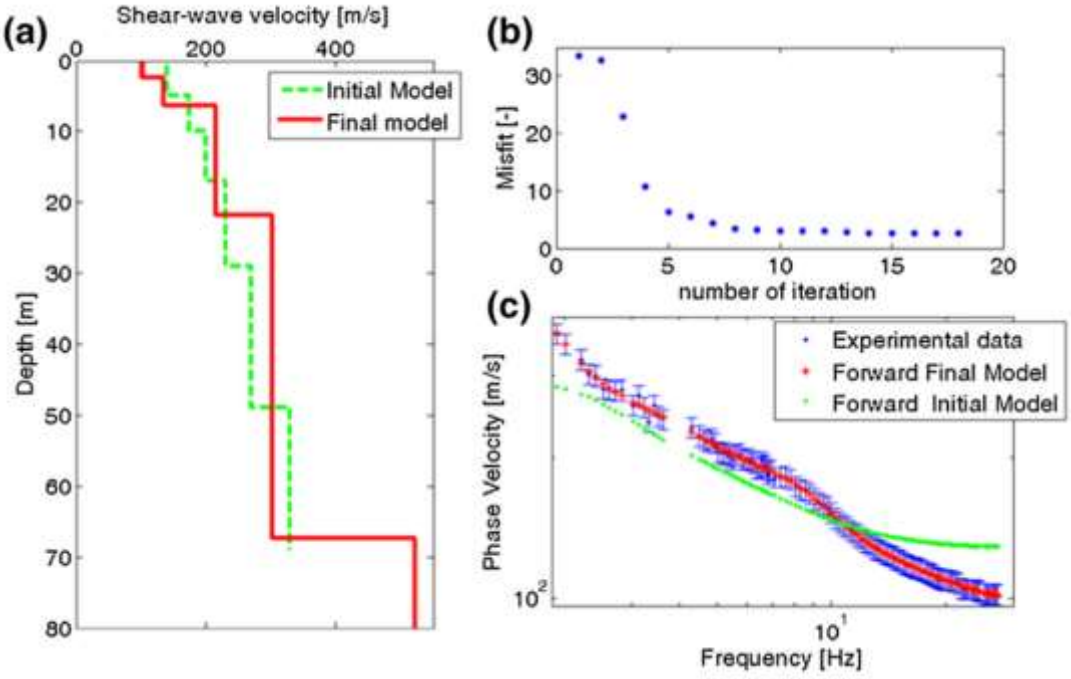

Figure 2.19: Typical result for Local search method (Foti et al., 2018)

In global search methods the search boundaries for each model parameter are defined. Then a large number of solution profiles is randomly generated with respect to the bounds of each model parameter. The misfit of the solution profiles relative to the experimental data is obtained. Inference is then made to find the profiles that represent acceptable solutions. It must also be borne in mind that the ability of global search methods to yield a set of profiles allows for the assessment of the uncertainty related to non-uniqueness of the solution. The global search methods include approaches like Monte Carlo, Genetic algorithms, simulated annealing, neighbourhood and from artificial intelligence point of view Artificial Neural Networks approach is used. (Strobbia, 2003 and Foti et al., 2018).

Figure 2.20 show an example of the solution for global search method. The red line in part “a” represents the profile with minimum misfit, the greed dotted lines represent the solution boundary (search area). Blue and yellow profiles are the acceptable profiles base on their misfit values. In “b” the red part is the experimental data and the blue and yellow are the accepted profiles. Lastly, part “c” compares experimental data (red) with the profile of minimum misfit value (Foti et al., 2018).

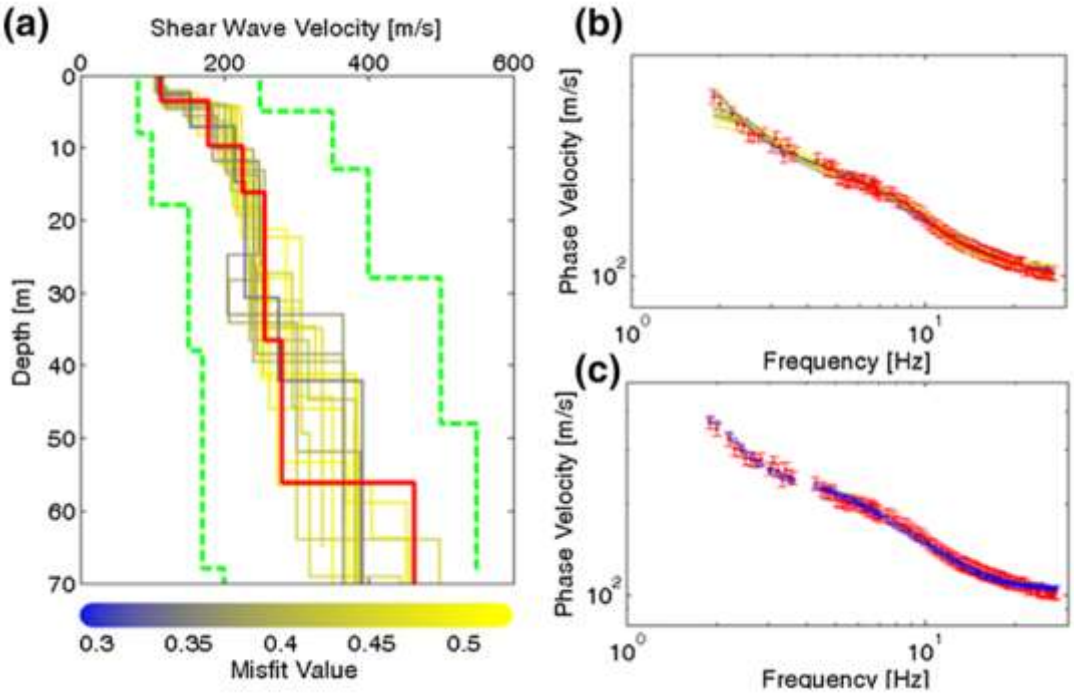

Figure 2.20: Typical result for Global search method (Foti et al., 2018)

According to Foti et al. (2018) global search methods are better than local search methods because solution of the local search methods depend strongly on the initial uncertain profile model. Also, the global search methods are able to investigate the uncertainties associated with non-uniqueness of the solution even though they are time and computation resource consuming.

2.11 Comparison of seismic tests

This chapter presents the work that was conducted in the past to compare active seismic tests.

Omar et al. (2011) conducted a research using SASW and CSW methods to predict the long-term settlement of a loaded pad on a soft clay site. The soil was treated as an anelastic material of viscoelastic property. The calculation of long-term settlement was carried out using the shear wave velocities obtained from SASW and CSW and damping factor (D) from the plate load test using a seismic formula that is based on the generalized viscoelastic time-dependent strain of materials. The formula is presented as Equation 2.26.

$$w = w_o(T/T_o)^{2/\pi Q} \qquad 2.26$$

Where:

w = predicted settlement

w_o = elastic deformation from input of shear wave velocity

T = total settlement time to be predicted

T_o = the period from the frequency of the dominant seismic event

Q = mechanical quality factor

Shear wave velocities for CSW were measured using a total of eleven survey lines whereby for each survey line forward and reverse tests were done to obtain an average shear wave velocity. For SASW, 2-D modelling to calculate dispersion curve was carried out using WinSASW. The shear wave velocity was obtained by using 3-dimensional stiffness matrix to match the theoretical from experimental dispersion curve to obtain the minimum root mean square (RMS) error. Table 2.5 shows the settlement results of SASW and CSW obtained by using Equation 2.26 relative to observed settlement. Thus, SASW and CSW were both considered able to predict long term settlement results that are close to observed settlements.

Table 2.5: CSW and SASW predicted settlements relative to Observed settlement (Omar et al., 2011)

Time	Calculated settlement (mm)		Observed settlement (mm)
	CSW	SASW	
0.067 s (elastic)	3.77	3.77	–
1 day	22.6	25.8	13.5
30 days	34.8	40.1	33.0
300 days	48.0	54.1	36.5

Equation 2.26 was revised to derive the form of equation that can be able to produce better predictions of long term settlement of soft clay. Equation 2.27 was therefore found to be a better version of Equation 2.26.

$$w = w_o(T/T_o)^{3.25D/\pi} \quad 2.27$$

Where:

D = damping factor related to quality factor by $\frac{1}{Q} = 2D$

Long term settlement results for SASW and CSW relative to observe settlement when using Equation 2.27 are shown in Figure 2.21. The difference between calculated and observed settlements were reduced by an average of 10 % when Equation 2.27 was used. Thus, both SASW and CSW were able to predict long-term settlement in soft clay with the results being improved when revised settlement equation was used.

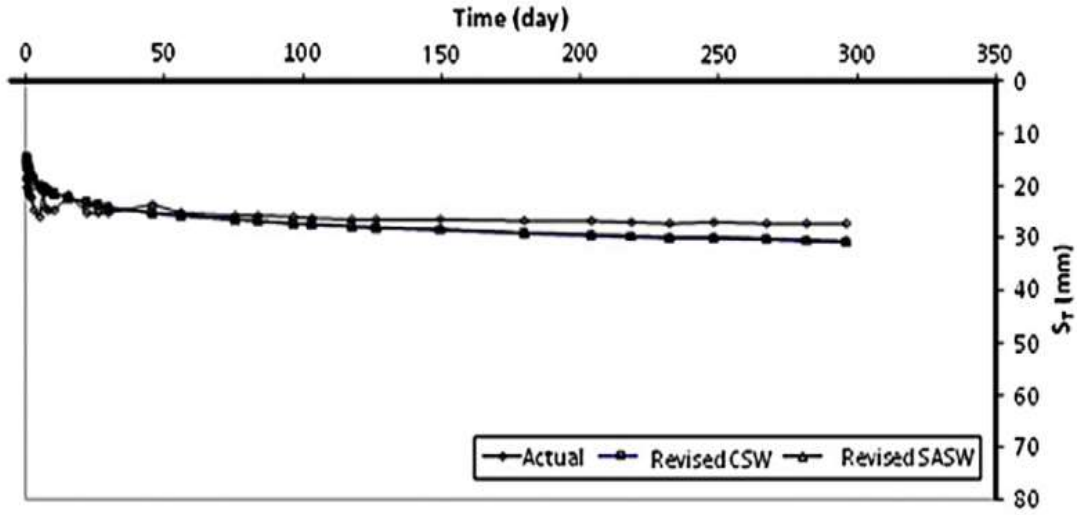

Figure 2.21: Predicted long-term settlements for CSW and SASW using revised seismic equation parameter relative to observed long term settlement (Omar et al., 2011)

Kim et al. (2013) conducted as comparative study for intrusive and non-intrusive seismic methods using Round Robin Test (RRT) performed at Seohae Ground Bridge site in Korea. Intrusive methods included borehole seismic tests such as downhole, cross hole, SPT based uphole, suspension logging methods as 1-D characterization of V_s profile. Non-intrusive surface wave methods included SASW, MASW, Harmonic Wavelet Analysis of Waves (HWAW) and ReMi were used for 1-D and 2-D characterization. Table 2.6 and Table 2.7 show the descriptions of intrusive and Non-intrusive methods used. The study focused on reliability and limitation for each method, cause of difference in results, suggestion for better V_s profile evaluation and feasibility of 2-D subsurface image mapping based on surface wave methods.

Table 2.6: Intrusive methods and their description (Kim et al., 2013)

Borehole seismic methods	Key features in this study
Crosshole seismic test (U1)	• Use two testing boreholes (BH-2 & BH-3, hole spacing = 3m) • Motor-driven impact source, horizontally propagating SH wave • Constant signal to noise ratio with depth in general • Agilent 35670A for data logger • Simple interpretation procedure (velocity = distance/travel time) • Most reliable field seismic test, but expensive
Inhole seismic test (U1)	• Use one testing borehole (BH-1) • Motor-driven impact source, vertically propagating SH wave • One serial body of source and receiver with air packer clamping system • Applicable to the non-cased testing hole • Agilent 35670A for data logger • Simple interpretation procedure (velocity = distance/travel time)
Downhole seismic test (U2, U3, C1, C3, C4, C5)	• Use one testing borehole (BH-1), vertically propagating SH wave • Simple surface source (wood or steel plate type with spike and overburden pressure) • Orientation for horizontal geophone (orientation rod or electric magnetic compass type) • Clamping system (air packer or motor-driven spring plate) • General-purpose data logger (Agilent 35670A), or commercialized equipments for seismic tests (Geometrix, OYO Mcseis, ABEM Mark 6+) • Relatively unclear interpretation procedure (direct method and refracted ray-path method)
Uphole seismic test (U2)	• Impact energy from sampler during SPT for underground source (Bang and Kim, 2007a) • Use one borehole, casing work is not required (BH-1) • Underground SV wave is changed to SH wave while propagating to the ground surface • Two-component surface geophones (more 2 sets) • Multi-channel data logger (Graphtec MA6000) • Similar interpretation procedure to the refracted ray-path method of downhole test
Suspension PS logging (C2, C3, C4, C5)	• Use one testing borehole (BH-1) • One body of source and two receivers connected serially • Simple field operation, automatic sourcing and sensing with depth measurement • Commercialized testing equipment from OYO company • Simple interpretation procedure (velocity = distance/travel time between two receivers) • Data processing S/W:Gelog-sus v.1.6 (C2, C4), Suspension for Win v.2.0 (C3), SU (C5)

Table 2.7: Non-intrusive methods and their description (Kim et al., 2013)

Surface wave methods	Key features in this study
SASW method (U2, U3)	• Phase velocities from phase differences between two receivers • Global property over receiver-spread area • Shear-wave velocity profile from the apparent phase velocities (superposed mode) • Dynamic stiffness matrix method • Comprehensive forward modeling (U2) or automatic inversion analysis (U3) • Impulsive source (U2, U3), swept-sine source, or random vibration source (U2) • Data interpretation S/W:WinSASW 1.2.3 (U2), WinSASW 2.3.2 (U3)
HWAW method (U2)	• One receiver-array with short spacing and source distance • Simple surface source like sledge hammer even for low frequency data acquisition • Time-frequency analysis using harmonic wavelet • Apparent phase velocity (U2) or normal modes • Shear-wave velocity profile from apparent phase velocity • Dynamic stiffness method • Comprehensive forward modeling • Data interpretation S/W:WinSASW 1.2.3
MASW method (C2, C3, C4, C5)	• Walk-away measurement with limited number of receivers (usually 12 or 24 receivers) • Impulsive source (C2, C3, C4, C5) or swept-sine source • Fundamental mode and higher modes • Global property over receiver-spread area • Shear-wave velocity profile from the fundamental mode (Transfer matrix method) • Automatic inversion analysis • Data interpretation S/W:SeisImager2D (C2, C4), Sufseis 1.5 (C3, C5)
ReMi method (C2)	• Passive surface wave method (measure the ground-borne vibration) • More than 24 receivers are used • Enough low frequency data without huge source • Phase velocity are determined from the slowness-frequency transform • Shear-wave velocity profile from the fundamental-mode phase velocities • Combined matrix method, comprehensive forward modeling • Data interpretation S/W:ReMi 2.0

* U1 = Kyeong-Hee University, U2 = KAIST, U3 = Joong-Ang University, C1 = HeeSong Geotek Co., Ltd, C2 = Subsurface Information Technologies, Inc., C3 = GEOMAX Co., Ltd, C4 = DIKE CO., Ltd, C5 = ASIA Geo-Consultants Co., Ltd.

For comparison of intrusive tests, similar trends V_s profile with depth of were observed for SPS logging and downhole tests. However, at deep depth SPS logging test yielded repeatable results than downhole test and at shallow depths downhole was more repeatable. Int terms of quality of signals traces, those of downhole test were better than those of SPS logging. On the other hand, Crosshole test provided V_s profile down to a depth of 11 m, however, the S/N ratio decreased with depth due to poor grouting work of casing. Inhole test provided V_s profile to a maximum depth range of 25 m - 34 m whereas Uphole test only provided V_s profile at shallow depth. V_s profile generated with SPT source was not good due to engine noise from drilling machine.

Furthermore, the V_s profile trends of Crosshole, Inhole and Uphole tests were also similar to those of SPS logging and downhole tests. However, SPS logging and downhole test were found to be more stable and economic to obtain V_s profile of a site compared to other field seismic tests.

With comparison of surface wave methods, ReMiures was able to produce V_s profile to over 30 m though it could not yield reliable V_s values at the shallow depth. SASW and

HWAW yielded V_s profiles to over 25 m. However, MASW produced small V_s values below the depth of 10 m as its dispersion curve had few low frequency information. Since SASW and HWAW use short testing lines, they were capable of getting reliable 2-D image of a site, and their contour plots were also able to better estimate line of bedrock and to show rapid change in stratigraphy than those of MASW.

2.12 Summary

This chapter provided a review of the information about three widely used active seismic surface wave tests being SASW, MASW, and CSW. The information covered the definition of these tests, the equipment (sources, receivers, and data logging devices), time sampling parameters, popular procedures used to set them up and to execute them. Different data processing techniques which include dispersion and inversion analysis were also included. Furthermore, the information covered possible factors that could affect the signal during the test's execution and in addition to this, signal quality enhancing practice was also included. Work done on comparison of seismic tests was also a part of this chapter.

Advantages, disadvantages and limitations discussed in this chapter were based on information reported by different authors and data acquired from different sites and in different regions. This makes it difficult to objectively compare these tests using only information available in the literature. Thus, this study is aimed at giving a fair, rigorous and unbiased comparison between these three tests. The tests will be conducted on the same sites using the same equipment and the same time sampling parameters. Sledge hammers, high and low frequency shakers will be used to generate signals and geophones and a seismograph will be used to capture and log the data.

Even though inversion was reviewed, it will only be performed for reflecting V_s profiles with depth and not for comparison purposes as it is associated with uncertainty and errors that might incorporate bias to the study. Dinver global search method in Geopsy computer program will be used to run inversion analysis.

3 METHODOLOGY

3.1 Introduction

This chapter presents methods used to acquire data for achieving the objectives of the study, this is comprised of the following:

- Site description
- Seismic equipment
- Experimental procedures
- Python codes procedures
- Inversion procedure

3.2 Shallow bedrock site description

SASW, MASW and CSW tests were conducted in the northern part of the University of Pretoria experimental farm about 120 m away from the Civil Engineering laboratory (Engineering 4.0). The site topography is generally flat with vegetation comprising mainly grass and scrub with thick stands of small to large trees. This is a shallow bedrock site with residual lava soils which have formed from the weathering of andesite lava bedrock at a depth of about 3.0 m. This was discovered during a site investigation that was conducted prior to construction of Engineering 4.0. At test pit TP7, the CAT 422E tractor-loader-backhoe encountered refusal on stiff to very stiff residual lava at a depth of 2.4 m. Test pit result for this site is shown in Table 3.1. The plan view of the test site can be seen in Figure 3.1 and the tests were performed along the red line in shown in the figure.

Figure 3.1: Google earth plan view of the Engineering 4.0 shallow bedrock site

Table 3.1: Engineering 4.0 test pit results

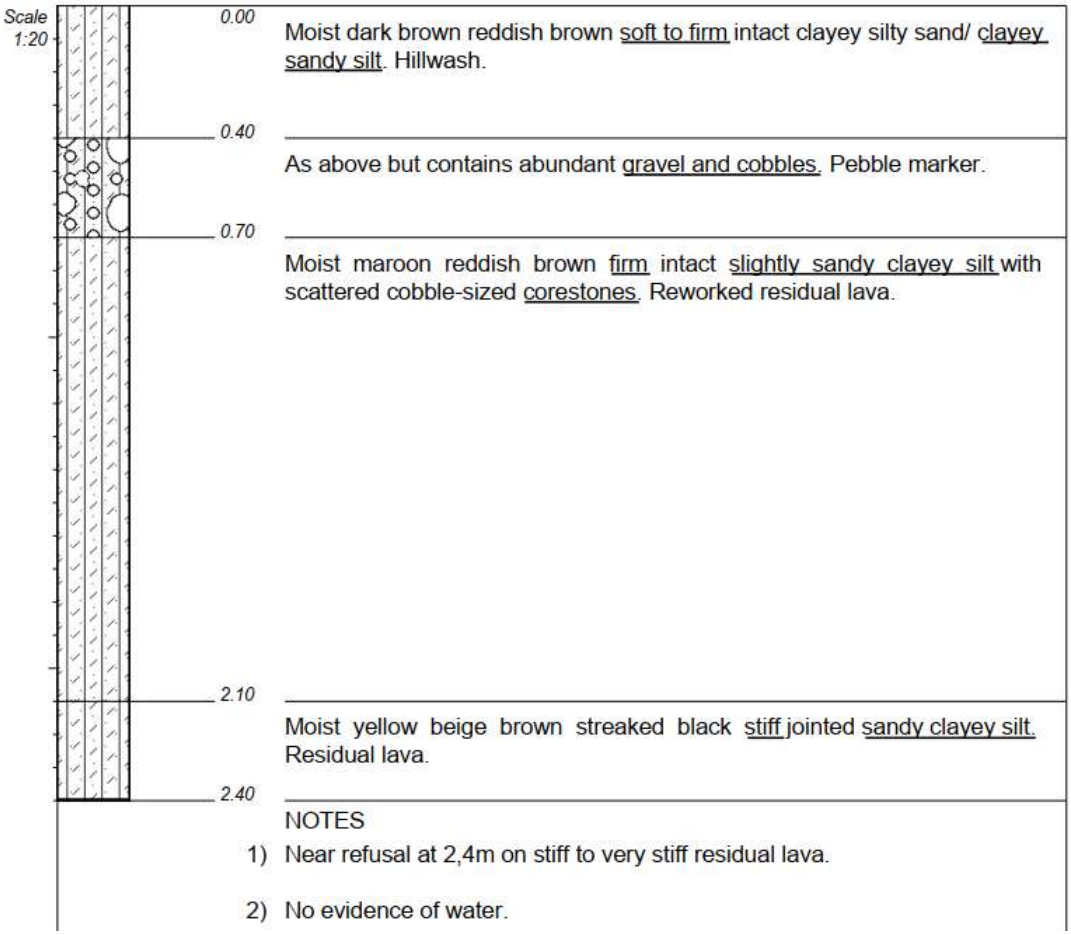

Seismic surface wave tests were performed along the side of the access road that was used during the construction of the Engineering 4.0 as can be seen in Figure 3.2. This place is considered as a quiet site as the only source of noise was the traffic from the N1 and N4 roads on the northern boundaries of the site. However, the traffic noise was negligible as the test site was about 230 m away from these two roadways. Figure 3.2 shows the yellow line which is where the tests were performed and the Global Positioning System (GPS) coordinates for this site were (25°44’36.57”S, 28°15’34.48”E).

Figure 3.2: View of the test site

3.3 Deep bedrock site description

The Wind Africa site is located on a farm near Vredefort in the Free State province of South Africa. This site is located in the vicinity of a bentonite mine which is not operating anymore near positions where piles were installed to study their behaviour in expansive clays. The topography of this site is flat with vegetation consisting of dense grass and short trees that are scattered around. This is a deep bedrock site with bedrock situated at a depth of about 12.0 m as can been seen in Table 3.2. Furthermore, this site is quiet as it is located in the middle of the farm where there are no heavy duty activities taking place. There is a gravel road with very little traffic about 200 m from the site. Figure 3.3 shows the Google earth image of the test site with the red line indicating the span of roughly 110 m over which the seismic tests were conducted and the GPS coordinates for this site were 27°15’15.95”S, 27°16’00.90”E. Figure 3.4 also shows the actual view of the site with its vegetation with the red line showing the location where the tests were performed.

Figure 3.3: Google earth plan view of Wind-Africa deep bedrock site

Figure 3.4: View of deep bedrock site

Table 3.2: Wind Africa test pit result

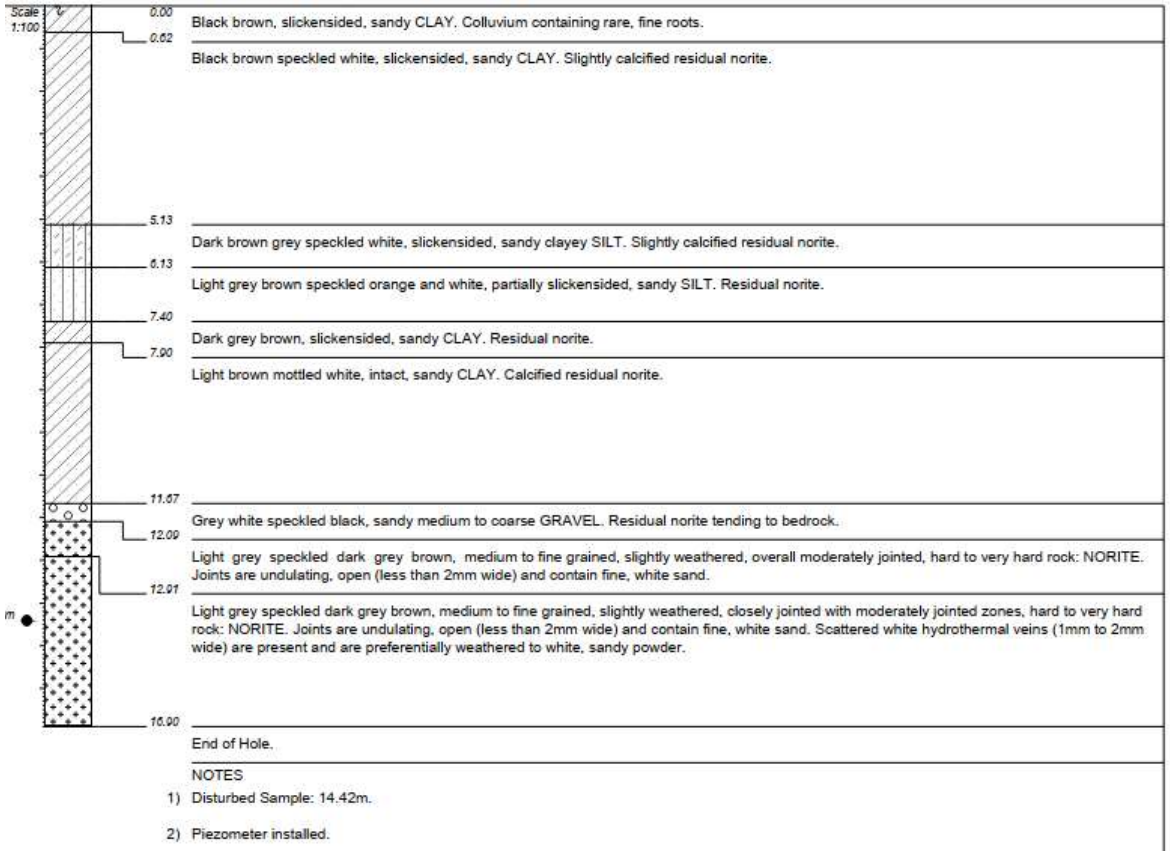

3.4 Seismic equipment

3.4.1 Sources

In this study, energy was produced by impacting a steel plate placed on the ground with sledge hammers for both SASW and MASW, whereas for CSW low and high frequency shakers for deep and shallow depths respectively were used to vibrate the ground. The sledge hammers used were 2.2 kg, 6.3 kg and 9.2 kg, and the plate was 185 mm in diameter and 30 mm thick as shown in Figure 3.5. The low frequency shaker had a total mass of 80 kg and generated a peak force of 6.3 kN at a frequency of 22 Hz whereas the high frequency shaker had a total mass of 70 kg and generated a peak force of 8.0 kN at the frequency of 90 Hz. These two shakers are shown in Figure 3.6.

Figure 3.5: Steel plate (top): Sledge hammers 2.2 kg (top) - 6.3 kg (middle) - 9.2 kg (bottom)

Figure 3.6: High frequency shaker (left) - Low frequency shaker (right)

3.4.2 Data acquisition devices

Seismic signals were acquired using 4.5 Hz resonant frequency geophones which were spiked rigidly into the ground. The signals detected by the geophones were transmitted to a PASI GEA 24 seismograph by means of a seismic cable. For CSW testing, a VAC-ON variable frequency drive (VFD) was used to adjust the frequency of the shaker. The signals of the propagating Raleigh waves were saved as files on the computer that was connected to the seismograph by a USB cable. Figure 3.7 shows the VFD, geophones and seismograph whereas Figure 3.8 shows the geophones connecting cable and trigger cable.

Figure 3.7: Variable frequency drive (left) - Seismograph (middle) - 4.5Hz Geophone (right)

Figure 3.8: Geophone connecting cable (left) - Trigger cable (right)

3.5 Experimental Procedures

3.5.1 Ambient noise measurements

This test was done with the two geophone configuration but without impacting the ground with any seismic source. The trigger was tapped so that the seismograph could log the background noise that was detected by the geophones.

3.5.2 SASW test execution

Common midpoint two receiver SASW tests were conducted for this study. The tests were done for six sets of receiver spacings which were 1 m, 2 m, 4 m, 8 m, 16 m and 32 m. For each receiver spacing, the ground was impacted three times on both sides of the centreline of the receivers using each of the 2.2 kg, 6.3 kg and 9.2 kg sledge hammers. The reason for the three shots was not for stacking but rather for assessment of the repeatability of the SASW test. Data was recorded for a period of 2 s with a logging frequency of 500 Hz. Figure 3.9 and Figure 3.10 show the SASW settings for a typical receiver spacings.

Figure 3.9: SASW test set at the shallow bedrock site

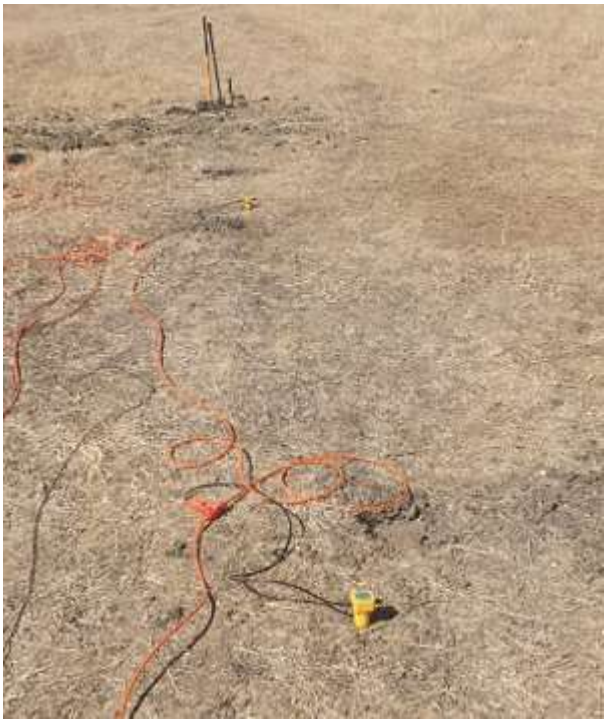

Figure 3.10: SASW test setup at the deep bedrock site

3.5.3 MASW test execution

Two sets of this test were conducted using a linear array of 24 geophones. The first test was done at a geophone spacing of 1 m whereas the second 2 m geophone spacing was used. This is because some researchers suggest a geophones spacing of 1 m and others a spacing of 2 m. Multiple source offsets for both sets of tests were used. This were as follows 1 m, 2 m, 4 m, 8 m and 16 m for 1 m geophone spacing. The source offsets for the 2 m geophone spacing were 2 m, 4 m, 8 m, 16 m and 32 m. Each of the 2.2 kg, 6.3 kg and 9.2 kg sledgehammers was used at each source offset impacting the steel plate three times. The variation of source offset was for investigation of near field effects. For both sets of tests, data was acquired for a time length of 2 s and 500 Hz logging frequency. Figure 3.11 and Figure 3.12 show typical MASW test configurations on the shallow and deep bedrock sites respectively.

Figure 3.11: Typical MASW test setup at the shallow bedrock site.

Figure 3.12: MASW set up at the deep bedrock site

3.5.4 CSW test execution

Monotonic and sweep CSW tests were done using an array of five geophones spaced at 1 m. Low and High frequency shakers were used to provide ground vibrations in the frequency ranges of 10 - 22 Hz and 22.5 - 90 Hz, respectively. The tests were done at three different source offset which were 1 m, 2 m and 4 m for the investigation of near field effects. Table 3.3 and Table 3.4 show the time sampling parameters for different shaker operation frequencies.

Table 3.3: Frequency increments for different frequency ranges

Frequency range (Hz)	Frequency increments (Hz)
10 - 20	0.5
20 - 45	1.5
45 - 70	2
70 - 90	3

Table 3.4: CSW acquisition time and logging frequency for different frequency ranges

Frequency range (Hz)	Logging frequency (Hz)	Acquisition time (s)
< 22	500	10
22 - 50	1000	5
50 - 90	2000	3

Figure 3.13: CSW test setup with high frequency shaker at the shallow bedrock site

Figure 3.14 CSW test setup with low frequency shaker at the deep bedrock site

Figure 3.15: CSW setup at the deep bedrock site

3.6 Python codes procedure

Sections 3.6.1 and 3.6.2 below give step by step procedures for the python codes that were used to analyse SASW and CSW data respectively. The codes were developed based on the analysis procedures described in Sections 2.9.1 and 2.9.2.

3.6.1 SASW python code procedure

Described below is the step by step procedure for how the developed was used to analyse SASW data. The actual code can be referred to in Appendix C. The functions mentioned in this procedure were not python built in functions but rather the function that were programmed to perform different tasks of the analysis.

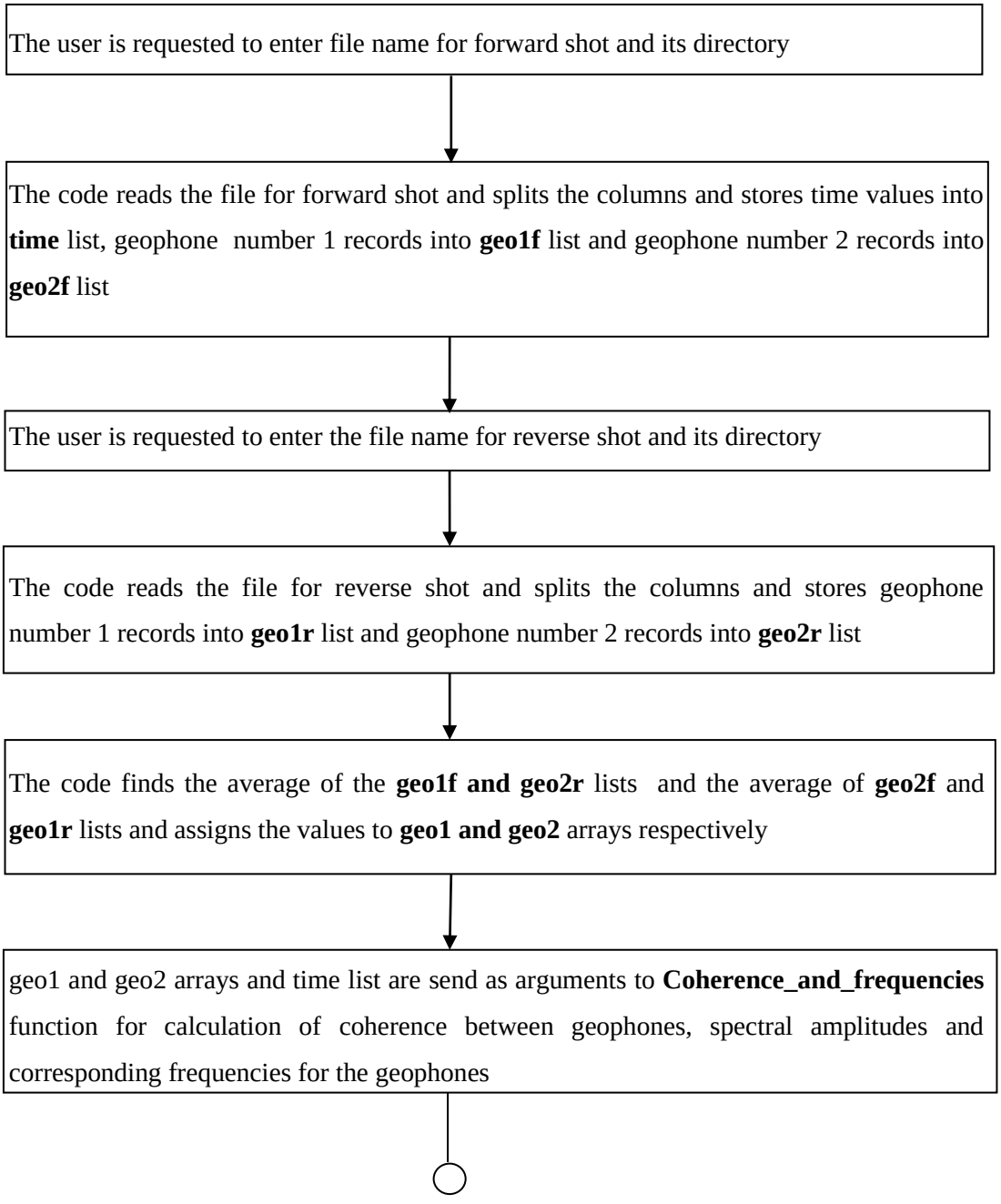

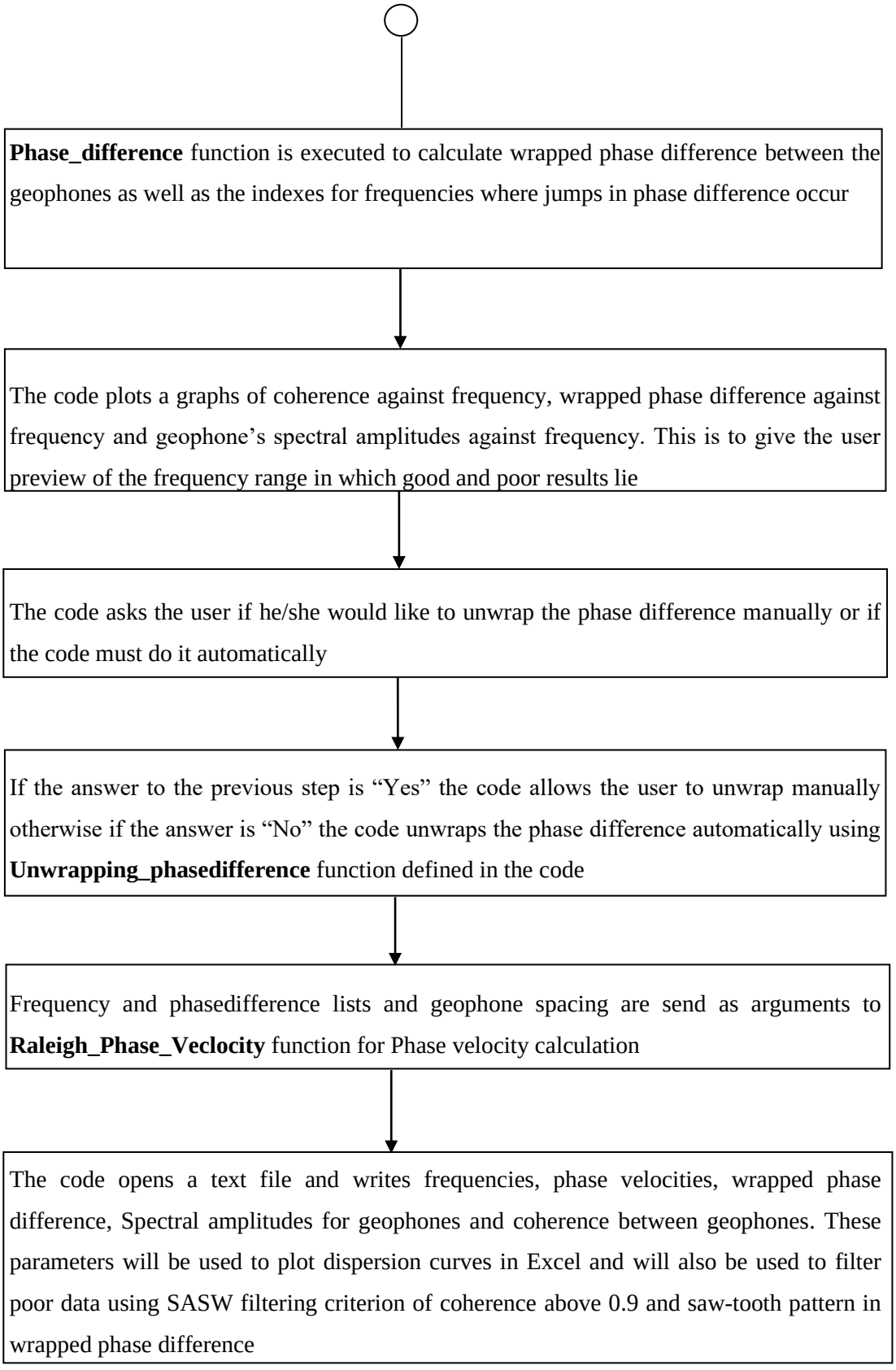
Phase_difference function is executed to calculate wrapped phase difference between the geophones as well as the indexes for frequencies where jumps in phase difference occur
The code plots a graphs of coherence against frequency, wrapped phase difference against frequency and geophone's spectral amplitudes against frequency. This is to give the user preview of the frequency range in which good and poor results lie
The code asks the user if he/she would like to unwrap the phase difference manually or if the code must do it automatically
If the answer to the previous step is "Yes" the code allows the user to unwrap manually otherwise if the answer is "No" the code unwraps the phase difference automatically using **Unwrapping_phasedifference** function defined in the code
Frequency and phasedifference lists and geophone spacing are send as arguments to **Raleigh_Phase_Veclocity** function for Phase velocity calculation
The code opens a text file and writes frequencies, phase velocities, wrapped phase difference, Spectral amplitudes for geophones and coherence between geophones. These parameters will be used to plot dispersion curves in Excel and will also be used to filter poor data using SASW filtering criterion of coherence above 0.9 and saw-tooth pattern in wrapped phase difference

3.6.2 CSW python code procedure

Described below is the step by step procedure for how the developed was used to analyse CSW data. The actual code can be referred to in Appendix D. In the same way as for SASW python code, the functions mentioned here are not python built in functions.

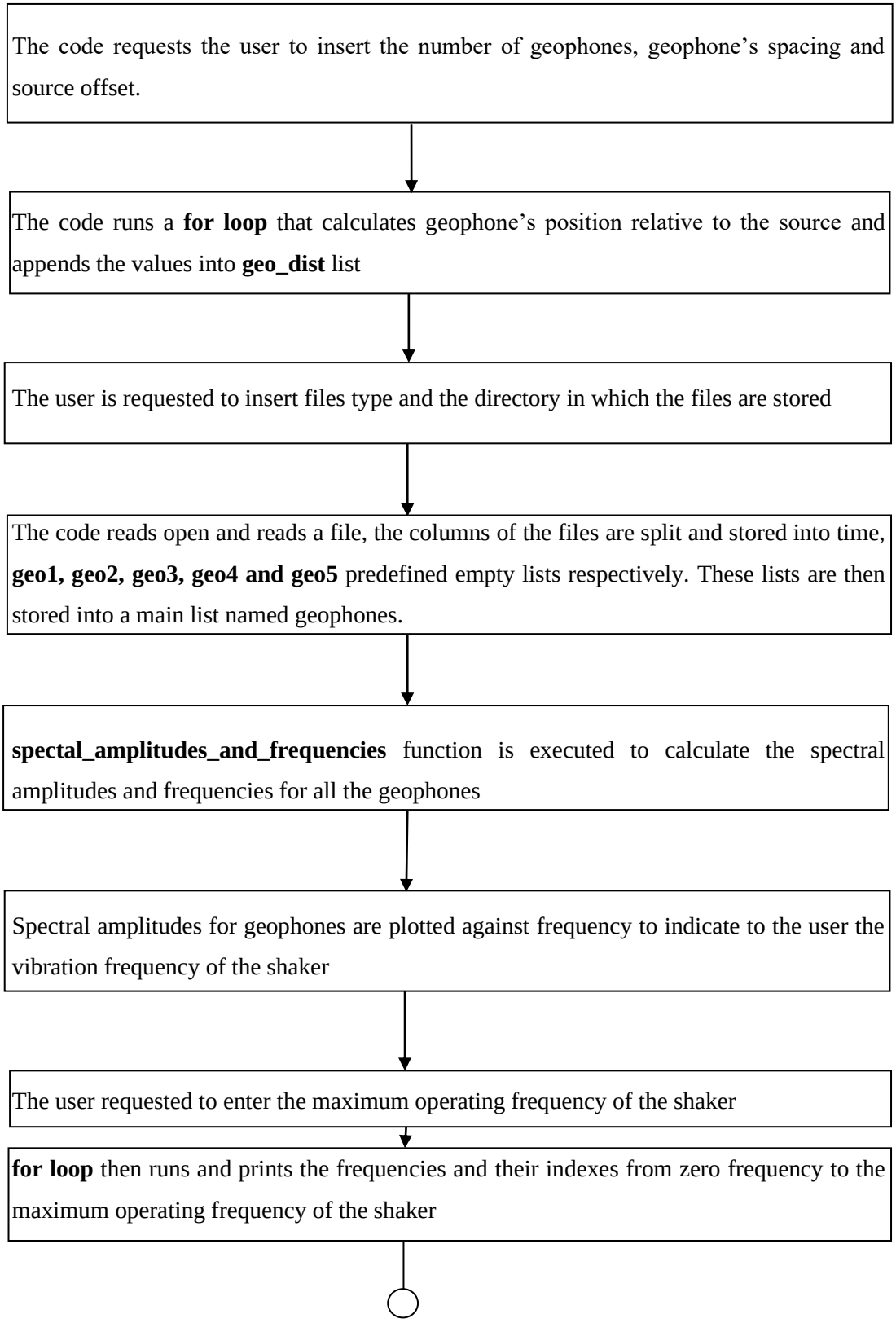

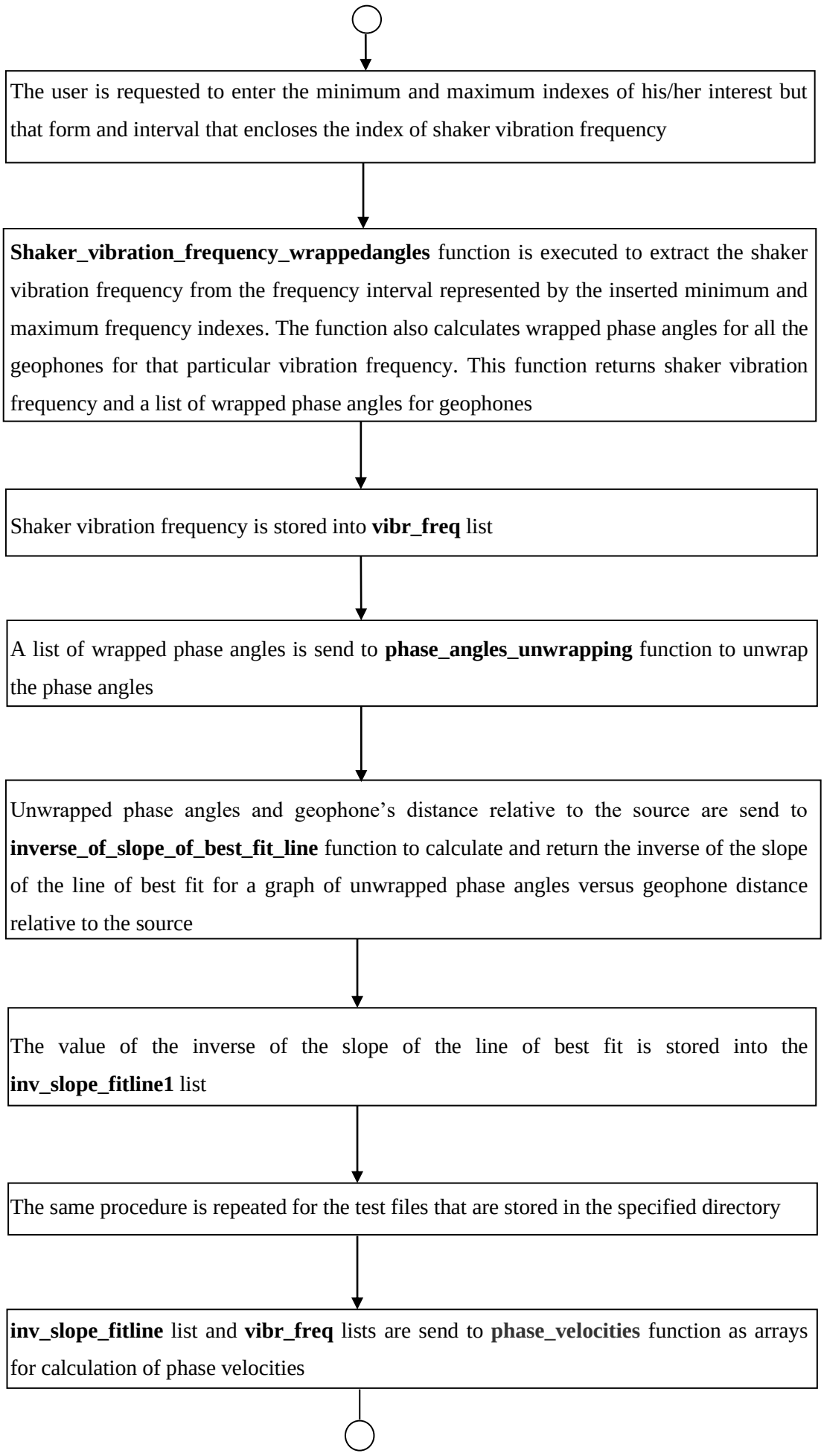
The user is requested to enter the minimum and maximum indexes of his/her interest but that form and interval that encloses the index of shaker vibration frequency
Shaker_vibration_frequency_wrappedangles function is executed to extract the shaker vibration frequency from the frequency interval represented by the inserted minimum and maximum frequency indexes. The function also calculates wrapped phase angles for all the geophones for that particular vibration frequency. This function returns shaker vibration frequency and a list of wrapped phase angles for geophones
Shaker vibration frequency is stored into **vibr_freq** list
A list of wrapped phase angles is send to **phase_angles_unwrapping** function to unwrap the phase angles
Unwrapped phase angles and geophone's distance relative to the source are send to **inverse_of_slope_of_best_fit_line** function to calculate and return the inverse of the slope of the line of best fit for a graph of unwrapped phase angles versus geophone distance relative to the source
The value of the inverse of the slope of the line of best fit is stored into the **inv_slope_fitline1** list
The same procedure is repeated for the test files that are stored in the specified directory
inv_slope_fitline list and **vibr_freq** lists are send to **phase_velocities** function as arrays for calculation of phase velocities

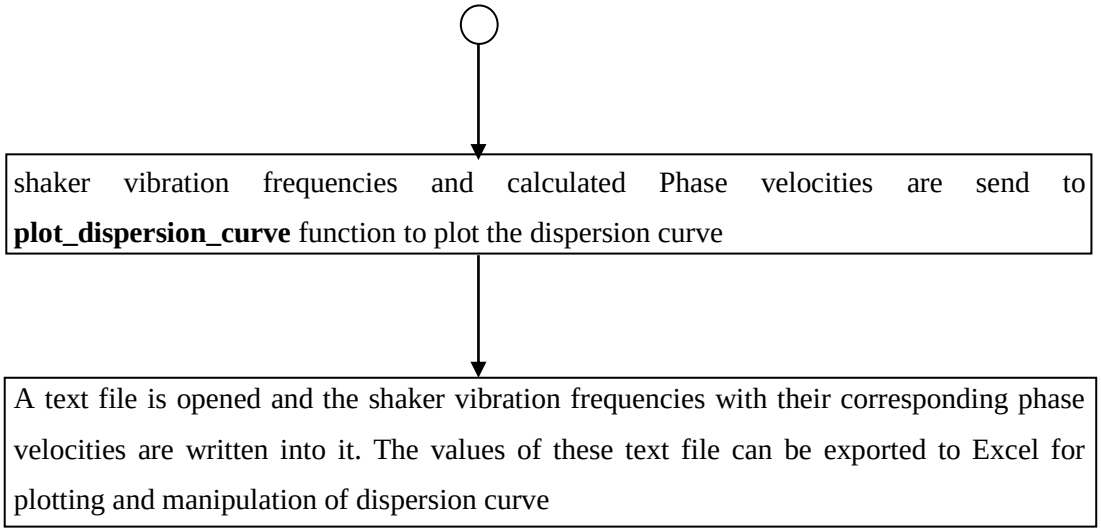
shaker vibration frequencies and calculated Phase velocities are send to **plot_dispersion_curve** function to plot the dispersion curve
A text file is opened and the shaker vibration frequencies with their corresponding phase velocities are written into it. The values of these text file can be exported to Excel for plotting and manipulation of dispersion curve

3.7 Inversion procedure

Inversion processes for SASW, MASW and CSW were carried out using Geopsy add-in called Dinver. Wavelet (2004) stated that in the inversion process the number of layers must range from five to ten. In this study the models were thus design to satisfy this criterion. In all the models, ν and ρ were fixed whereas layer thickness and V_s were allowed to vary. The fixed value of 0.35 was used for ν as Dal Moro (2007) suggested this value for soils of V_s lower than 1500 m/s. ρ value of 1800 kg/m^3 for stiff cohesive soils was used for stiff silts of the shallow bedrock site whereas a value of 1600 kg/m^3 for soft cohesive soils was used for soft clays of the deep bedrock site. These values of ρ these are stated by Look (2007). V_p was calculated using Equation 3.1. The inversion models that were used are represented in the tables below.

$$V_p = V_s\sqrt{\frac{1-\nu}{0.5-\nu}} \qquad 3.1$$

Table 3.5: SASW inversion model for shallow bedrock site

Layer No.	Thickness (m)	V_s range (m/s)	Density (kg/m^3)	Poisson ratio
1	1.5	100-375	1800	0.35
2	1.5	100-375	1800	0.35
3	2.5	100-375	1800	0.35
4	3.0	150-700	1800	0.35
5	3.0	150-700	1800	0.35
6	3.5	200-3000	1800	0.35
7	3.5	200-3000	1800	0.35
8	3.5	200-3000	1800	0.35
9	3.5	200-3000	1800	0.35
Half space	-	200-3000	1800	0.35

Table 3.6: MASW inversion model for shallow bedrock site

Layer No.	Thickness (m)	V_s range (m/s)	Density (kg/m^3)	Poisson ratio
1	2.5	100-375	1800	0.35
2	2.5	100-375	1800	0.35
3	2.5	150-700	1800	0.35
4	2.5	150-700	1800	0.35
5	3.0	150-700	1800	0.35
6	3.0	200-3000	1800	0.35
7	3.0	200-3000	1800	0.35
8	3.0	200-3000	1800	0.35
Half space	-	200-3000	1800	0.35

Table 3.7: CSW inversion model for shallow bedrock site

Layer No.	Thickness (m)	V_s range (m/s)	Density (kg/m^3)	Poisson ratio
1	1.0	100-375	1800	0.35
2	1.0	100-375	1800	0.35
3	1.0	100-375	1800	0.35
4	1.0	100-375	1800	0.35
5	2.0	150-700	1800	0.35
6	2.0	150-700	1800	0.35
7	2.0	150-700	1800	0.35
8	2.0	150-700	1800	0.35
Half space	-	150-700	1800	0.35

Table 3.8: SASW inversion model for deep bedrock site

Layer No.	Thickness (m)	V_s range (m/s)	Density (kg/m^3)	Poisson ratio
1	1.5	100-200	1600	0.35
2	1.5	100-300	1600	0.35
3	2.5	150-400	1600	0.35
4	3.0	150-400	1600	0.35
5	3.0	150-400	1600	0.35
6	3.5	200-3500	1600	0.35
7	3.5	200-3500	1600	0.35
8	3.5	200-3500	1600	0.35
Half space	-	200-3500	1600	0.35

Table 3.9: MASW inversion model for deep bedrock site

Layer No.	Thickness(m)	V_s range (m/s)	Density (kg/m^3)	Poisson ratio
1	1.5	100-200	1600	0.35
2	1.5	100-300	1600	0.35
3	2.0	150-400	1600	0.35
4	2.0	150-400	1600	0.35
5	2.0	150-400	1600	0.35
6	3.0	150-400	1600	0.35
7	3.0	200-3500	1600	0.35
8	3.0	200-3500	1600	0.35
9	3.0	200-3500	1600	0.35
Half space	-	200-3500	1600	0.35

Table 3.10: CSW inversion model for deep bedrock site

Layer No.	Thickness (m)	V_s range (m/s)	Density (kg/m^3)	Poisson ratio
1	1.0	100-200	1600	0.35
2	1.0	100-300	1600	0.35
3	1.0	150-300	1600	0.35
4	1.0	150-400	1600	0.35
5	1.5	150-400	1600	0.35
6	1.5	150-400	1600	0.35
7	2.0	150-400	1600	0.35
8	2.0	150-400	1600	0.35
Half space	-	150-400	1600	0.35

3.8 Summary

The equipment and methods used to conduct all the tests for this study were described in this chapter, this included site description, seismic sources and data acquisition devices, ambient noise measurements, SASW, MASW, and CSW test procedures. Also, the step by step procedures for python codes developed for SASW and CSW data analysis were explained and lastly the models for the inversion analysis were presented. The next chapter includes the analysis and discussion of the acquired data.

4 DATA ANALYSIS AND DISCUSSION

4.1 INTRODUCTION

The aim of this chapter is to analyse and discuss the test results so that the conclusions to the objectives of the study can be drawn. The structure of this chapter is as outlined below.

- Analysis of background noise for shallow and deep bedrock sites
- Unbiased comparison of SASW, MASW and CSW in terms of near field effects, repeatability and sampling depth at the shallow bedrock site.
- Shear wave profiles for shallow bedrock site produced with SASW, MASW and CSW.
- Unbiased comparison of SASW, MASW and CSW in terms of near field effects, repeatability and sampling depth at the deep bedrock site.
- Shear wave profiles for deep bedrock site produced with SASW, MASW and CSW.

SASW and CSW data were analysed using Python codes presented in Appendix C and D respectively whereas MASW was analysed using Geopsy software. The results will all be presented in the form of dispersion curves which is the relationship between Raleigh phase velocity (v_r) response of a soil profile and frequency (f) or wavelength (λ).

For CSW and MASW, the following nomenclature is used throughout the dissertation.

CSW1m - CSW performed with the source at 1 m offset

CSW2m - CSW performed with the source at 2 m offset

CSW4m - CSW performed with the source at 4 m offset

MASW1m - MASW performed with 1 m geophones spacing

MASW2m - MASW performed with 2 m geophones spacing

MASW(geophone spacing)(source offset)(sledgehammer size) - MASW test performed at particular geophone spacing and source offset and specific sledgehammer size e.g MASW1m2m2.2kg for MASW performed at 1 m geophones spacing, 2 m source offset and 2.2 kg sledgehammer.

4.2 Background noise analysis

In this study, background tests were performed to investigate whether the ambient noise levels would warrant the stacking of the test records. Thus, as it was mentioned in Chapter 3, both test sites were located on farms where the only possible source of noise could be wind since these sites were experiencing virtually no traffic and there were also no heavy machinery running on these sites. Thus Figure 4.1 and Figure 4.7 show the background noise detected on the shallow and deep bedrock sites respectively. Since the sledgehammers were used for offsets of 1 m to 32 m and shakers for offsets of 1 m to 4 m, it was necessary to compare the signal strength of these sources relative to the noise strengths at multiple offsets in order to check if the noise was a major concern.

Figure 4.2 to Figure 4.6 show plots of the background noise and the signal strength of the sources at multiple source offsets at the shallow bedrock site. It is clear in these figures that the signal strength of the source decreases with increased offset. However, the noise plots as almost zero relative to source's signals for all the offsets. The same behaviour at the deep bedrock site can be seen from Figure 4.8 to Figure 4.12. This therefore justifies that these two sites were quiet, hence the acquired data was less contaminated, hence the stacking of records was also not necessary.

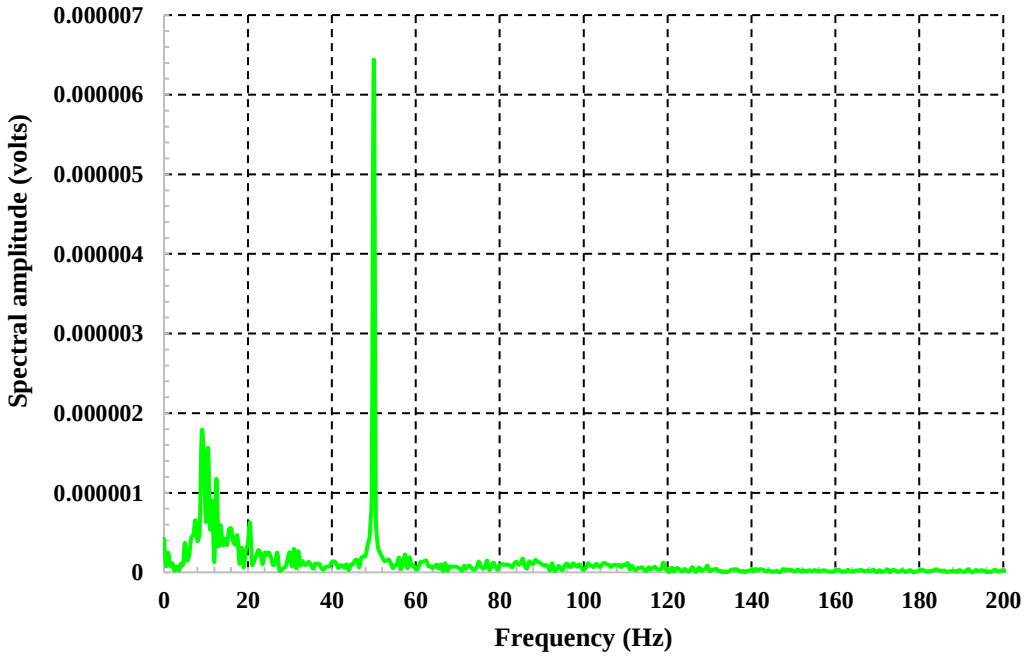

Figure 4.1: Background noise at shallow bedrock site

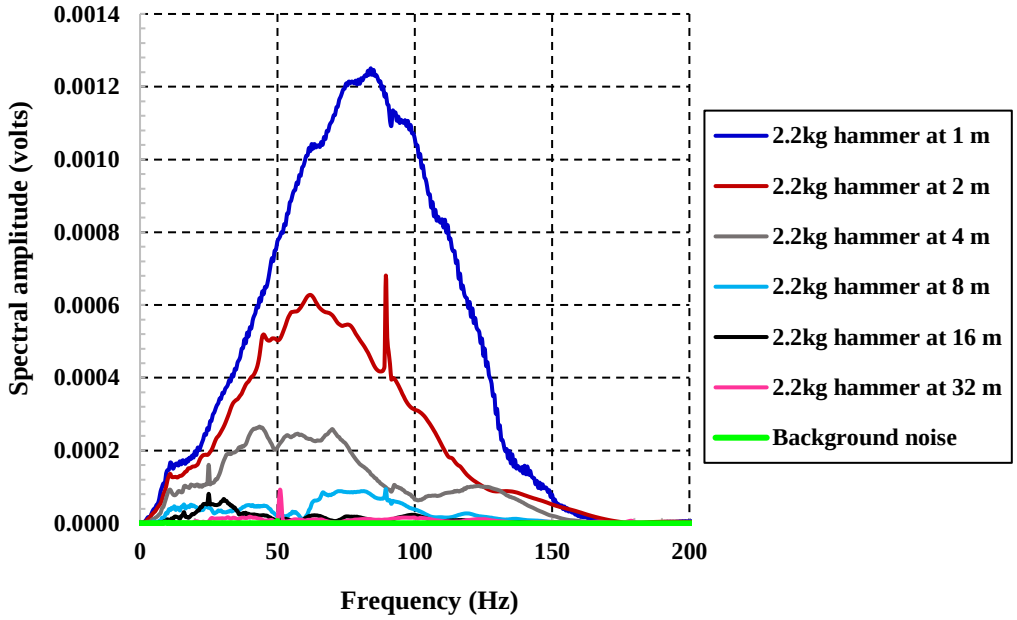

Figure 4.2: Noise strength relative to 2.2 kg hammer's signal strength at multiple offsets at the shallow bedrock site

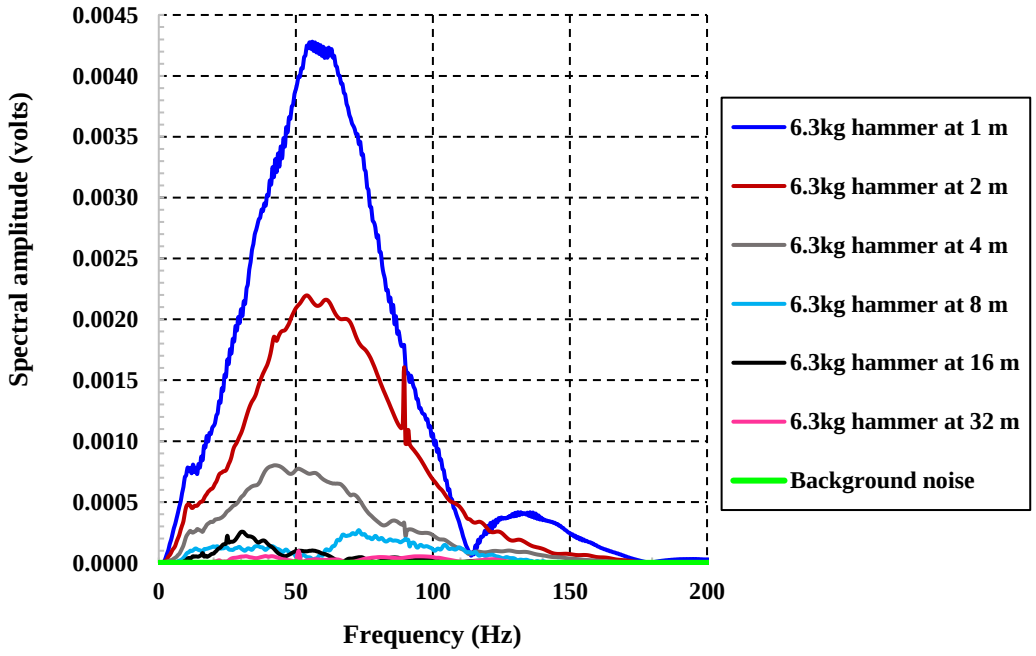

Figure 4.3: Noise strength relative to 6.3 kg hammer's signal strength at multiple offsets at the shallow bedrock site

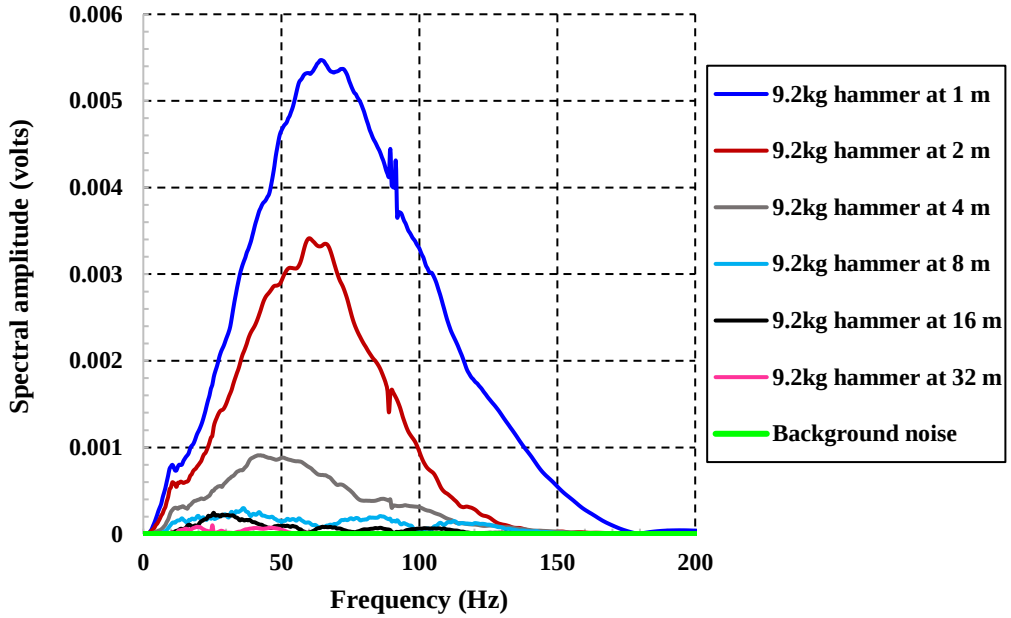

Figure 4.4: Noise strength relative to 9.2 kg hammer's signal strength at multiple offsets at the shallow bedrock site

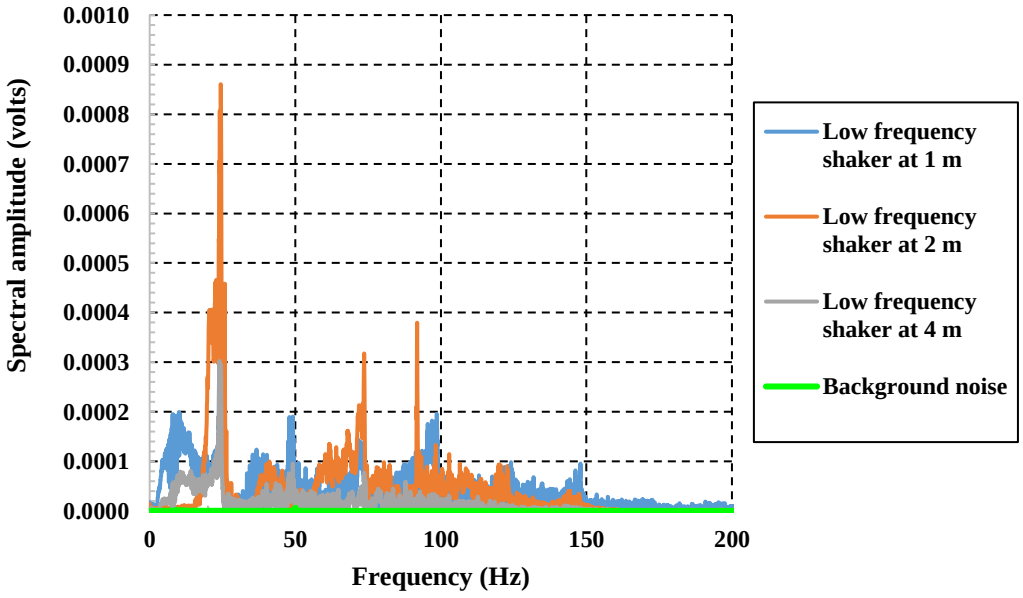

Figure 4.5: Noise strength relative to Low frequency shaker's signal strength at multiple offsets at the shallow bedrock site

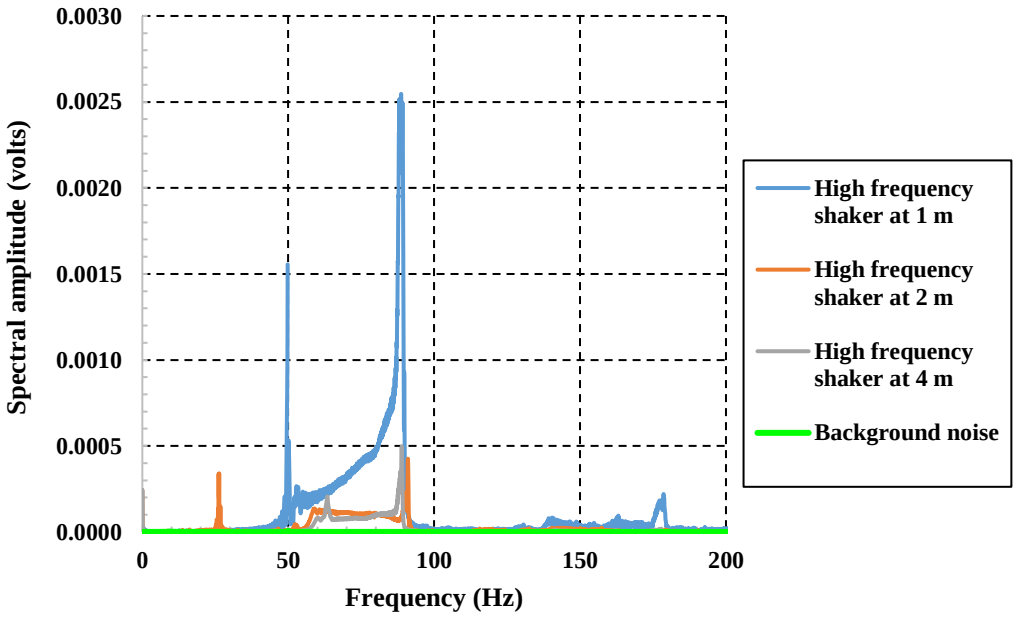

Figure 4.6: Noise strength relative to High frequency shaker's signal strength at multiple offsets at the shallow bedrock site

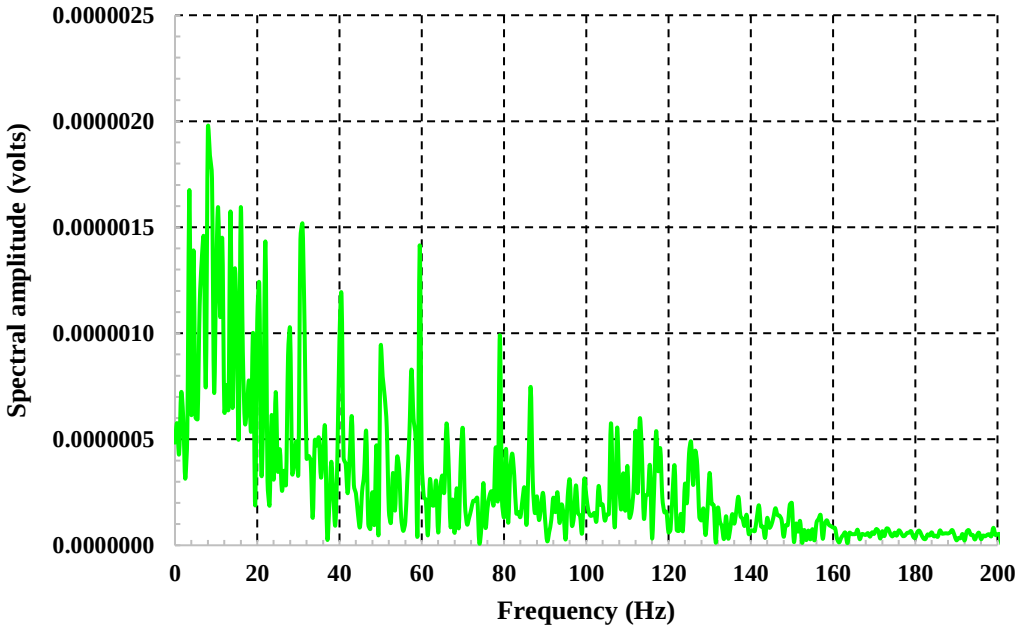

Figure 4.7: Background noise at deep bedrock site

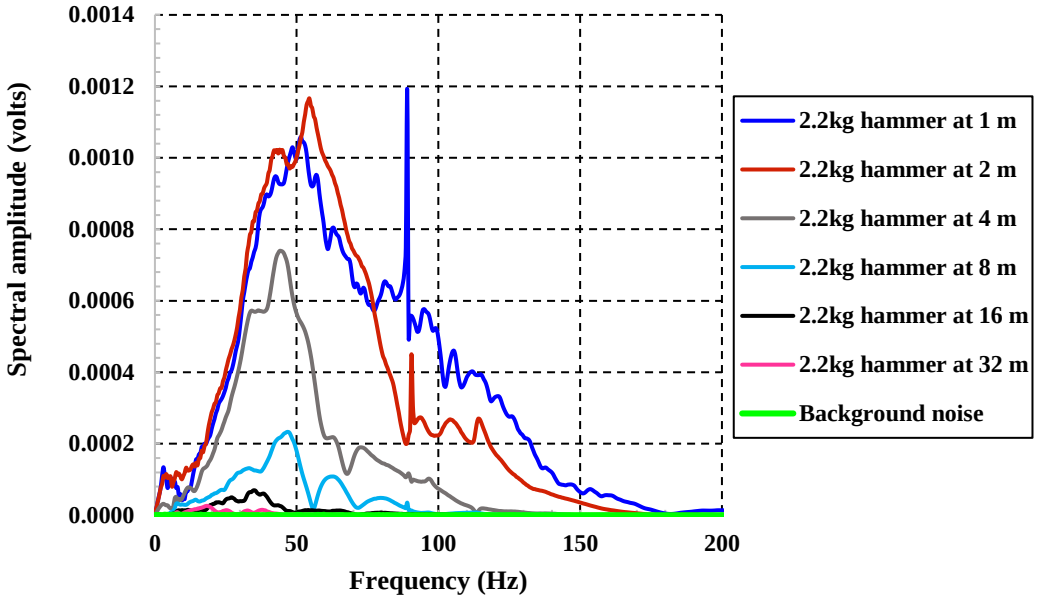

Figure 4.8: Noise strength relative to 2.2 kg hammer's signal strength at multiple offsets at the deep bedrock site

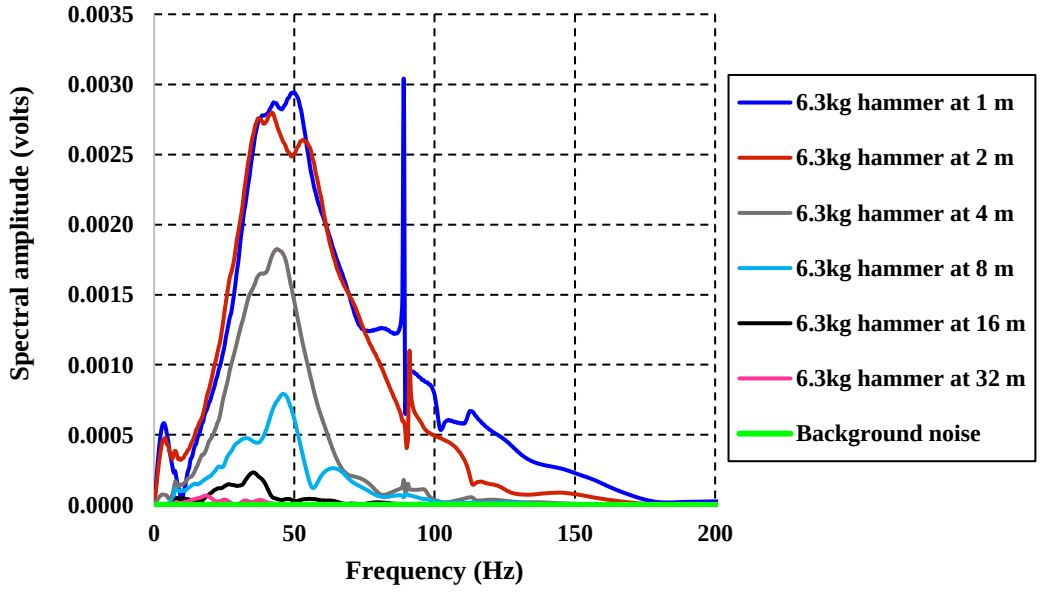

Figure 4.9: Noise strength relative to 6.3 kg hammer's signal strength at multiple offsets at the deep bedrock site

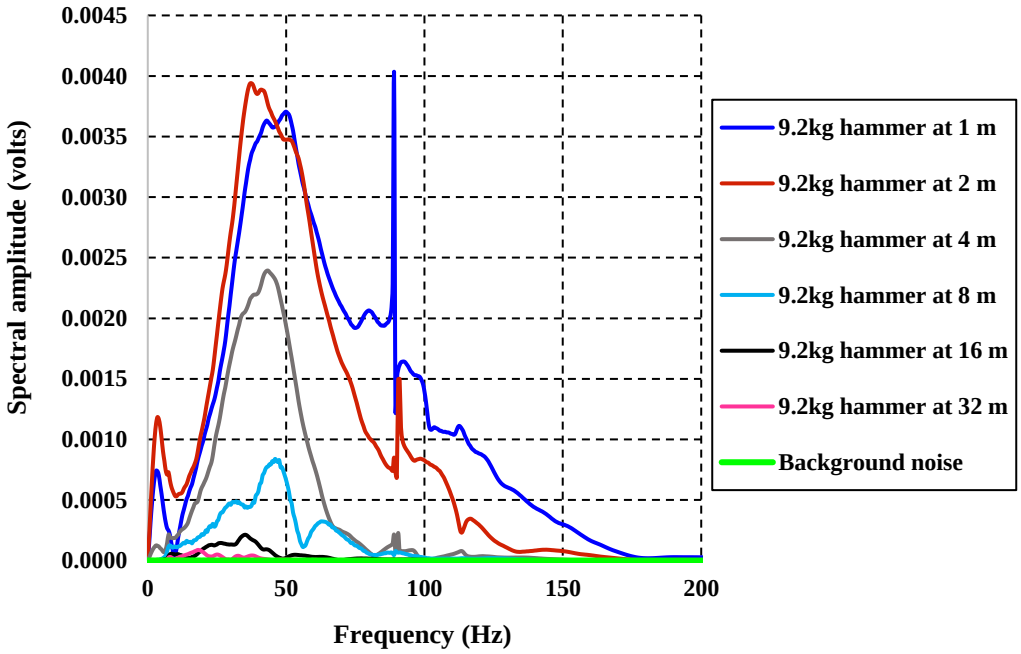

Figure 4.10: Noise strength relative to 9.2 kg hammer's signal strength at multiple offsets at the deep bedrock site

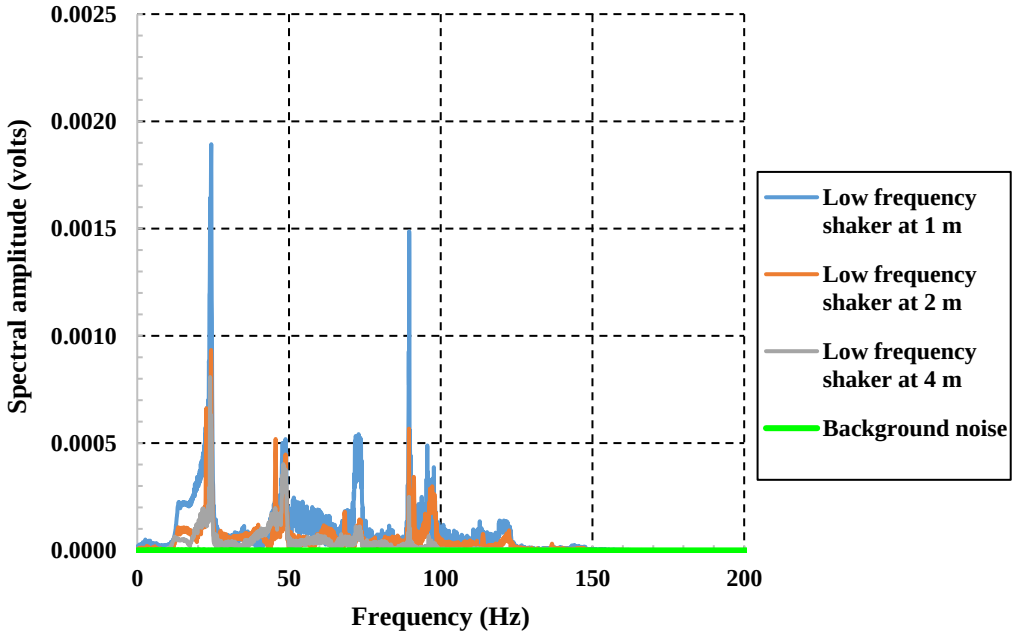

Figure 4.11: Noise strength relative to Low frequency shaker's signal strength at multiple offsets at the deep bedrock site

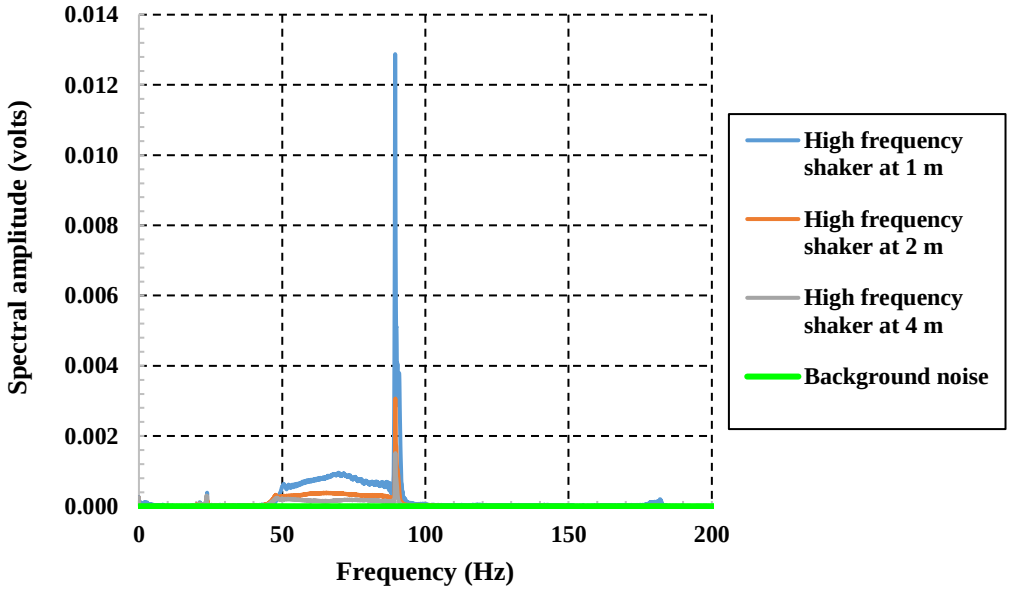

Figure 4.12: Noise strength relative to High frequency shaker's signal strength at multiple offsets at the deep bedrock site

4.3 Shallow bedrock data analysis

4.3.1 Repeatability comparison

This section focuses on the repeatability of the three tests SASW, MASW and CSW. It is worth noting that MASW dispersion curves presented in this chapter were extracted from overtone images using Geopsy's algorithm of automatic curve extraction. The purpose of this is to be as unbiased as possible and typical examples of overtone images and extracted curves for 2.2 kg, 6.3 kg and 9.2 kg sledgehammers are shown in Figure 4.13, Figure 4.14 and Figure 4.15.

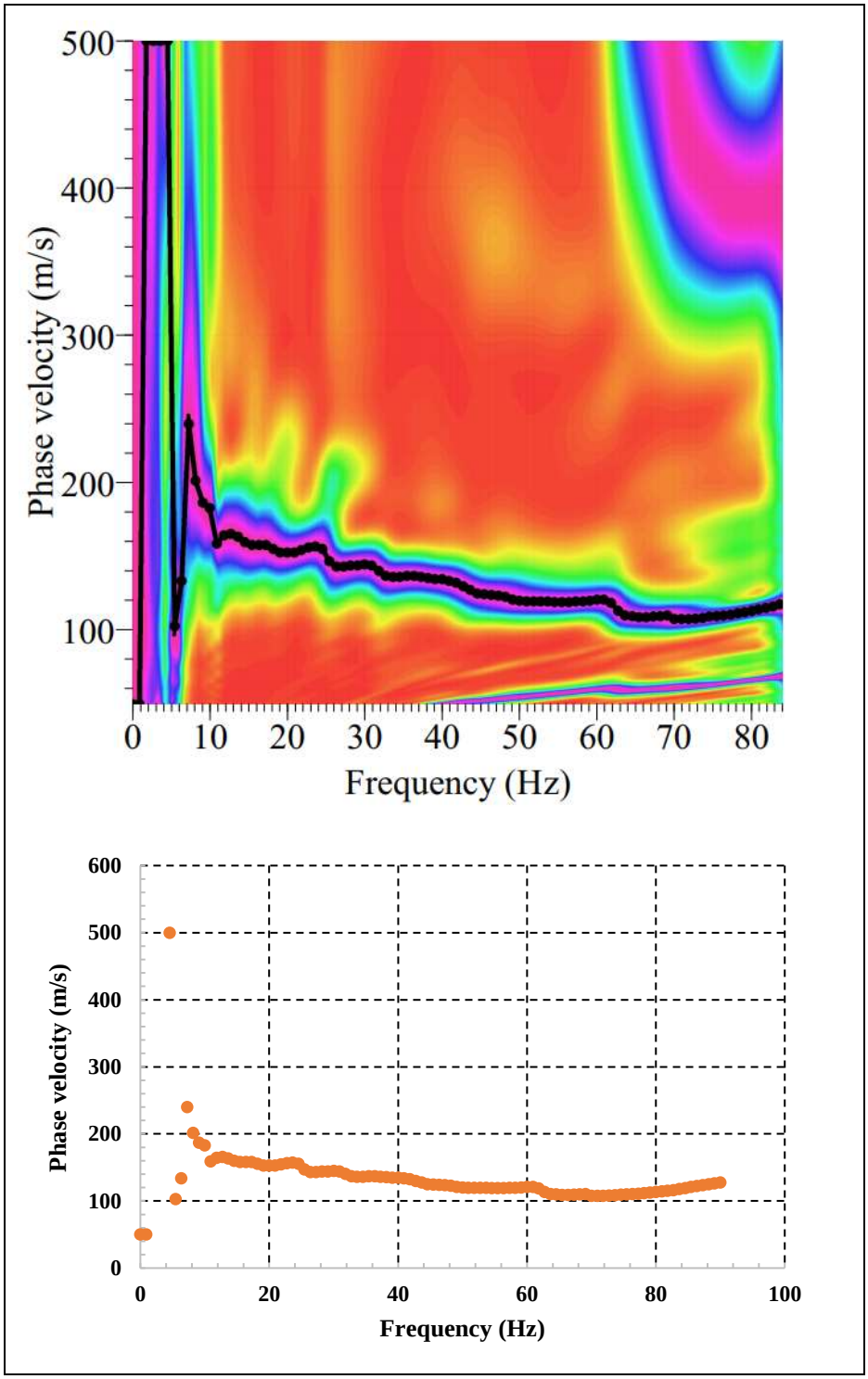

Figure 4.13: Typical Geopsy overtone image obtained with 2.2 kg sledgehammer (top) and the extracted dispersion curve (bottom)

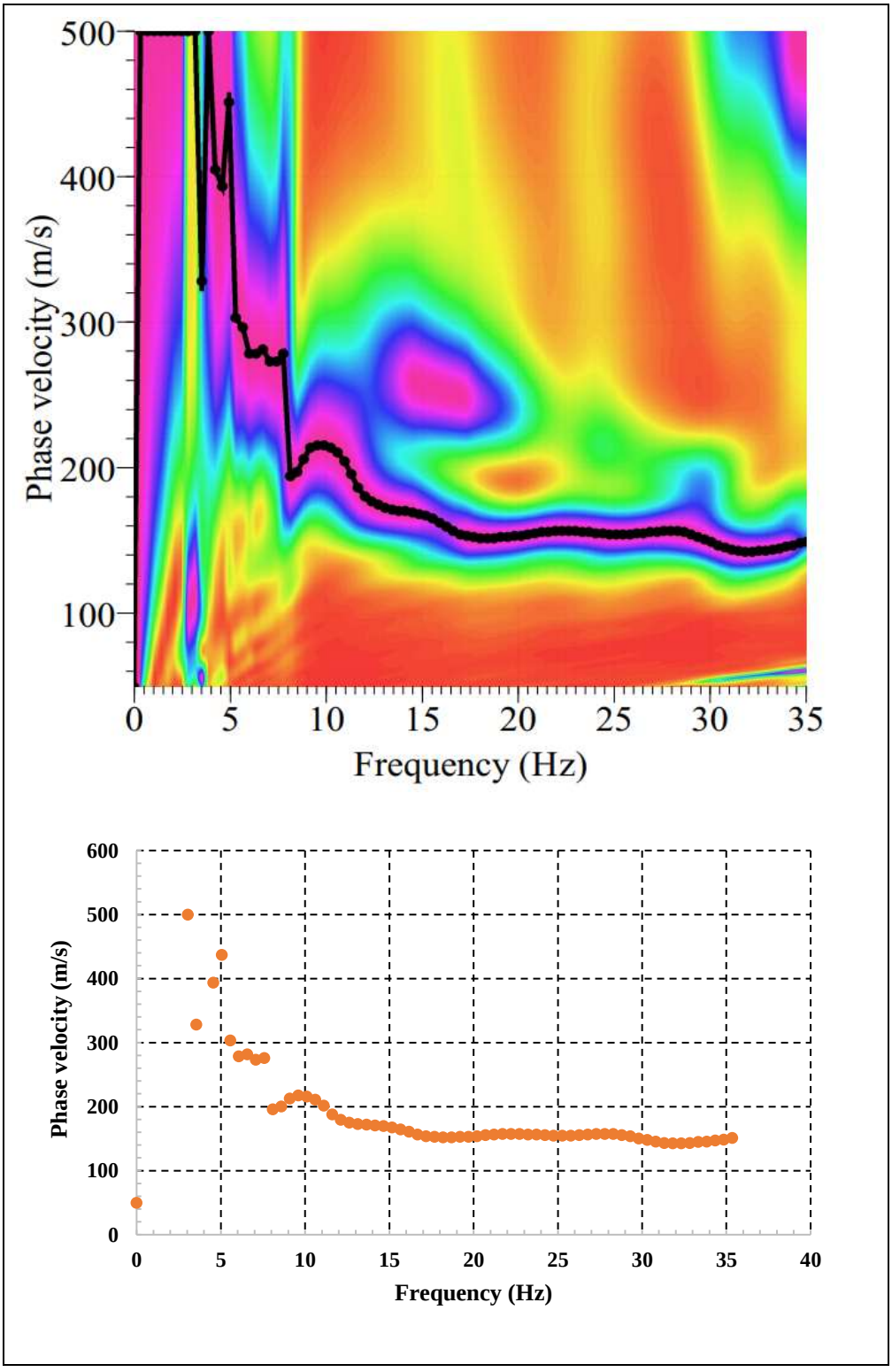

Figure 4.14: Typical Geopsy overtone image obtained with 6.3 kg sledgehammer (top) and the extracted dispersion curve (bottom)

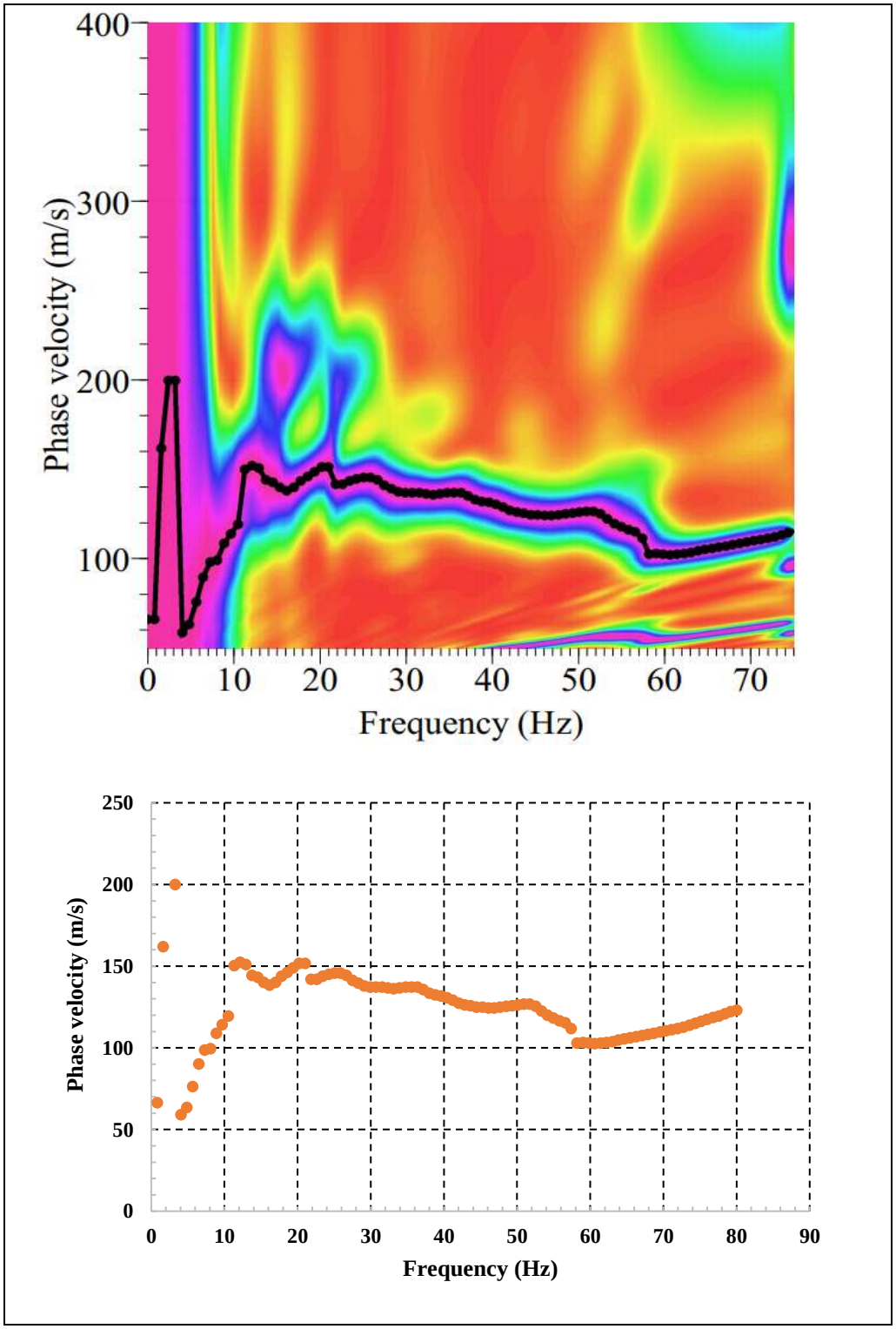

Figure 4.15: Typical Geopsy overtone image obtained with 9.2 kg sledgehammer (top) and the extracted dispersion curve (bottom)

In Figure 4.16, Figure 4.17 and Figure 4.18 are the repeatability dispersion curves for CSW and those of SASW and MASW obtained with 2.2 kg, 6.3 kg and 9.2 kg sledgehammers respectively. In these three figures, similar trends can be seen. Firstly, it is clear that for SASW, the curves loose repeatability for frequencies above 80 Hz where the dispersion curves start to offset from each other. However, the repeatability is good for frequencies below 80 Hz down to about 7- 8 Hz below which the dispersion curves follow similar trends but with scatter. The lack of repeatability in the high frequency range can be attributed to the limit of production of short waves for the sledge hammers used and hence data in the high frequency range can be considered unreliable as most of it did not satisfy the SASW filtering criteria of a saw tooth pattern and coherence value greater 0.9.

For MASW1m and MASW2m, the dispersion curves show good repeatability from the high frequency end of the fundamental mode down to the frequency of 10 Hz below which the scattering of the data points is apparent hence loss of repeatability. The scatter in the dispersion curves for MASW and SASW for frequencies below 10 Hz can be attributed to the fact that sledge hammers are limited to frequencies above 10 - 8 Hz as was stated by Foti et al. (2018).

CSW dispersion curves show fundamental mode with some higher modes. Though some of the data points are scattered, good repeatability is observed throughout the entire frequency band over which the shakers operated. This can be seen on both the fundamental mode as well as on higher modes. The good repeatability of CSW can be attributed to the fact that the source (shaker) generates a near sinusoidal wave at a single frequency, unlike in the SASW and MASW tests where the energy generated by the sledgehammer could vary from test to test.

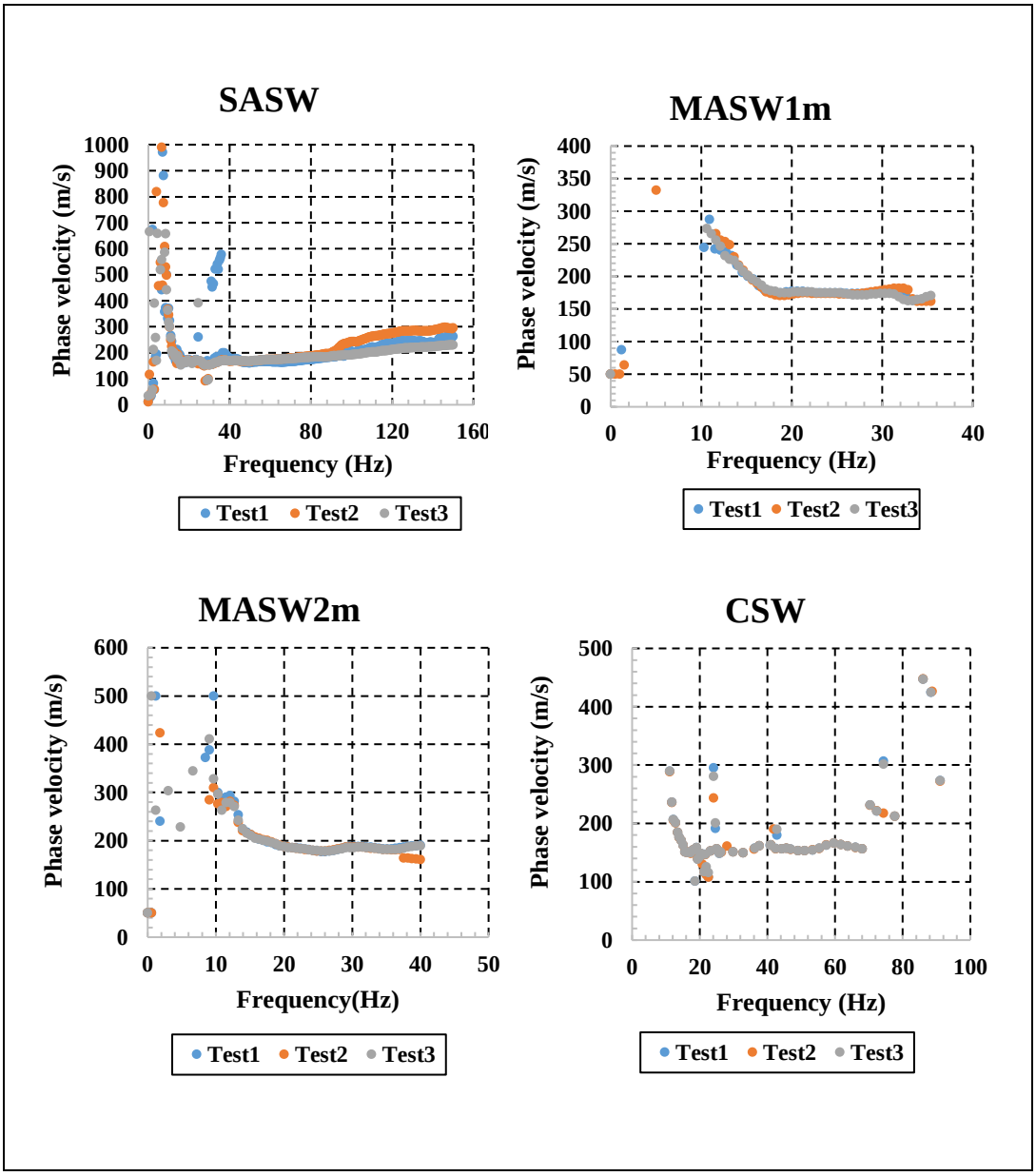

Figure 4.16: Repeatability dispersion curves for SASW and MASW performed with 2.2 kg sledgehammer and CSW at the shallow bedrock site

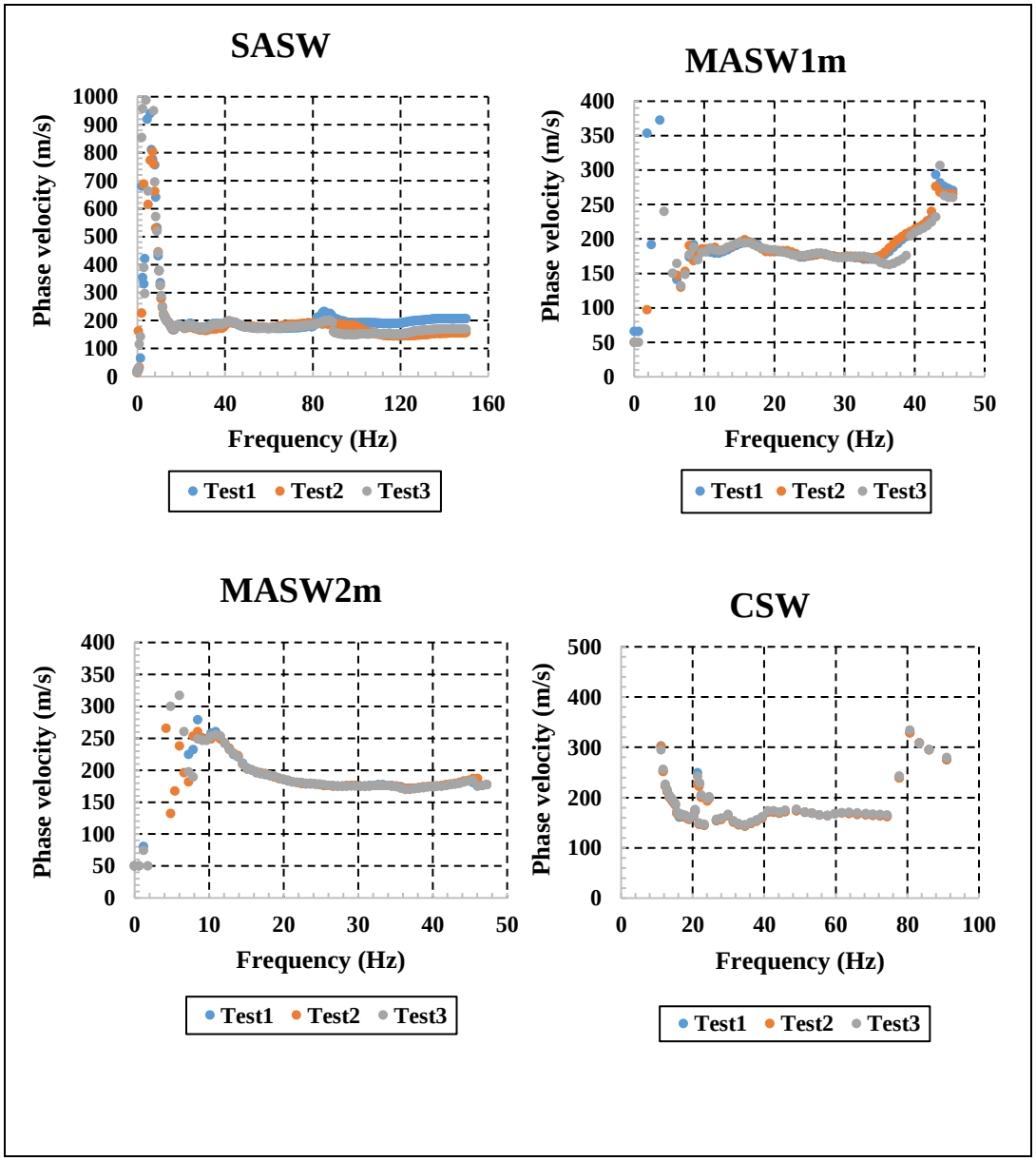

Figure 4.17: Repeatability dispersion curves for SASW and MASW performed with 6.3 kg sledgehammer and CSW at the shallow bedrock site

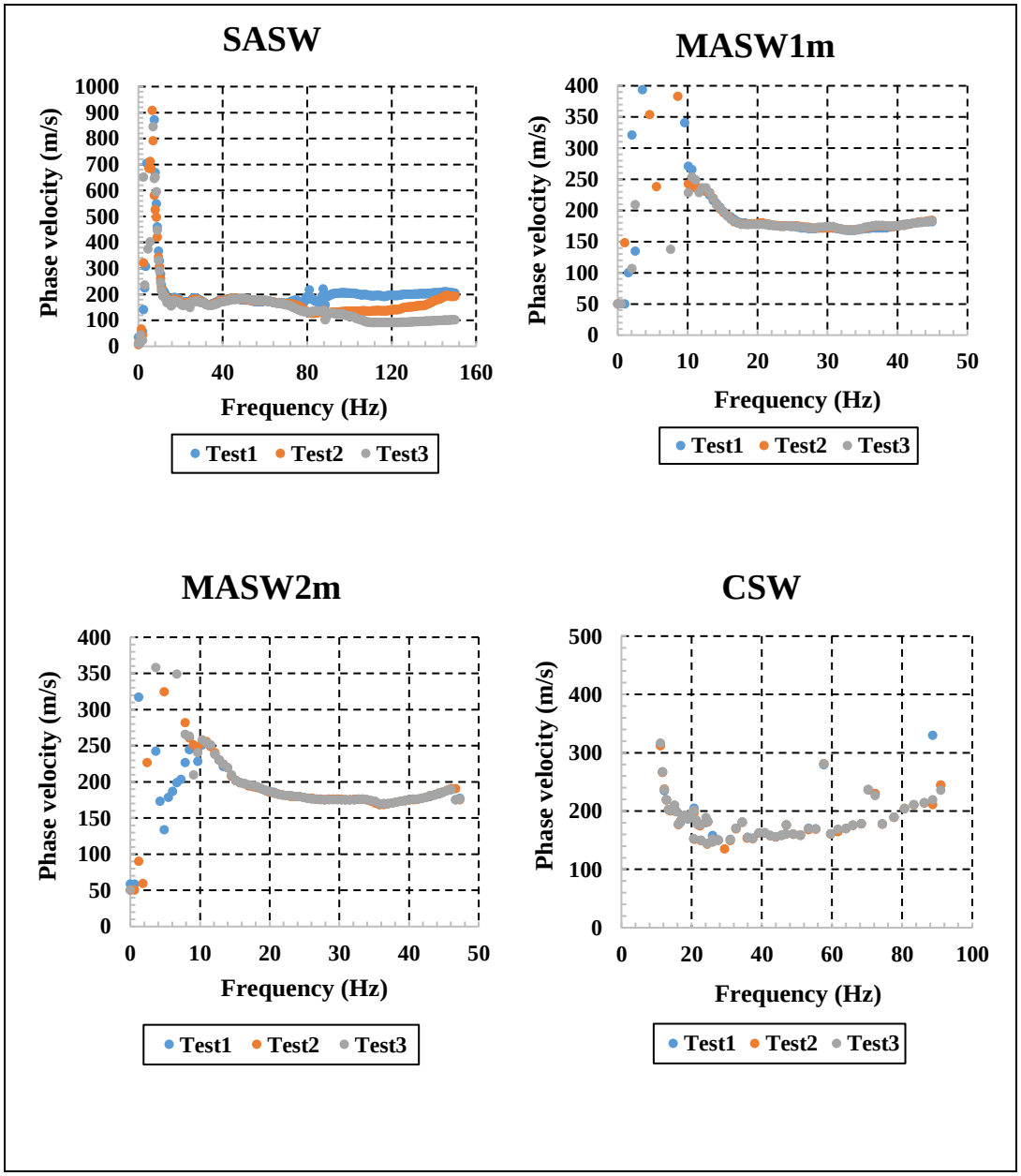

Figure 4.18: Repeatability dispersion curves for SASW and MASW performed with 9.2 kg sledgehammer and CSW at the shallow bedrock site

4.3.2 Near field effects comparison

As described in Chapter two, near field effects are effects that result from non-planar Raleigh and Body waves propagating cylindrically and spherically respectively in the near field region which is the region it the vicinity of the source excitation point. Thus, it is clear that these effects will be prevalent when the source is placed too close to the receivers. However, there is also an aspect of far field effect which is due to geometric spreading and material damping when the source is placed too far from the receivers. According to Zywicki and Rix (2005) near field effects can further be caused by model incompatibility which results from using analysis methods that model a cylindrically propagating wave as a plane wave. Also, irregular variation of ground stiffness increases the severity of near field effects due to the complexity of wave fields for such soil profiles (Yoon and Rix, 2009 and Olafsdottir et al., 2018).

Near field effects lead to errors when estimating Raleigh phase velocity as many researchers who did numerical analysis, laboratory simulation and field tests found that due to near field effects, phase velocity is underestimated in the low frequency range (Yoon and Rix, 2009 and Olafsdottir et al., 2018). This is an important consideration for seismic tests as the poor estimation of phase velocity in the low frequency range affects the maximum investigation depth. On the other hand, far field effects result in overestimation of Raleigh phase velocity, generation of multiple modes due to superimposed body waves and attenuation of the fundamental mode components in the higher frequencies due to material damping (Zywicki and Rix, 2005 and Yoon and Rix, 2009).

In this study, tests were performed with the source placed at multiple offsets in order to investigate the susceptibility of SASW, MASW and CSW to near field effects. As it was explained in Chapter 3, SASW was performed using the source offsets of 1 m, 2 m, 4 m, 8 m, 16 m and 32m. MASW1m tests were performed at source offsets of 1 m, 2 m, 4 m, 8 m and 16 m whereas MASW2m tests were performed at source offsets of 2 m, 4 m, 8 m, 16 m and 32 m. On the other hand, CSW was performed using the offsets of 1 m, 2 m and 4 m. Hunter and Crow (2015) suggested the guide represented in Equation 4.1 to avoid near field effects:

$$d > \frac{\lambda_{max}}{2} \tag{4.1}$$

Where d is the source offset and λ_{max} is the maximum wavelength of plane Raleigh wave that can be analysed.

In all the figures below, the diagonal lines based on Equation 4.1 are included as a guide to differentiate between near field and non near field segments of the dispersion curves for different source offsets. Based on the essence of Equation 4.1, the dispersion curve segment to the left of this cut-off line is considered to include near field effects whereas the segment to the right is unaffected by the near field effects.

SASW, MASW1m and MASW2m dispersion curves shown in Figure 4.19, Figure 4.20 and Figure 4.21 are for 2.2 kg, 6.3 kg and 9.2 kg sledgehammers respectively. It is clear in these figures that for SASW, small source offsets result in under estimation of phase velocity and this effect also becomes significant with increased size of the source.

On MASW1m dispersion curves, it is clear in these three figures that the dispersion curves obtained with source offsets of 1 m and 2 m are entirely in the near field zone. Also, these dispersion curves together with dispersion curve for source at 4 m do not portray clear fundamental mode trends but instead they show severe scattering. This behaviour can be associated with near field effects since the dispersion curves improved with increased source offset (8 m and 16 m). The improved behaviour can clearly be explained by nearfield cut-off lines that show that the tests performed at 8 m and 16 m can only experience near field effects only for frequencies below 10 Hz. However, relative to 16 m source offset, 8 m source offset underestimated phase velocity which explains that near field effects were still included at this offset even though their impact was less severe compared to 1 m, 2 m and 4 m source offsets. The same behaviour is seen for the dispersion curves obtained using 6.3 kg and 9.2 kg sledgehammers.

On MASW2m dispersion curves near field effects were not as severe because the curves for different source offsets lie close to each though underestimation of phase velocity is still apparent to a certain extent.

Moreover, it is clear from the CSW dispersion curves and near field guidelines that when performing CSW with source positioned at 1 m away from the receivers, the obtained dispersion curve is entirely in the near field zone. However, with increased offset of 2 m and greater, part of the dispersion curve in the low frequency range will be afflicted by near field effects whereas the segment in the high frequency range will be free of near field effects. CSW near field effects in the figures below appear to be more distinct in the frequency range below 20 Hz which is the data obtained with the low frequency shaker. It is worth noting that CSW is also affected by high modes at high frequencies which is another aspect of near field effects (far field).

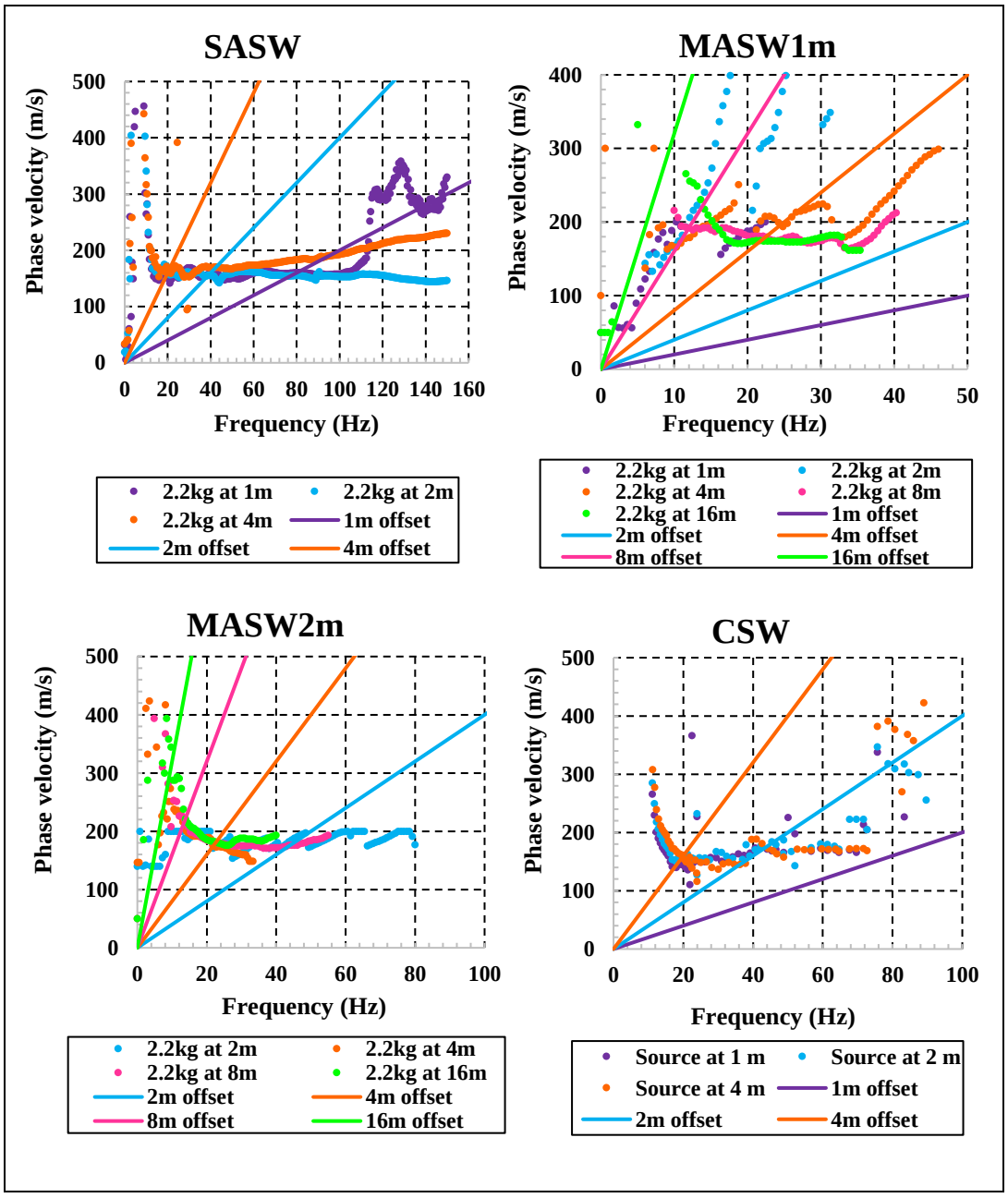

Figure 4.19: SASW, MASW and CSW dispersion curves (obtained with 2.2 kg sledgehammer for SASW and MASW) and their near field guidelines at the shallow bedrock site

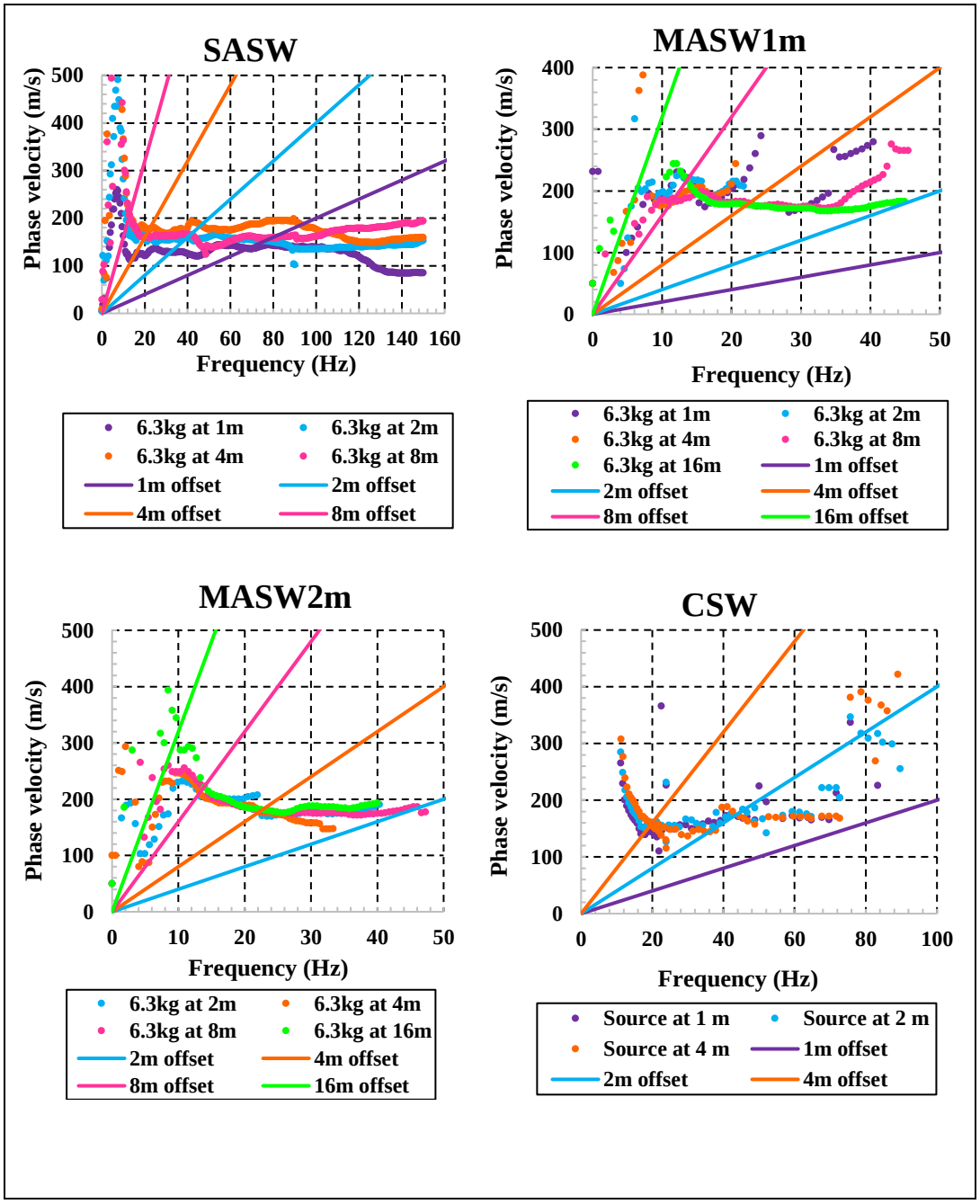

Figure 4.20: SASW, MASW and CSW dispersion curves (obtained with 6.3 kg sledgehammer for SASW and MASW) and their near field guidelines at the shallow bedrock site

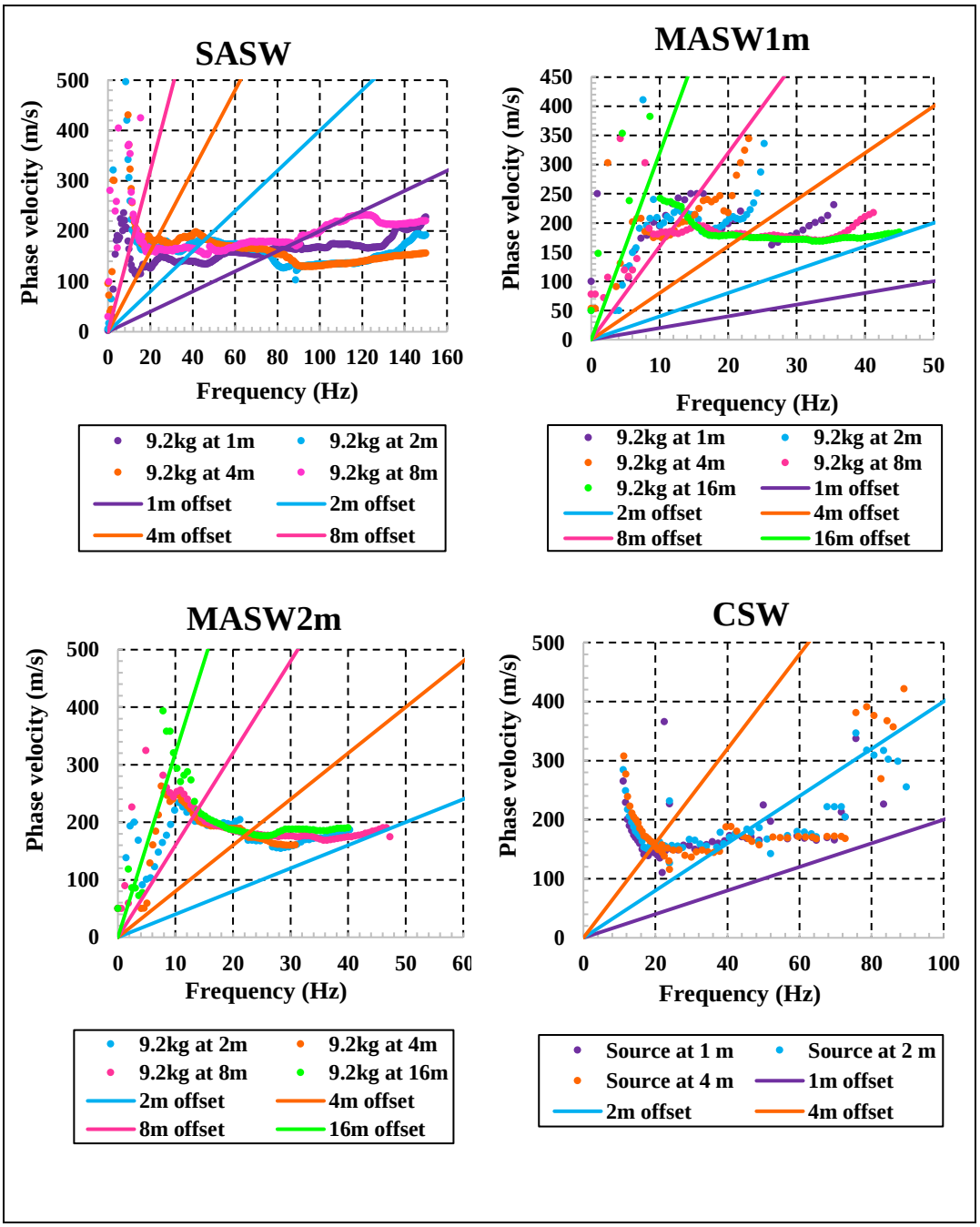

Figure 4.21: SASW, MASW and CSW dispersion curves (obtained with 9.2 kg sledgehammer for SASW and MASW) and their near field guidelines at the shallow bedrock site

In conclusion, near field effects seem to be inevitable in seismic surface wave testing. MASW appear to be the most susceptible to near field effects with MASW1m being affected the most as compared to MASW2m. However, near field effects for MASW at small source offsets can be a result of model incompatibility caused by analysing

cylindrically propagating waves with the Geopsy software that assumes plane Raleigh wave propagation.

4.3.3 Sampling depth comparison

This section focuses on the sampling depths of these three tests and their respective depths are shown in Figure 4.22 and Figure 4.23. It is also worth mentioning beforehand that the MASW tests with small source offsets i.e 1 m, 2 m and 4 m did not yield good data hence nothing could be deduced from their dispersion curves. This is not a surprise since Foti et al. (2018) stated that for good practice, MASW must be performed with source offsets that are three to five times the geophones' spacing. Thus, MASW was nonetheless compared with the other two tests but using the dispersion curves for the sources offsets that were able to yield good data. Sampling depths were determined using Equation 4.2 which is used by many researchers.

$$z = \frac{\lambda}{2} \qquad 4.2$$

Where z is the sampling depth and λ is the measured wavelength.

The fundamental mode of the dispersion curves alone was used to determine the sampling depths. The points in low frequency range (7-10 Hz) where the dispersion curves were starting to experience scatter were used to evaluate the maximum sampling depths whereas the points at end of the fundamental mode in the higher frequency range were used to determine the minimum sampling depths.

Only the extreme values for the average depths in the tables in Appendix A were used to compare the three tests. The figures below show comparison of SASW, CSW and MASW1m as well as comparison of SASW, CSW and MASW2m Thus, it can be seen from Figure 4.22 that the deepest that SASW test could sample was 28.8 m and could also sample as shallow as 0.55 m. On the other hand, it can be seen that with MASW1m16m2.2kg the maximum depth of 12.5 m and the minimum depth of 2.4 m were reached. Furthermore, the maximum depth of 15.3 m and minimum depth of 2.0 m were sampled with MASW1m2m6.3kg and MASW1m16m6.3kg respectively. MASW1m4m9.2kg was capable of sampling down to 14.0 m and a shallow depth of 2.0 m was achieved with MASW1m4m16m9.2kg. CSW test was capable of sampling to a maximum depth of 14.1 m with the source positioned at a distance of 4 m from the closest geophone and a minimum depth of 1.1 m was attained with the source placed 2 m away.

In Figure 4.23 it is clear that the maximum depths obtained by MASW2m tests were 14.2 m, 19.9 m and 25.0 m and these depths were less than that obtained by SASW tests but greater than that obtained by CSW. Furthermore, the minimum depths of 1.7 m, 1.9 m and 2.5 m sampled by MASW2m tests were deeper than those of SASW and CSW even though that of CSW was also deeper than for SASW

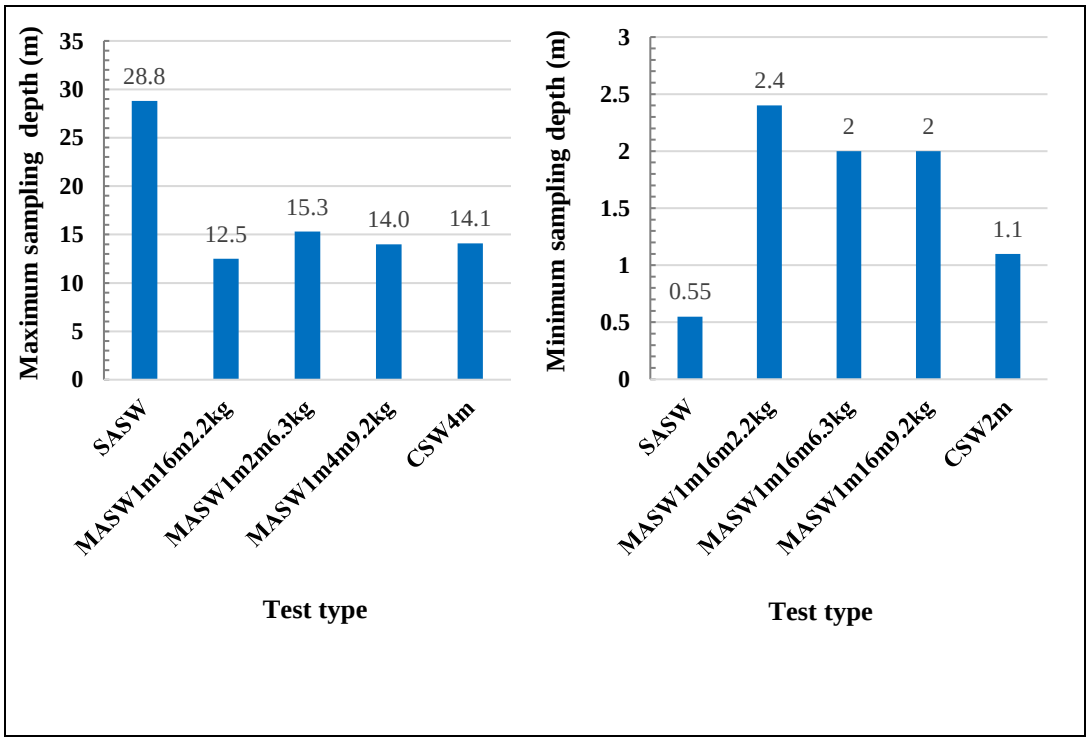

Figure 4.22: Maximum and minimum sampling depths for SASW, MASW1m and CSW at the shallow bedrock site

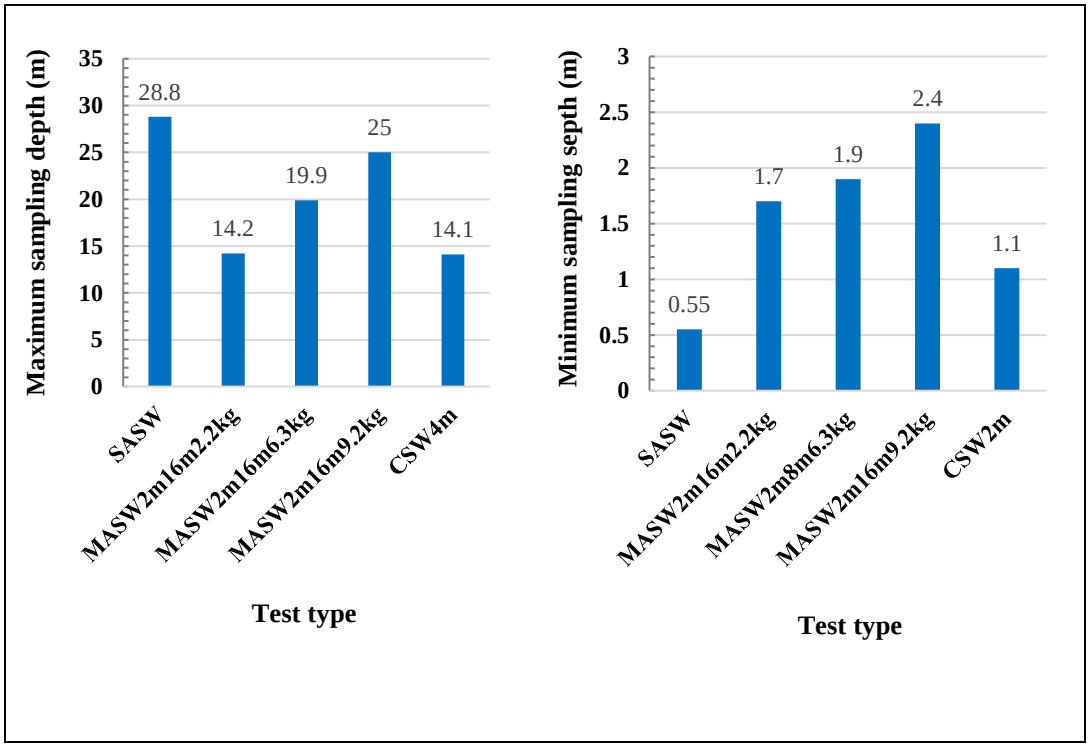

Figure 4.23: Maximum and minimum sampling depths for SASW, MASW2m and CSW at the shallow bedrock site

From the presented data above it is clear that on a shallow bedrock site the SASW test can sampled deeper, followed by the MASW test and lastly the CSW test. The inability of CSW to sample to great depths was anticipated since this was stated in the literature by (Clayton et al., 2012 and Hunter and Crow, 2015) that the profiling depth of CSW is limited by the frequency range over which the shaker can operate. On the other hand, SAWS was also found to sample shallower, followed by CSW and MASW.

In addition, it is noteworthy that with MASW2m the investigation depth was deeper as opposed to that of MASW1m. This is in accordance with what was stated by Hunter and Crow (2015) that for great depths of roughly 30 m, a geophone spacing must be increased to 2 m to 3 m.

The dispersion curves that were used to determine the investigation depth for MASW are presented in the repeatability section and in Appendix A and those of CSW are also presented in the repeatability section. However, the composite dispersion curves that were used to determine the investigation depths for SASW are shown below.

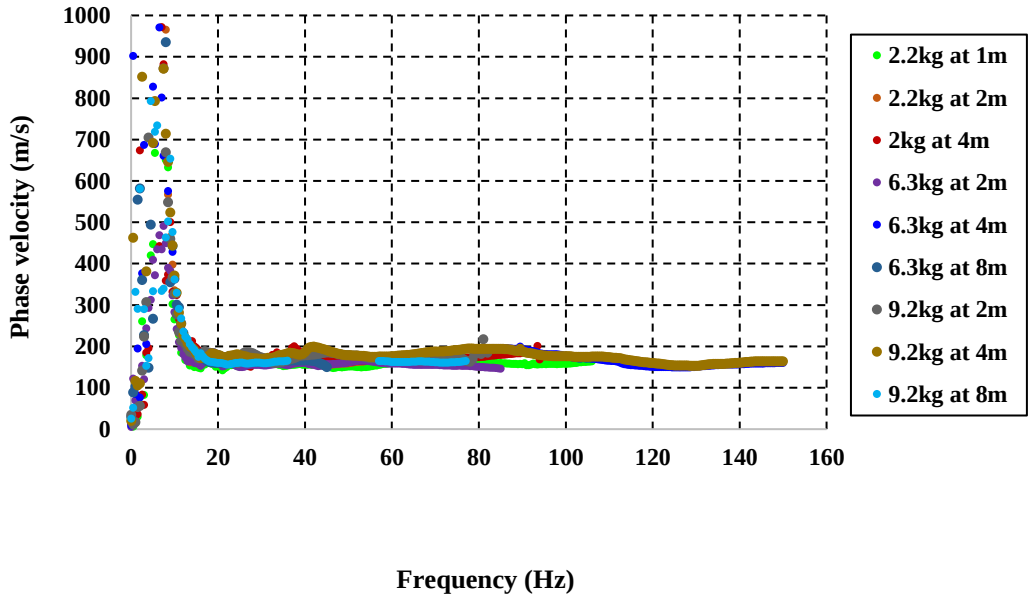

Figure 4.24: SASW composite dispersion curve for test 1 at the shallow bedrock site

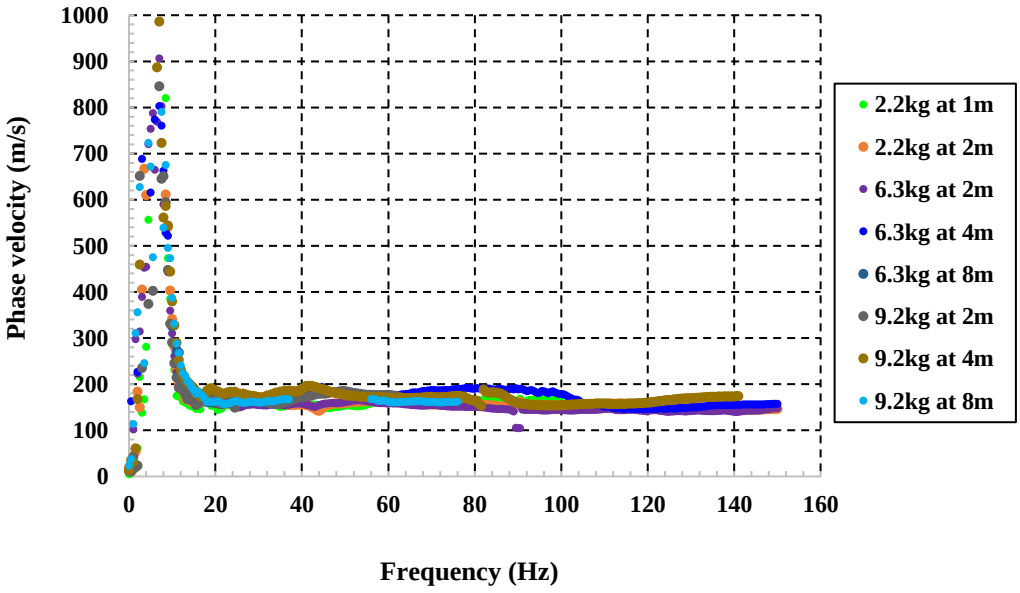

Figure 4.25: SASW composite dispersion curve for test 2 at the shallow bedrock site

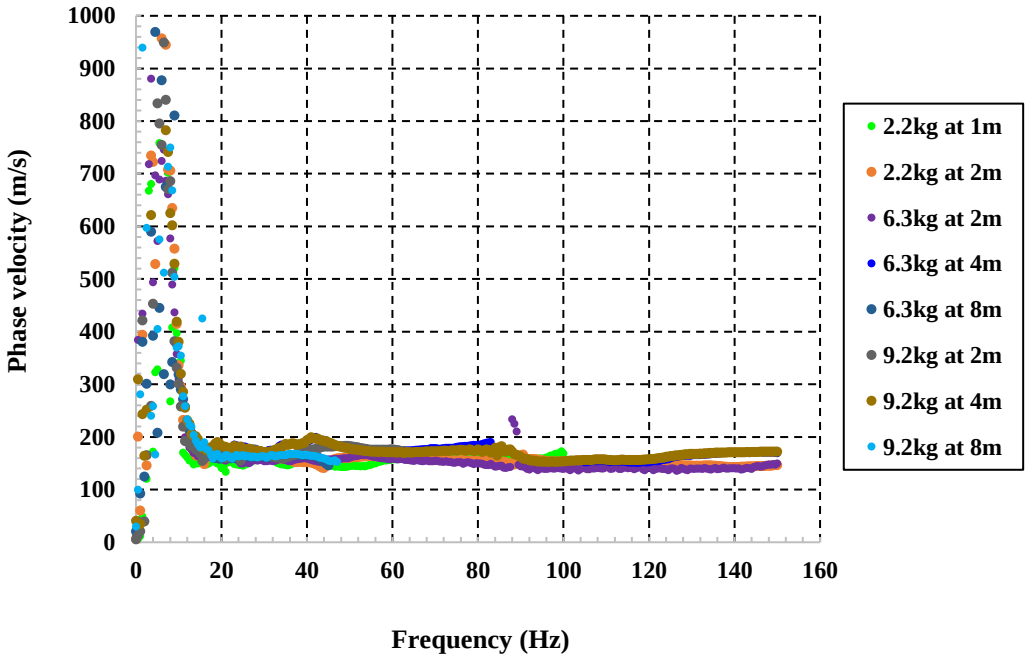

Figure 4.26: SASW composite dispersion curve for test 3 at the shallow bedrock site

4.3.4 Shear wave velocity profiles for shallow bedrock site

This section represents the shear wave profiles for the shallow bedrock site. The objective of this section is not to compare the three tests but to show how V_s varies with depth. The inversion was performed with maximum allowable misfit of 10 %. The red graphs represented the solutions with the minimum misfit values and these values were 0.059, 0.028 and 0.047 for SASW, MASW and CSW respectively. The fitting of theoretical dispersion curves to experimental dispersion curves for these three tests are also presented. It can be seen from the shear wave velocity profiles yielded by SASW, MASW and CSW that this site is normally dispersive as V_s increases with depth.

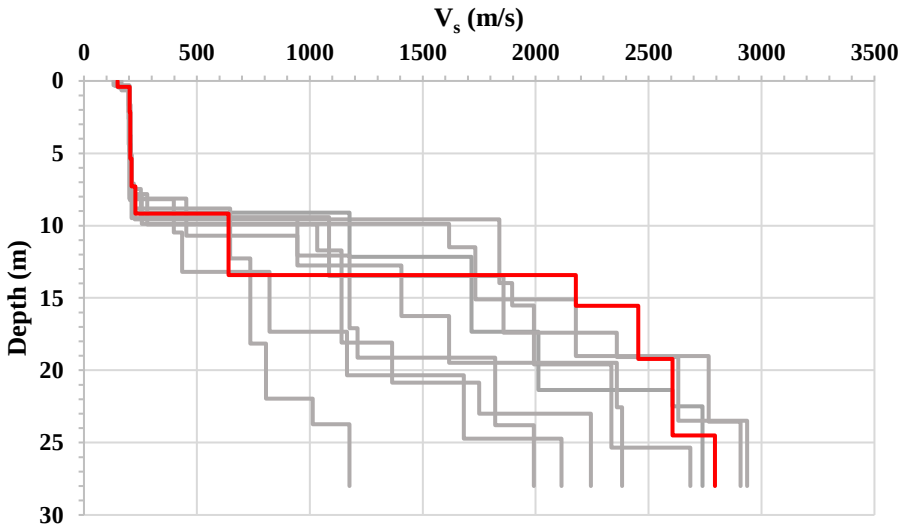

Figure 4.27: Shear wave velocity profile represented by SASW at the shallow bedrock site

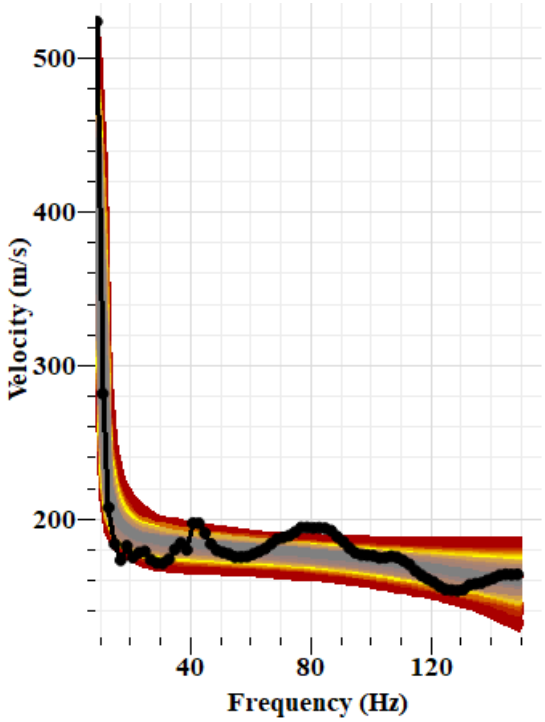

Figure 4.28: Fitting of theoretical dispersion curve to SASW dispersion curve at the shallow bedrock site

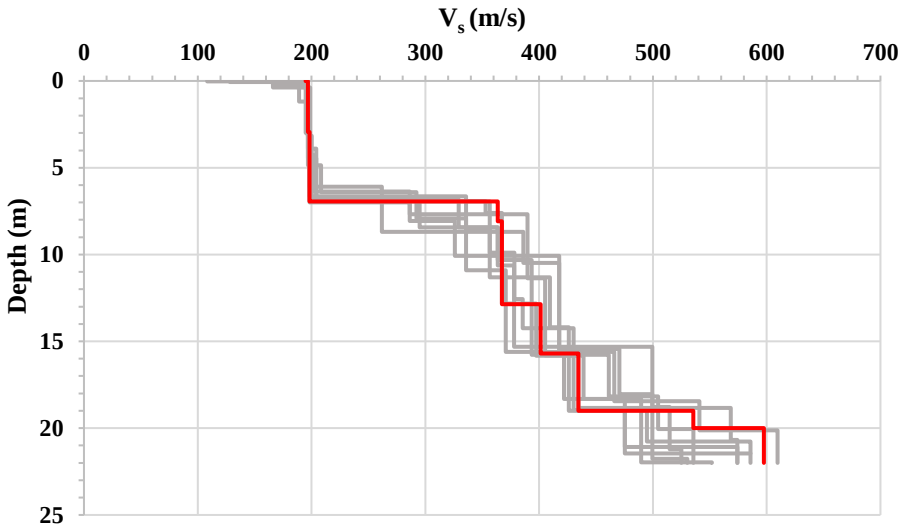

Figure 4.29: Shear wave velocity profile represented by MASW at the shallow bedrock site

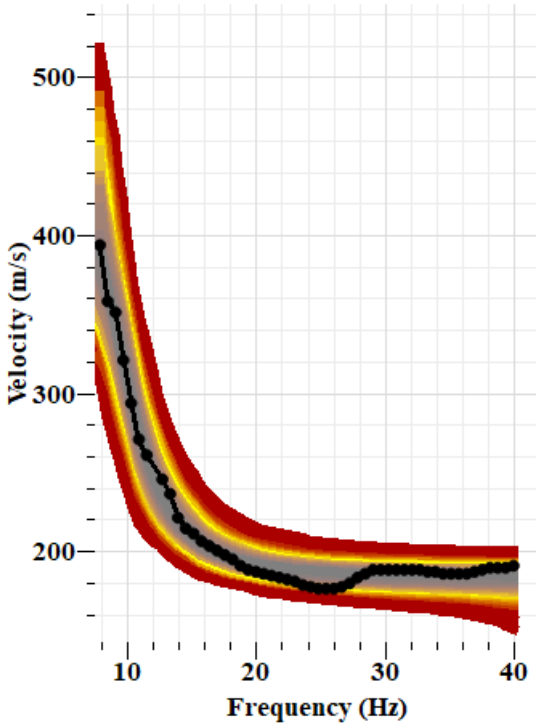

Figure 4.30: Fitting of theoretical dispersion curve to MASW dispersion curve at the shallow bedrock site

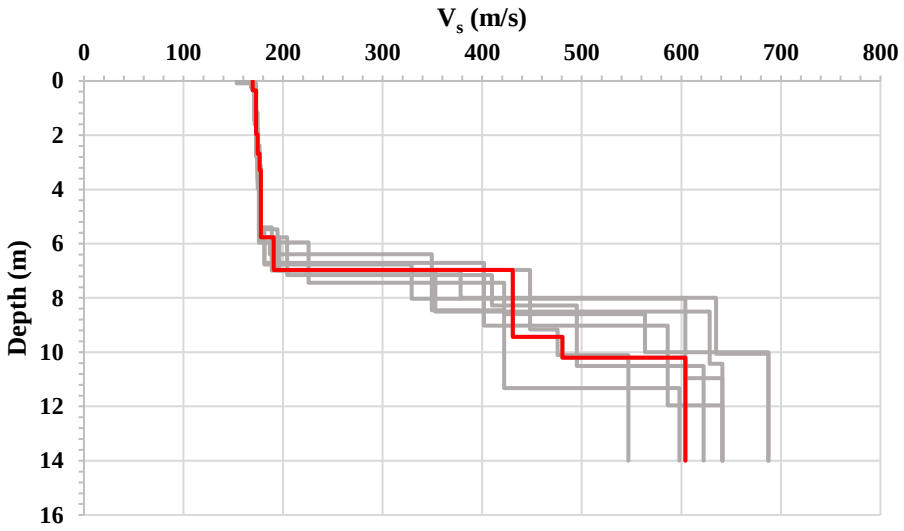

Figure 4.31: Shear wave profile represented by CSW at the shallow bedrock site

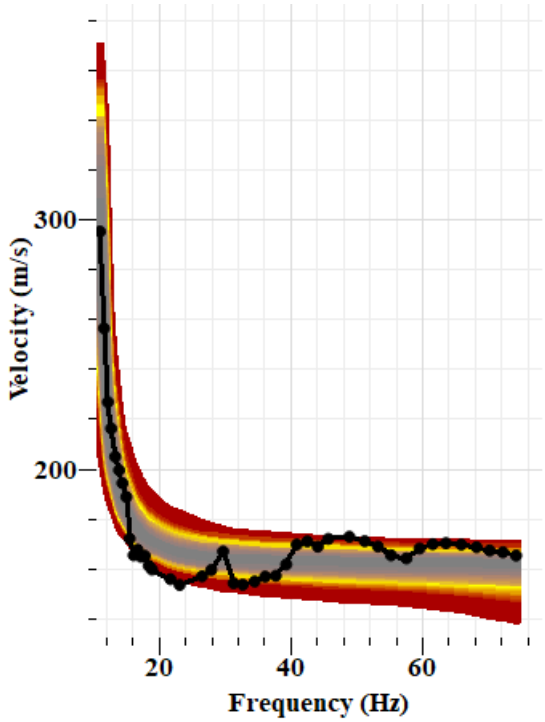

Figure 4.32: Fitting of theoretical dispersion curve to CSW dispersion curve at the shallow bedrock site

4.4 Deep bedrock data analysis

4.4.1 Repeatability comparison

In the same way as with the analysis of repeatability at the shallow bedrock site, the repeatability dispersion curves for SASW, MASW and CSW at the deep bedrock site are presented. MASW and SASW dispersion curves presented in Figure 4.33, Figure 4.34 and Figure 4.35 are for 2.2 kg, 6.3 kg and 9.2 kg sledge hammers respectively.

From the dispersion curves it is clear that SASW is repeatable in the low frequency range however, the repeatability deteriorates for frequencies above 60 - 80 Hz. This is the same behaviour as that seen for the shallow bedrock site hence this behaviour could be attributed to the same reason stated in Section 4.3.1. It can also be concluded that SASW is site independent as far as repeatability is concerned.

Repeatability for MASW and CSW was excellent as their dispersion curves were repeatable throughout the entire range of the fundamental mode as well as for higher mode in the case of CSW. However, it is worth noting that below the frequency of 10 Hz the repeatability for MASW was not as good as that of CSW. As the tests were done with the same equipment and by the same operator then different behaviours reflected by MASW at shallow and deep bedrock sites indicates that MASW is site dependent when it comes to repeatability.

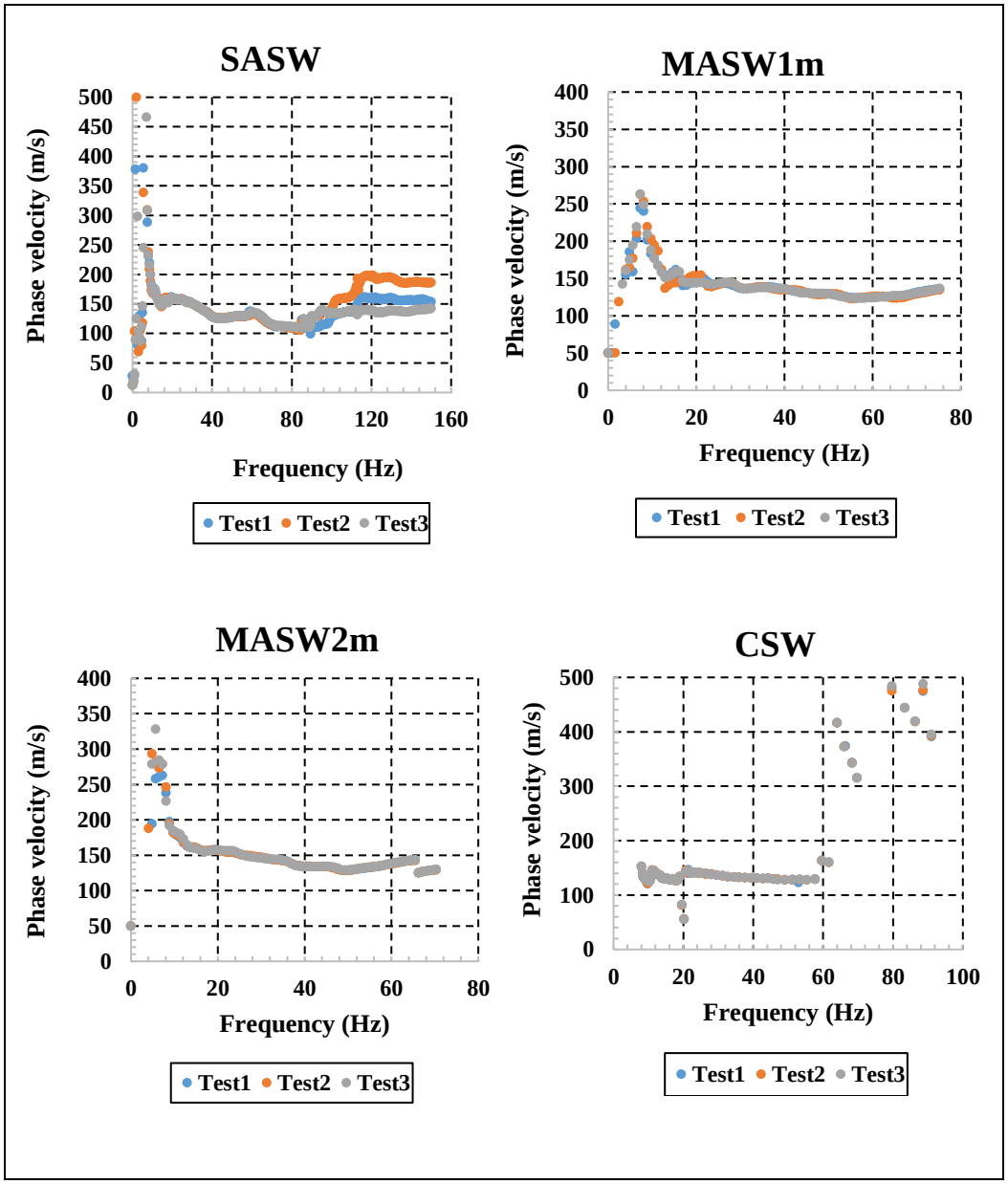

Figure 4.33: Repeatability dispersion curves for SASW and MASW performed with 2.2 kg sledgehammer and CSW at the deep bedrock site

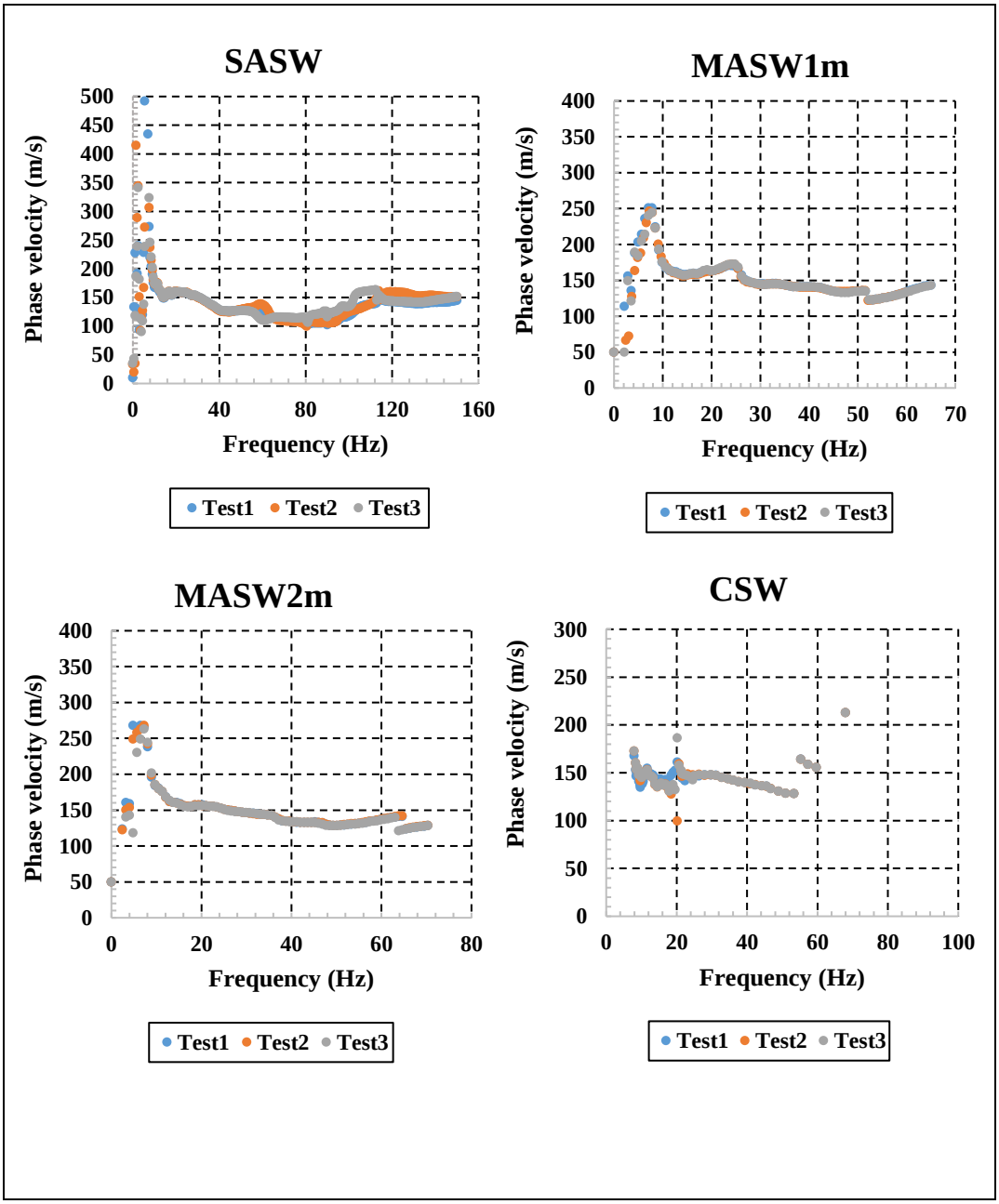

Figure 4.34: Repeatability dispersion curves for SASW and MASW performed with 6.3 kg sledgehammer and CSW at the deep bedrock site

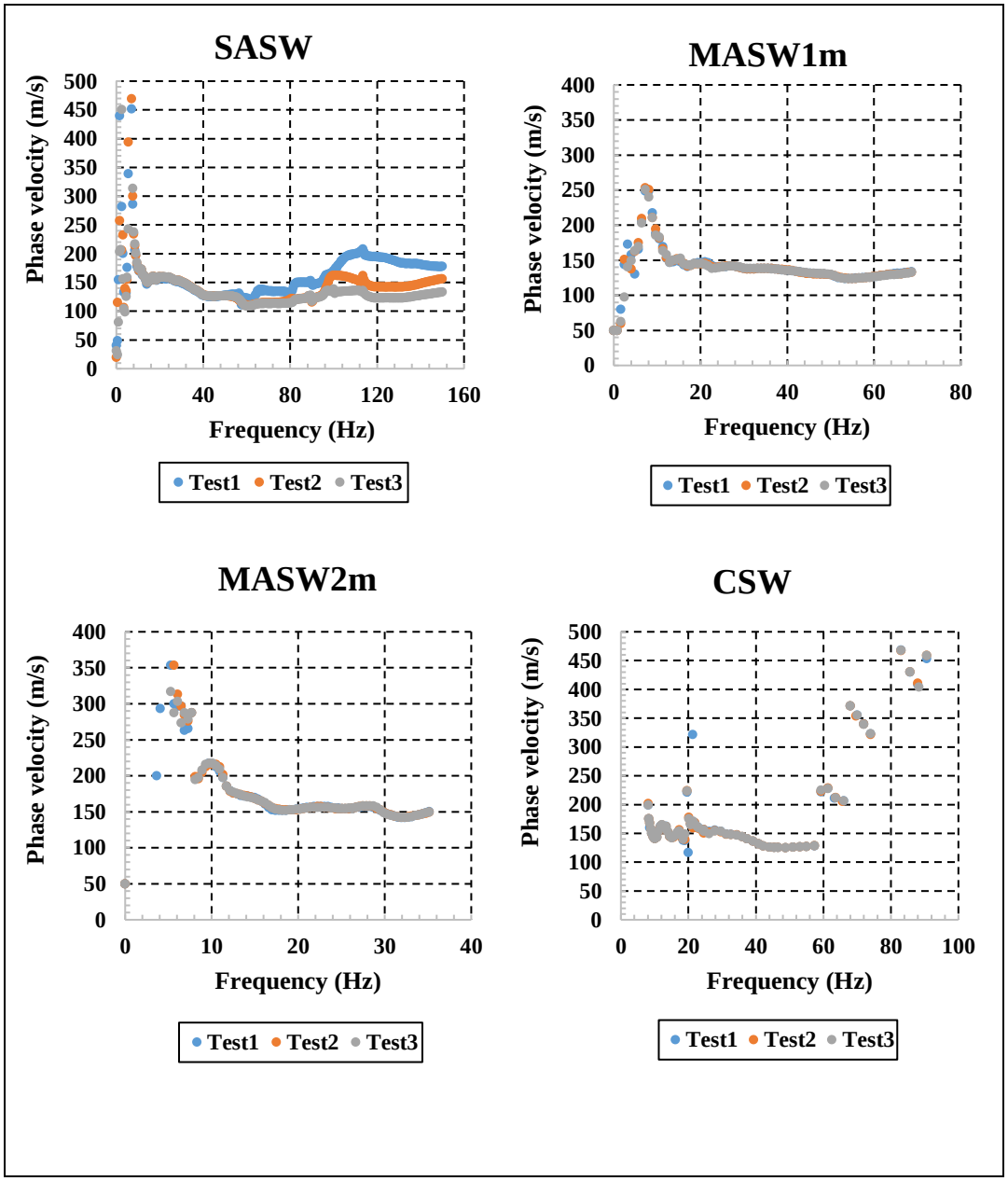

Figure 4.35: Repeatability dispersion curves for SASW and MASW performed with 9.2 kg sledgehammer and CSW at the deep bedrock site

4.4.2 Near field effects comparison

In this section the comparison of the three tests with respect to the susceptibility to near field effects at the deep bedrock site will be discussed. The near field guide lines were calculated using Equation 4.1 presented in Chapter 4.3.2. At this site it is evident from Figure 4.36, Figure 4.37 and Figure 4.38 that for SASW tests, near field effects are apparent for 1 m source offset. However, for source offsets of 2 m and greater, the dispersion curves alternate between each other in different frequency ranges with no obvious under estimation of Raleigh phase velocity.

For MASW1m it can be seen that the dispersion curves from multiple source offsets coincide for frequencies above 40 Hz. However, for frequencies below 40 Hz the dispersion curves start to differ and the phase velocity is higher for increased source offsets. The behaviour below 40 Hz frequency can be considered as the manifestation of the near field effects. As for MASW2m not much of near field effects were observed as the dispersion curves obtained from different source offsets correspond fairly well. It was only for tests at 2 m source offsets where Raleigh phase velocity was underestimated in frequencies below 10 Hz, 20 Hz and 10 Hz for 2.2 kg, 6.3 kg and 9.3 kg sledgehammers respectively.

Lastly, CSW is affected by near and far field effects since the phase velocity seems to decrease with decrease in source offset in the low frequency range below 40 Hz. On the other hand, high modes are more dominant in the higher frequency range which also hampered the ability of CSW to sample to very shallow depths.

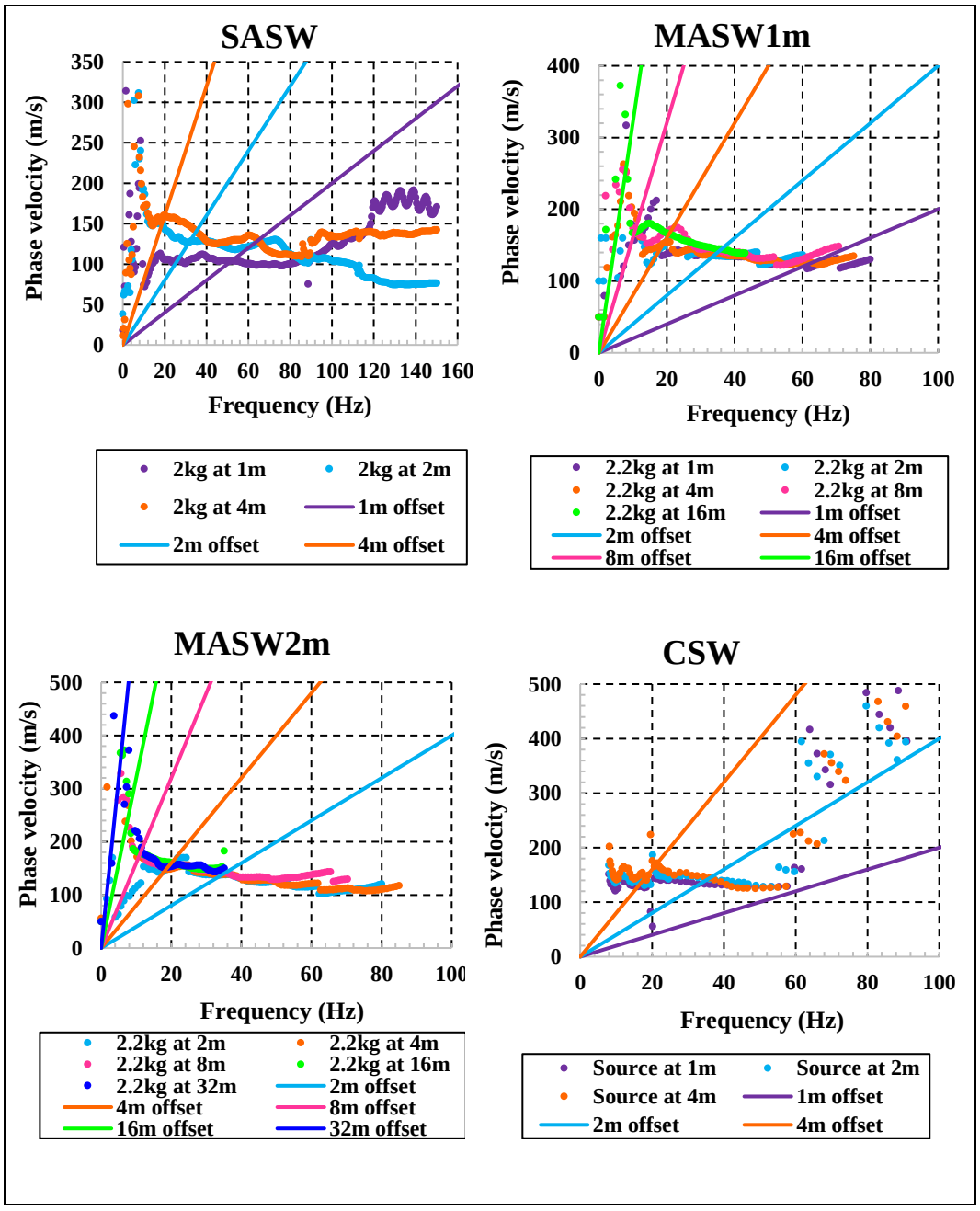

Figure 4.36: SASW, MASW and CSW dispersion curves (obtained with 2.2 kg sledgehammer for SASW and MASW) and their near field guidelines at the deep bedrock site

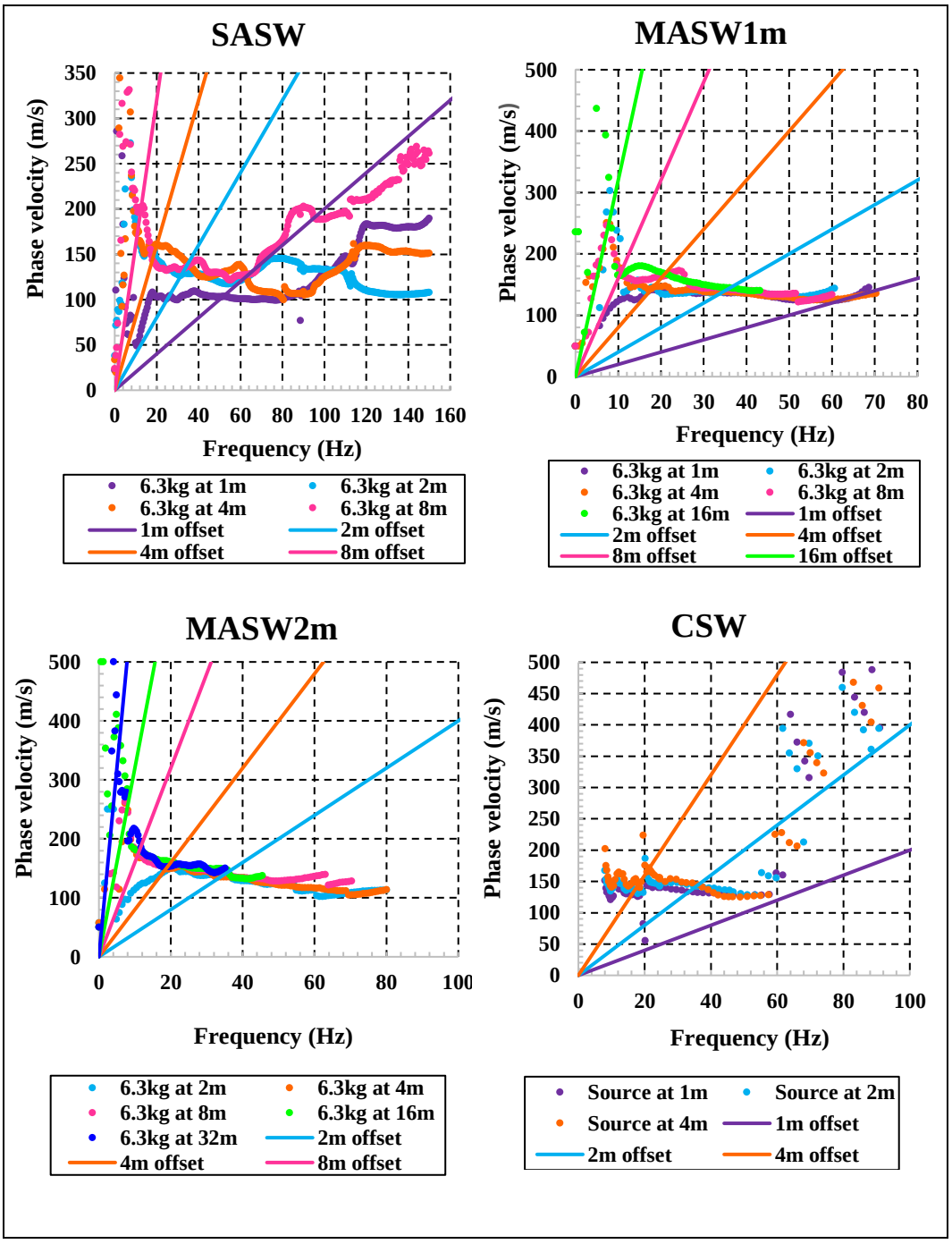

Figure 4.37: SASW, MASW and CSW dispersion curves (obtained with 6.3 kg sledgehammer for SASW and MASW) and their near field guidelines at the deep bedrock site

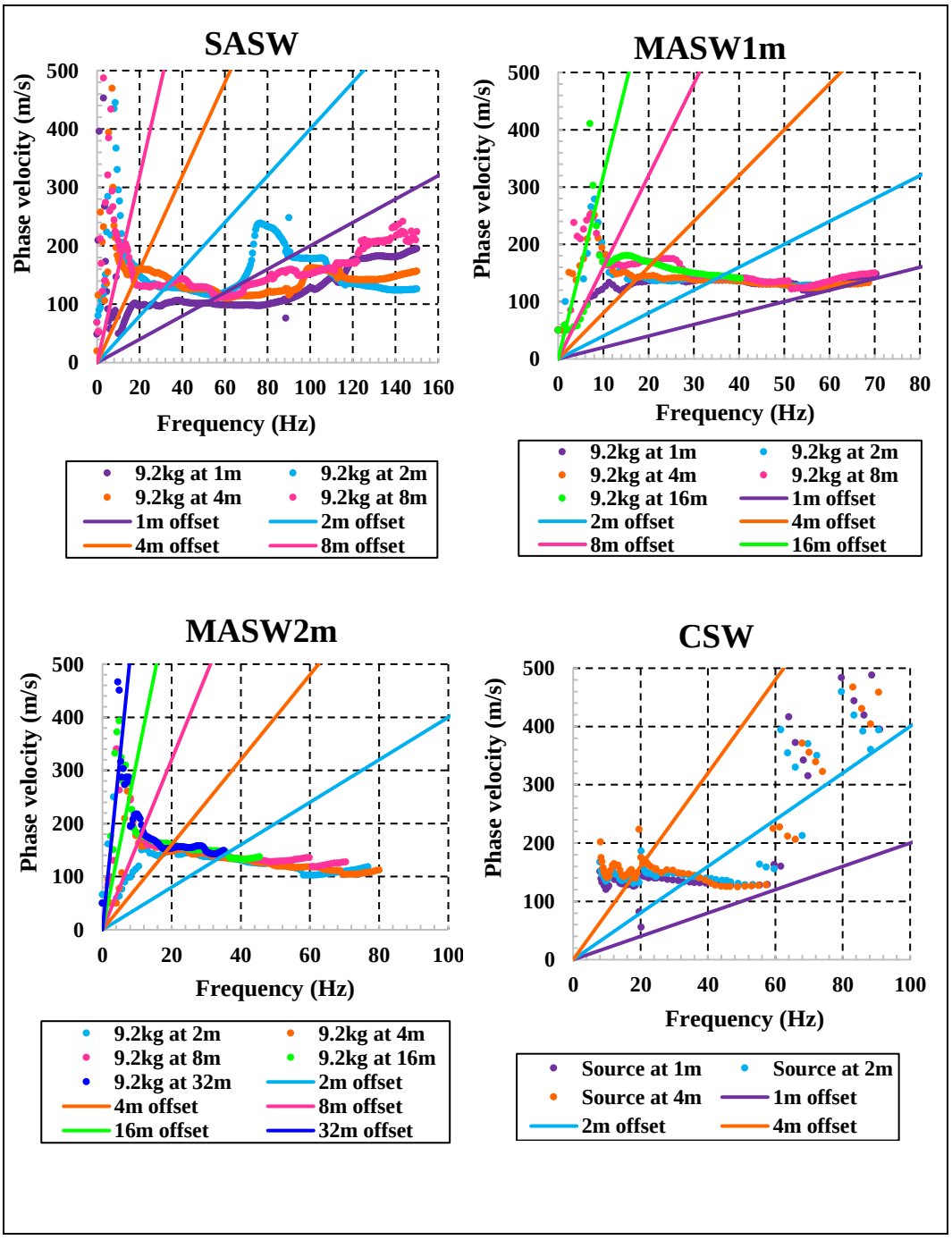

Figure 4.38: SASW, MASW and CSW dispersion curves (obtained with 9.2 kg sledgehammer for SASW and MASW) and their near field guidelines at the deep bedrock site

In conclusion, MASW1m was found to be more prone to near field effects, followed by SASW, CSW and MASW2m with geophones spaced at 2 m. Also, in terms of near field effects, the results obtained from the deep bedrock site were generally less affected by near field effects as opposed to the results from the shallow bedrock site. Therefore, this clearly affirms that the severity of near field effects is site-dependent. This agrees with the literature that near field effects are more extreme for irregular soil profiles as opposed to regular profiles (Yoon and Rix, 2009 and Olafsdottir et al., 2018).

4.4.3 Sampling depth comparison

The sampling depths at the deep bedrock site were determined using the same procedure as described in Chapter 4.3.3 and detailed data for sampled depths can be found in tables in Appendix B. However, it is still worth mentioning that only the fundamental mode was used to determine the depths. Figure 4.39 compares SASW, MASW1m and CSW whereas Figure 4.40 compares SASW, MASW2m and CSW. In Figure 4.39 it is clear that the SASW test was able to sample as deep as 24.7 m and as shallow as 0.78 m. On the other hand, MASW1m2m2.2kg sampled to a depth of 16.5 m and MASW1m4m2.2kg sampled the shallowest depth of 0.91 m. Furthermore, MASW1m16m6.3kg sampled to a maximum depth of 20.1 m whereas MASW1m4m6.3kg sampled the shallowest depth of 0.96 m. MASW1m16m9.2kg sampled to a maximum depth of 19.5 m and the shallowest depth of 0.97 was attained by MASW1m4m9.2kg.

Furthermore, as can be seen in Figure 4.40 MASW2m16m2.2kg sampled a maximum depth of 18.4 m and the shallowest depth sampled was 0.69 m by MASW2m4m2.2kg. MASW2m16m6.3kg sampled as deep as 21.2 m and MASW2m4m6.3kg reached the shallowest depth of 0.71 m. Furthermore, the maximum depth of 23.6 m was achieved by MASW2m16m9.2kg. The shallowest depth of 0.70 m was then achieved by MASW2m4m9.2kg. Lastly, with CSW, the maximum depth of 12.3 m and a minimum depth of 1.1 m were reached.

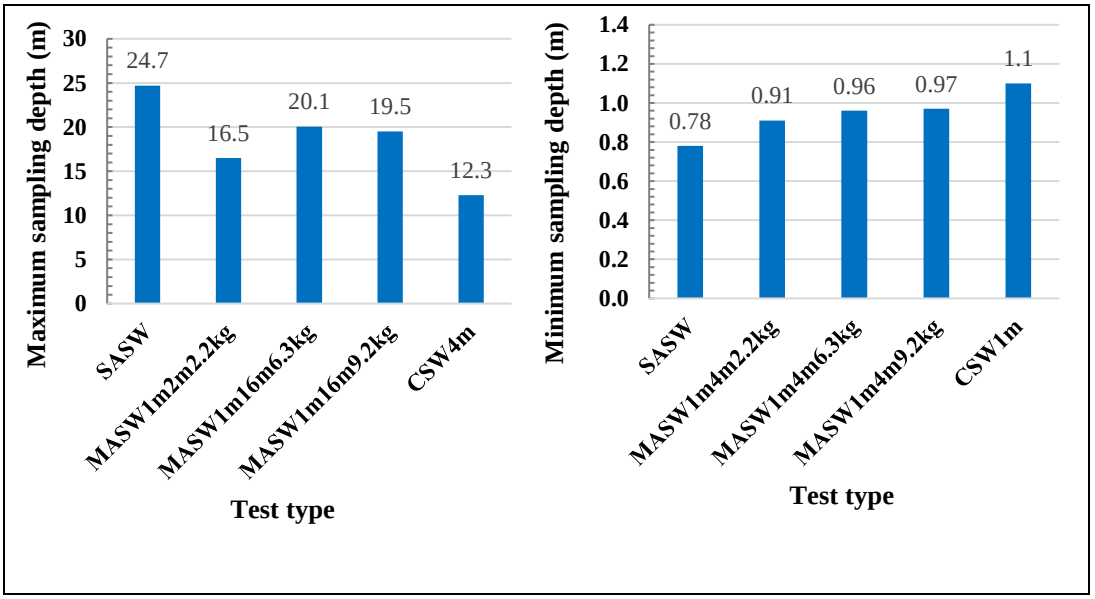

Figure 4.39: Maximum and minimum sampling depths for SASW, MASW1m and CSW at the deep bedrock site

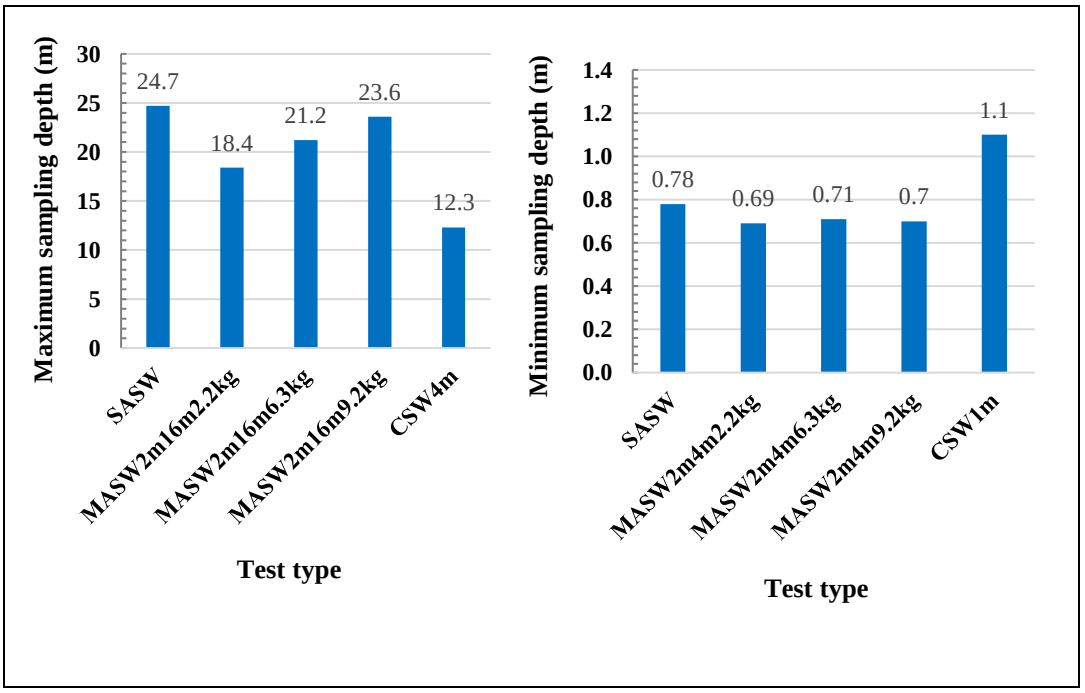

Figure 4.40: Maximum and minimum sampling depths for SASW, MASW2m and CSW at the deep bedrock site

With respect to the deep bedrock site, the conclusion is that SASW test has shown the ability to sample deeper, followed by MASW test then the CSW test. On the other hand, it can be concluded that the shallowest depths sampled by MASW and SASW fall fairly in

the same range, and these depths are shallower than that sampled by CSW. In addition, the MASW2m was found to sample deeper and shallower than MASW1m. Lastly, the maximum depths sampled by SASW, MASW and CSW at the deep bedrock site were shallower than those attained at the shallow bedrock site. Since the tests were conducted using the same equipment methodology, and personnel, it is clear that this behaviour is due to the difference in response behaviour of these two sites.

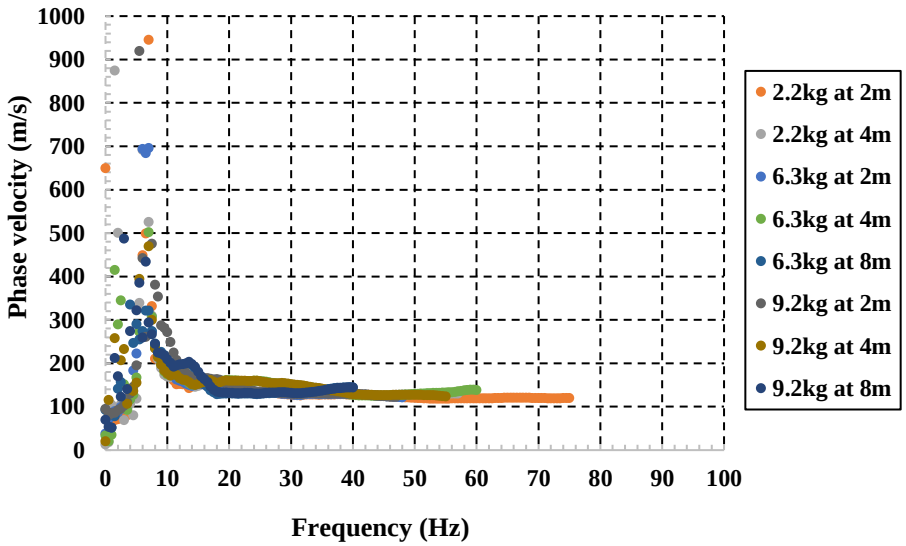

Figure 4.41: SASW composite dispersion curve for test 1 at the deep bedrock site

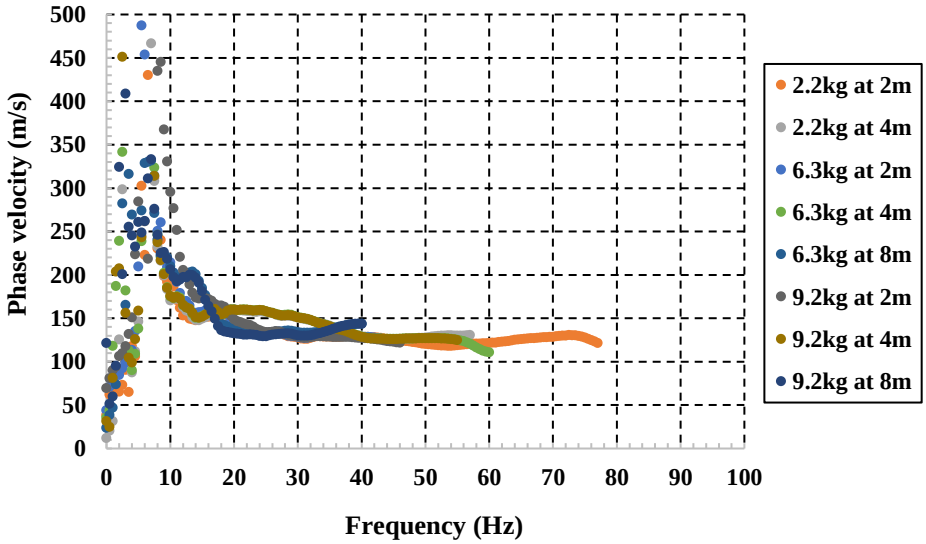

Figure 4.42: SASW composite dispersion curve for test2 on deep bedrock site

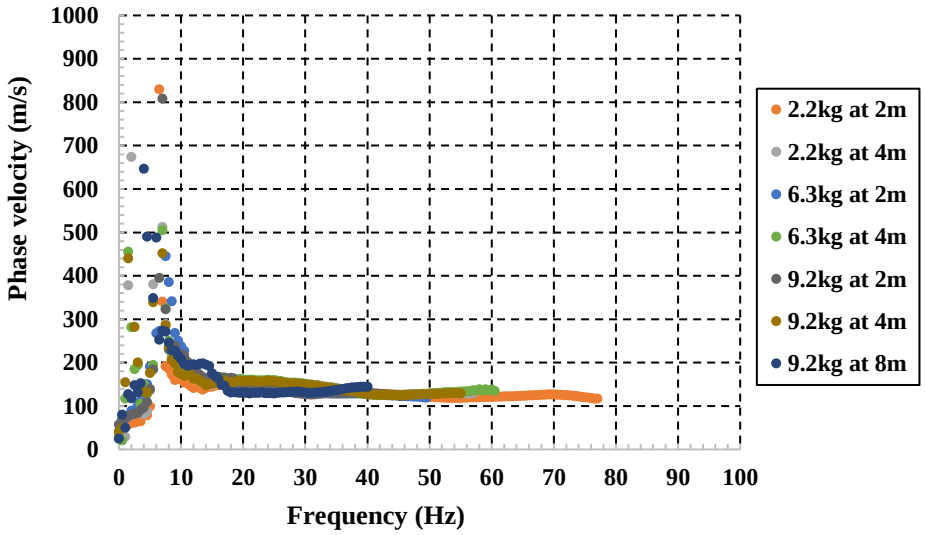

Figure 4.43: SASW composite dispersion curve for test 3 at the deep bedrock site

4.4.4 Shear wave velocity profiles for deep bedrock site

In the same way as in Section 4.3.4 the shear wave velocity profiles are presented in this section to show how shear wave velocity varies with depth at the deep bedrock site. The inversion was done at 10 % maximum allowable misfit and lowest misfit obtained for SASW, MASW and CSW were 0.026, 0.036 and 0.035 respectively and the graphs corresponding to this misfit values are represented in red. As with the shallow bedrock site it can be seen from the V_s profiles produced by SASW, MASW and CSW that the deep bedrock site has a normally dispersive profile as the V_s increases with depth.

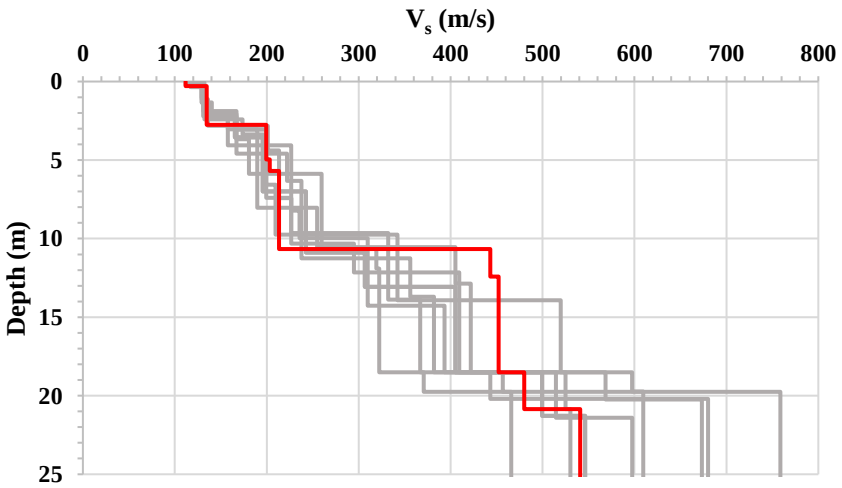

Figure 4.44: Shear wave velocity profile represented by SASW at the deep bedrock site

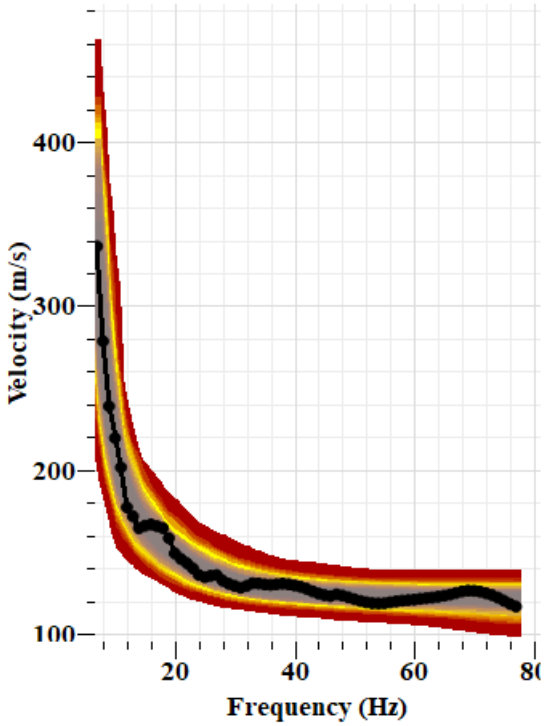

Figure 4.45: Fitting of theoretical dispersion curve to SASW experimental dispersion curve at the deep bedrock site

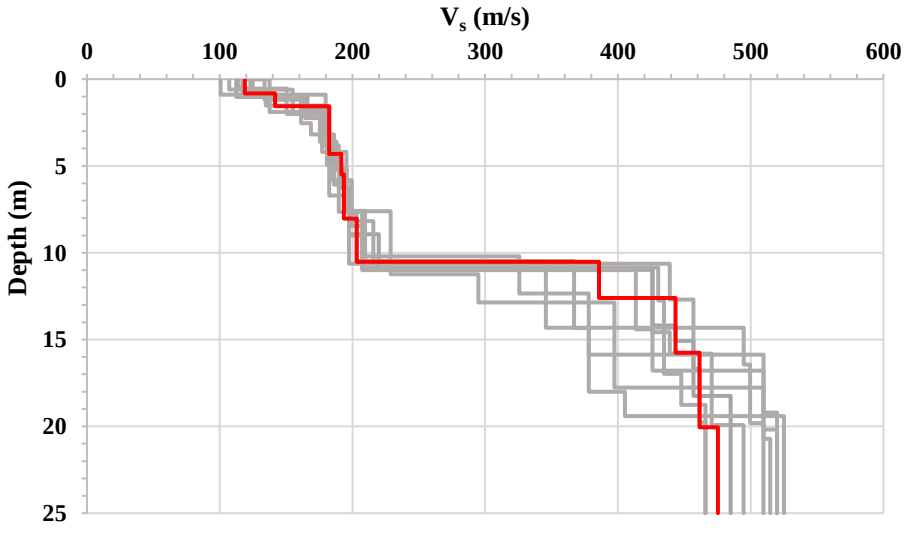

Figure 4.46: Shear wave velocity profile represented by MASW at the deep bedrock site

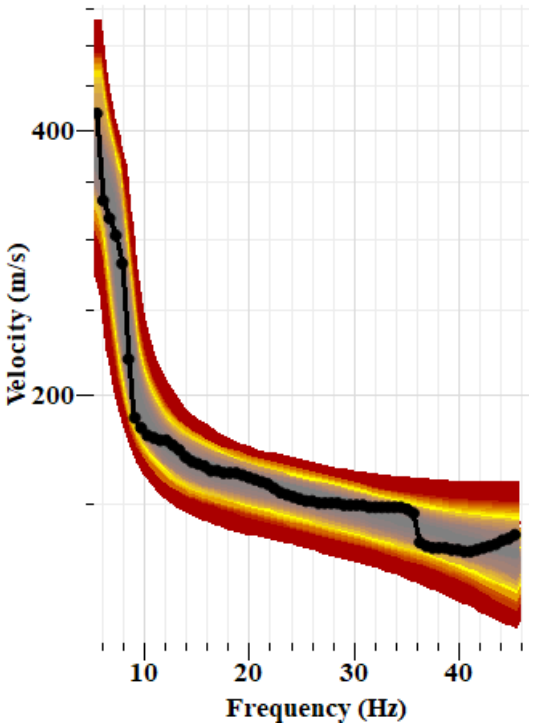

Figure 4.47: Fitting of theoretical dispersion curve to MASW experimental dispersion curve at the deep bedrock site

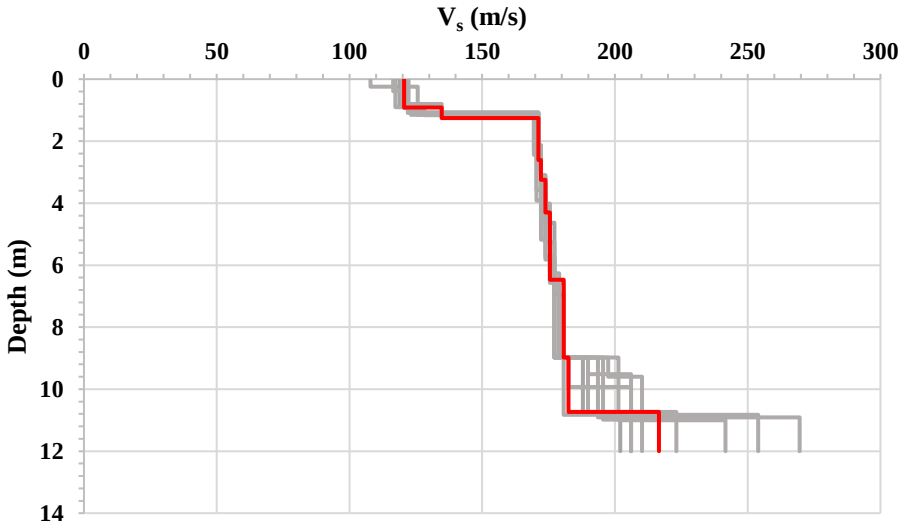

Figure 4.48: Shear wave velocity profile represented by CSW at the deep bedrock site

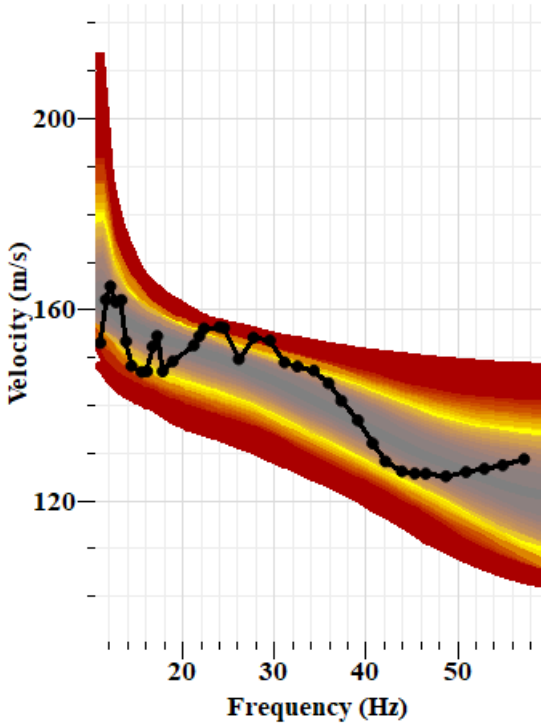

Figure 4.49: Fitting of theoretical dispersion curve to CSW experimental dispersion curve at the deep bedrock site

4.5 Summary

MASW, SASW and CSW data acquired from shallow and deep bedrock sites were analysed and presented in this chapter to compare these three tests. The comparison was in terms of repeatability, susceptibility to near field effects and investigation depth. The tests were compared using the fundamental modes of their dispersion curves. For SASW and CSW the dispersion curves were obtained by using Python codes that were developed for each of them whereas MASW dispersion were obtained by using Geopsy software.

At the shallow bedrock site, the tests seemed to be all fairly repeatable even though for SASW the repeatability was not good for frequencies above 80 Hz in many cases. On the other hand, MASW was repeatable down to a frequency of 10 Hz below which scatter was observed. As for CSW, it was repeatable throughout its entire dispersion range, and this could be attributed to the reliability of the shaker. Also, it was found that near field effects are prevalent in these three tests, however, MASW seemed to be more susceptible to near field effects as there was a significant under estimation of Raleigh phase velocities seen on its dispersion curves. SASW was the second most prone to near field effects and CWS was less affected. SASW was able to investigate deeper and shallower than MASW and CSW.

MASW was able to investigate deeper than CSW, but CSW sampled shallower than MASW.

At the deep bedrock site, the repeatability of the three tests were better than for the shallow bedrock site. For MASW and CSW, the repeatability was seen throughout their dispersion curves whereas for SASW the repeatability was poor for frequencies above 60 - 80 Hz. Near field effects were evident for the three tests, however, MASW1m was strongly affected, followed by SASW, CSW then MASW2m. SASW was found to investigate deeper than MASW and CSW, however, the minimum depths sampled by MASW and SASW were in the same range, and these depths were shallower than those sampled by CSW as the CSW tests generated higher modes at high frequencies.

The performance of MASW2 m was better than that of MASW1m on all the aspects of the study. Furthermore, the 6.3 kg and 9.2 kg sledgehammers produced results that were similar in many regards both at the shallow and deep bedrock sites. It can therefore be concluded that for MASW any sledgehammer weighing between 6.3 kg and 9.2 kg can be used to acquire the same results. Furthermore, for SASW the energy produced by the 2.2 kg sledgehammer was sufficient only up to an offset of 4 m whereas the energy for the 6.3 kg and 9.2 kg sledgehammers was meaningful up to an 8 m offset.

The inversion analysis was also part of this chapter though it was not meant for comparison but to indicate the dispersive modes of the two sites. It was therefore found from the V_s profiles produced by SASW, MASW and CSW that the two sites are normally dispersive.

5 CONCLUSIONS AND RECOMMENDATIONS

5.1 Conclusions

Active seismic tests are used worldwide, however people in different parts of the world often use a specific test based on the availability of the tests and not the capabilities of the tests. Thus, it was important to compare the capabilities of these tests in an unbiased way. This study compared SASW, MASW and CSW in terms of repeatability (reliability), susceptibility to near field effects and depth of investigation both on shallow and deep bedrock sites. After the analysis and the evaluation of the results obtained from the field tests, the following conclusions are made.

At the shallow bedrock site:

- The three tests were found to be repeatable and CSW being the most repeatable throughout its entire dispersion data range. For MASW, scatter was observed for frequencies less than 10 Hz. As for SASW, insignificant difference in dispersion data was seen for frequencies above 80 Hz. Therefore, it is concluded that the three tests are reliable even though their reliability levels differ slightly. However, when geo practitioners conduct any of these three tests, reliability should not be a major concern.
- MASW was found to be more prone to near field effects with MASW1m (1 m geophone spacing) being more affected than MASW2m (2 m geophone spacing). SASW was the second most affected and CSW was the least affected.
- SASW was found to investigate deeper and shallower than MASW and CSW. SASW was able to investigate as deep as 28.8 m and as shallow as 0.55 m. MASW1m sampled to depths of 12.5 m, 15.3 m and 14.0 m deep and as shallow as 2.4 m, 2.0 m and 2.0 m. On the other hand, MASW2m achieved maximum depths of 14.2 m, 19.9 m and 25.0 m and minimum depths of 1.7 m, 1.9 m and 2.4 m. The values were obtained with the 2.2 kg, 6.3 kg and 9.2 kg sledgehammers respectively. CSW attained a maximum depth of 14.1 m and a minimum depth of 1.1 m. It is therefore concluded that for the test methodology adopted for this project, SASW investigated deeper, followed by MASW then CSW. For shallow measurements, SASW sampled shallower, followed by CSW then MASW.

At the deep bedrock site:

- The repeatability was better for the three tests compared with the shallow bedrock site. For MASW and CSW, good repeatability was observed throughout the frequency range of their dispersion data. SASW was also repeatable, however the repeatability was not as good for frequencies above 60 - 80 Hz even though the loss was not that meaningful. Thus, the results of the three tests indicate that just as for the shallow bedrock site, the repeatability of these three tests is not a major concern.
- Near field effects were present but not as severe as for the shallow bedrock site. MASW1m geophones spacing was affected the most, followed by SASW, then CSW. MASW2m showed little near field effects. Therefore, the MASW2m test performed better than at the shallow bedrock site.
- SASW sampled down to a maximum depth of 24.7 m and to a minimum depth of 0.78 m. MASW1m geophone spacing attained maximum depths of 16.5 m, 20.1 m and 19.5 m and shallow depths of 0.91 m, 0.96 m and 0.97 m. MASW2m attained maximum depths of 18.4 m, 21.2 m and 23.6 m and shallow depths of 0.69 m, 0.71 m, 0.70 m. These were obtained with the 2.2 kg, 6.3 kg and 9.2 kg sledgehammers respectively. CSW investigated to a maximum depth of 12.3 m and a minimum depth of 1.1 m. It is concluded that SASW sampled deeper, followed by MASW and then CSW. On the other hand, SASW and MASW sampled roughly to the same minimum depth which was shallower than that of the CSW test.

5.2 Recommendations

Based on the results from the study, the following information is given as recommendations for future research.

- This dissertation compared SASW, MASW and CSW tests using field results; therefore, it is recommended that numerical analysis be conducted to compare the tests to see if the finding of the study can be confirmed.
- The tests should also be compared at noisy sites especially with regard to repeatability to investigate which one is least affected by noise, in order to conclude which tests will perform well on sites where noise cannot be avoided.
- SASW was found to sample deeper than CSW and MASW, but MASW was found to sample deeper with increased geophone spacing. Therefore, it is recommended that SASW be compared with MASW performed with a geophone spacing of more than 2 m to investigate how they compare with respect to investigation depth when a larger MASW array is used.

6 REFERENCES

Alexander, D.R., 1992. *In Situ Material Characterization for Pavement Evaluation by the Spectral-Analysis-of-Surface-Waves (SASW) Method* (No. WES/TR/GL-92-10). Army engineer waterways experiment station Vicksburg ms geotechnical lab.

Aung, A.M.W. and Leong, E.C., 2011. Stiffness profiles of residual soil sites using continuous surface wave method. *Unsaturated Soils: Theory and Practice 2011*.

Bertel, J.D., 2006. *Analytical study of the Spectral-Analysis-of-Surface-Waves method at complex geotechnical sites*. Doctoral dissertation. University of Missouri--Columbia.

Bignardi, S., 2011. *Complete waveform inversion approach to seismic surface waves and adjoint active surfaces.* Doctoral dissertation. Università degli Studi di Ferrara.

Bouazza, A. and Kavazanjian, E., 2000, November. Characterization of municipal solid waste sites using the continuous surface wave method. In *ISRM International Symposium*. International Society for Rock Mechanics and Rock Engineering.

Clayton, C.R., Heymann, G. and Matthews, M.C. 2012. The value of stiffness Measured in field seismic surveys. *International Journal of Geo-Engineering,4(2)*, pp 17-36.

Clayton, C.R., Matthews, M.C. and Simons, N.E. 1982. *Site investigation*. 2nd ed. Granada, London.

Dal Moro, G., Pipan, M. and Gabrielli, P., 2007. Rayleigh wave dispersion curve inversion via genetic algorithms and marginal posterior probability density estimation. *Journal of Applied Geophysics*, *61*(1), pp.39-55.

Foti, S., 2000. *Multistation methods for geotechnical characterization using surface waves*. PhD Thesis. Politecnico di Torino.

Foti, S., 2005. Surface wave testing for geotechnical characterization. *Surface Waves in Geomechanics: Direct and Inverse Modelling for Soils and Rocks* (pp. 47-71). Springer, Vienna.

Foti, S., Hollender, F., Garofalo, F., Albarello, D., Asten, M., Bard, P.Y., Comina, C., Cornou, C., Cox, B., Di Giulio, G. and Forbriger, T., 2018. Guidelines for the good practice of surface wave analysis: A product of the InterPACIFIC project. *Bulletin of Earthquake Engineering*, *16*(6), pp. 2367-2420.

Foti, S., Lai, C., Rix, G.J. and Strobbia, C., 2014. *Surface wave methods for near-surface site characterization*. CRC press, London.

Groenewold, F., 2016. *Comparison of SASW systems for coastal and offshore applications*. Master's Thesis. University of Rhode Island.

Gucunski, N. and Woods, R.D., 1992. Numerical simulation of the SASW test. *Soil dynamics and earthquake engineering*, *11*(4), pp.213-227.

Hebeler, G.L. and Rix, G.J., 2001. Site characterization in Shelby County, Tennessee using advanced surface wave methods. *MAE Center CD Release 06-02*.

Heisey, J.S., Stokoe, K.H., Hudson, W.R. and Meyer, A.H., 1981. *Determination of in situ shear wave velocities from spectral analysis of surface waves*. Master's thesis. University of Texas at Austin.

Heymann, G., 2007. Ground stiffness measurement by the continuous surface wave test. *Journal of the South African Institution of Civil Engineering*, 49(1), pp.25-31.

Hunter, J.A.M. and Crow, H.L., 2015. *Shear wave velocity measurement guidelines for Canadian seismic site characterization in soil and rock*. Natural Resources Canada.

Hwang, S., 2014. *Experimental investigation of near-field effects on the SASW dispersion curve*. Doctoral dissertation. University of Texas at Austin.

Joh, S.H., Hwang, S.K. and Nayan, K.A.M., 2011, January. Real-time spatial profiling of subgrade stiffness for quality assurance of field compaction. *The 90th Annual Meeting of the Transportation Research Board, Washing ton, DC, January*, pp. 1-20.

Kim, D.S., Park, H.J. and Bang, E.S., 2013. Round Robin test for comparative study of in-situ seismic tests. *Geotechnical and Geophysical Site Characterization: Proceedings of the 4th International Conference on Site Characterization ISC-4*, Vol. 1, pp. 1427-1434. Taylor & Francis Books Ltd.

Lin, C.P., Lin, C.H. and Chien, C.J., 2017. Dispersion analysis of surface wave testing–SASW vs. MASW. *Journal of Applied Geophysics*, *143*, pp.223-230.

Lin, Y.C., 2007. *Characterizing Vs profiles by the SASW method and comparison with other seismic methods*. Doctoral dissertation. University of Texas at Austin.

Look, B.G., 2007. *Handbook of geotechnical investigation and design tables*. Taylor & Francis, London, UK.

Matthews, M.C., Hope, V.S. and Clayton, C.R.I., 1996. The use of surface waves in the determination of ground stiffness profiles. *International Journal of Rock Mechanics and Mining Sciences and Geomechanics Abstracts*, Vol. 8, No. 33, pp. 360A-361A.

McCaskill, A., 2014. *A Study on the benefits of including near-field effects in active-source surface wave data collection and interpretation*. Doctoral dissertation. University of Missouri--Columbia.

Mothkuri, R.P., 2014. *Non-destructive SASW Evaluation of Controlled Low Strength Material As A Pipeline Bedding Material*. Master's thesis. University of Texas at Arlington.

Olafsdottir, E.A., Erlingsson, S. and Bessason, B., 2017. Tool for analysis of multichannel analysis of surface waves (MASW) field data and evaluation of shear wave velocity profiles of soils. *Canadian Geotechnical Journal*, *55(2)*, pp.217-233.

Olafsdottir, E.A., Bessason, B. and Erlingsson, S., 2018. Combination of dispersion curves from MASW measurements. *Soil Dynamics and Earthquake Engineering*, *113*, pp.473-487.

Omar, M.N., Abbiss, C.P., Taha, M.R. and Nayan, K.A.M., 2011. Prediction of long-term settlement on soft clay using shear wave velocity and damping characteristics. *Engineering geology*, *123*(4), pp.259-270.

Park, C.B., Miller, R.D. and Miura, H., 2002. Optimum field parameters of an MASW survey. *Proceedings of the Society of Exploration Geophysicists*, pp.22-23.

Park, C.B., Miller, R.D. and Xia, J., 1998. Imaging dispersion curves of surface waves on multi-channel record. *SEG Technical Program Expanded Abstracts 1998* (pp. 1377-1380). Society of Exploration Geophysicists.

Stokoe, K.H., Joh, S.H. and Woods, R.D., 2004, September. Some contributions of in situ geophysical measurements to solving geotechnical engineering problems. *Proceedings International Conference on Site Characterization ISC-2*, pp. 97-132.

Strobbia, C., 2003. *Surface wave methods. Acquisition, processing and inversion*. PhD Thesis. Politecnico di Torino.

Svensson, M. and Möller, B., 2001. *Geophysics in soil mechanics-in situ shear moduli determined by SASW-technique and more traditional geotechnical methods*. Swedish Geotechnical Institute. Report No.508. Linkoping.

Wathelet, M., Jongmans, D. and Ohrnberger, M., 2004. Surface-wave inversion using a direct search algorithm and its application to ambient vibration measurements. *Near surface geophysics*, *2*(4), pp.211-221.

Yoon, S. and Rix, G.J., 2009. Near-field effects on array-based surface wave methods with active sources. *Journal of Geotechnical and Geoenvironmental Engineering*, *135*(3), pp.399-406.

Zahari, M.N.H., 2014. *Development of Testing System Based on Surface Wave Spectral Analysis (SASW) Technique*. Doctoral dissertation. Universiti Tun Hussein Onn Malaysia.

Zywicki, D.J. and Rix, G.J., 2005. Mitigation of near-field effects for seismic surface wave velocity estimation with cylindrical beamformers. *Journal of geotechnical and geoenvironmental engineering*, *131*(8), pp.970-977.

7 APPENDIX A: DETAILED DATA FOR SHALLOW BEDROCK SITE

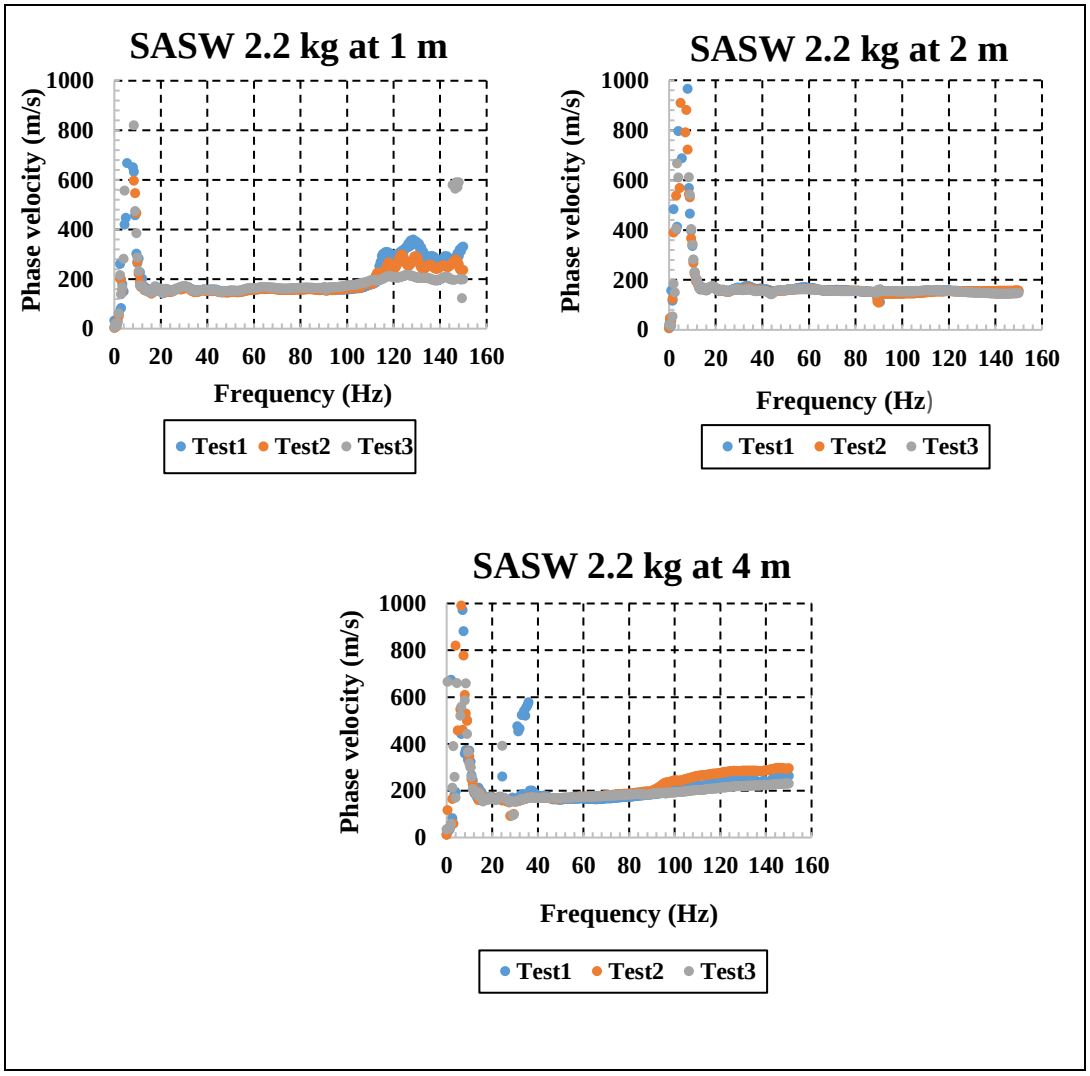

Figure 7.1: SASW repeatability dispersion curves for 2.2 kg sledgehammer at the shallow bedrock site

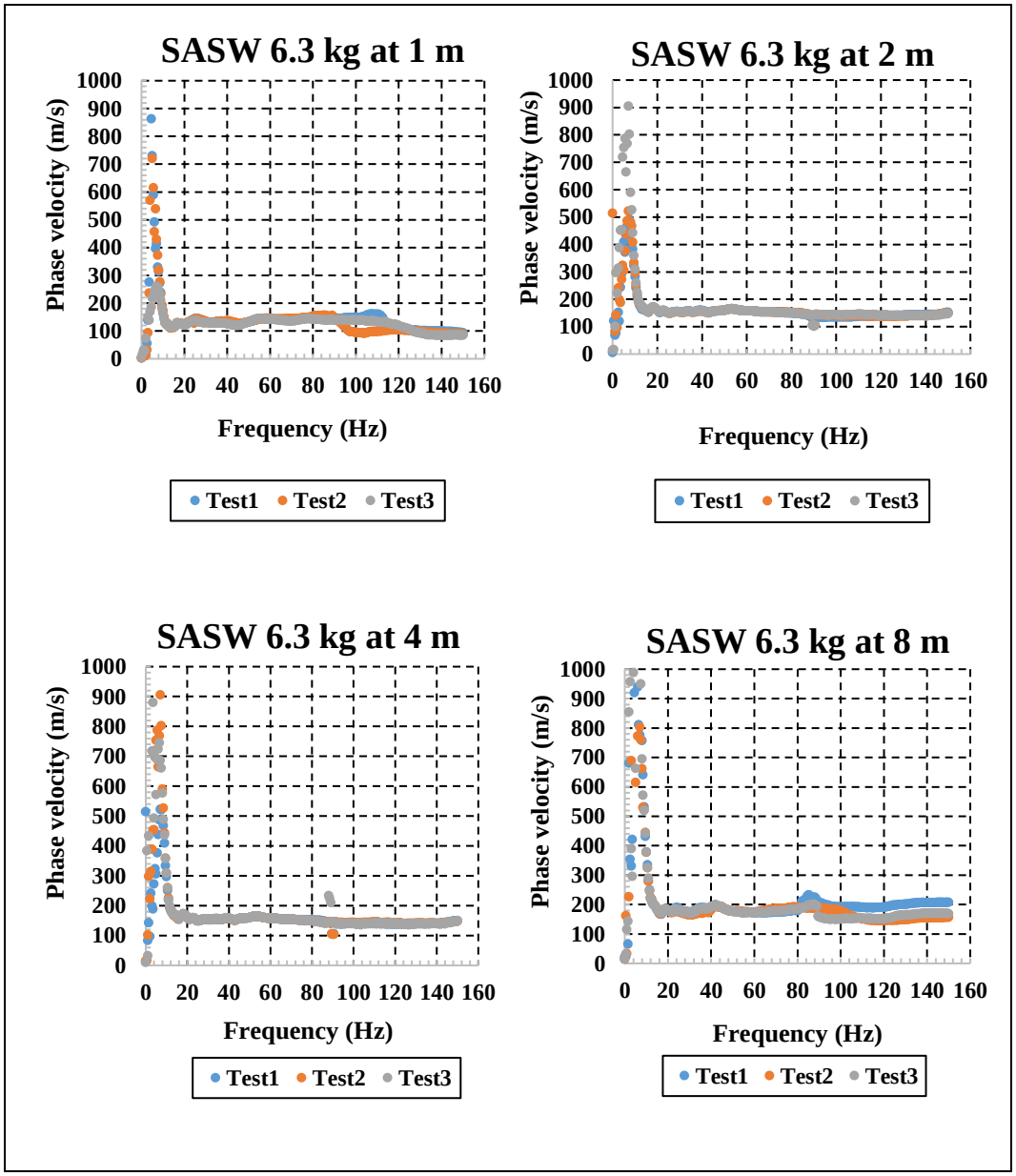

Figure 7.2: SASW repeatability dispersion curves for 6.3 kg sledgehammer at the shallow bedrock site

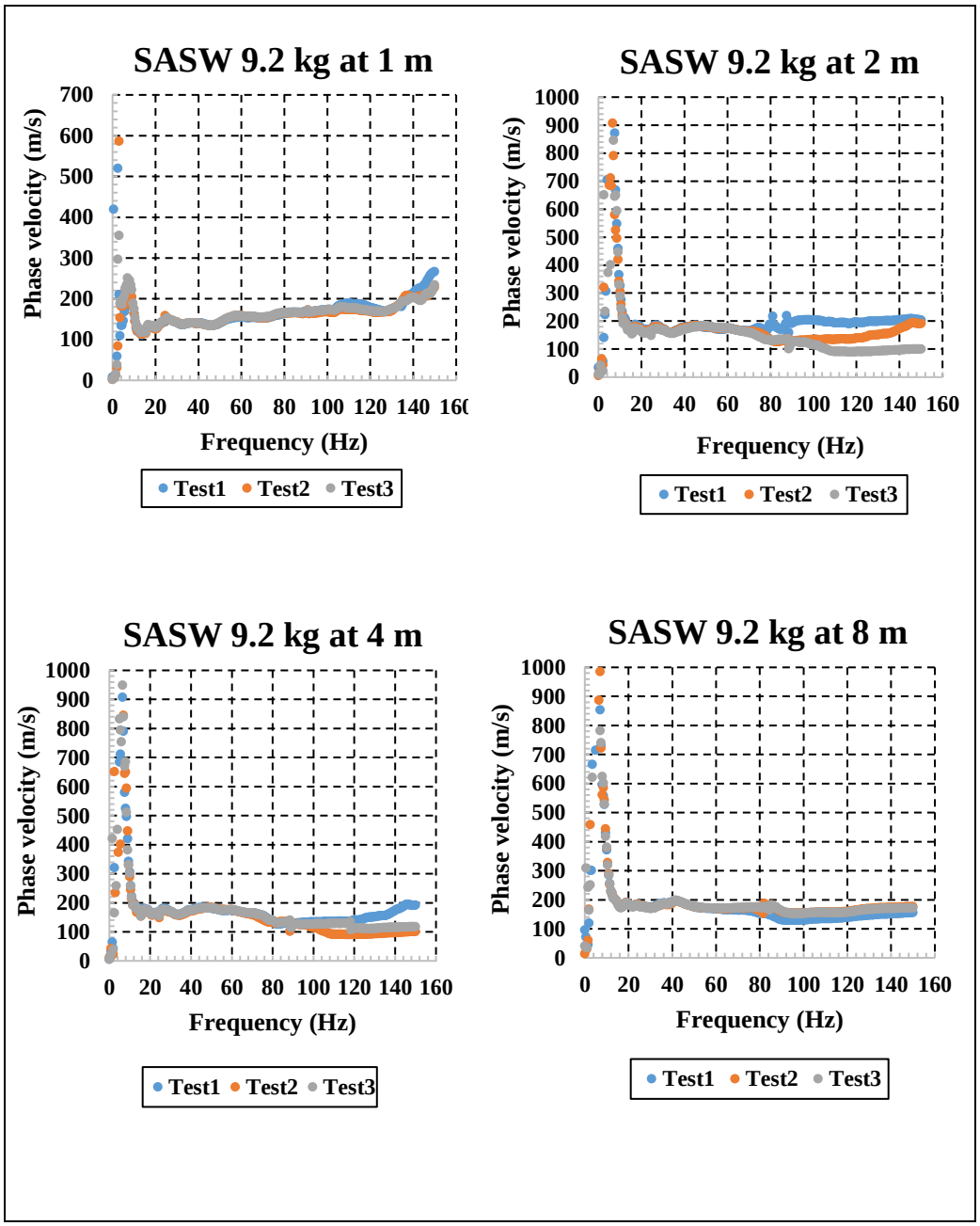

Figure 7.3: SASW repeatability dispersion curves for 9.2 kg sledgehammer at the shallow bedrock site

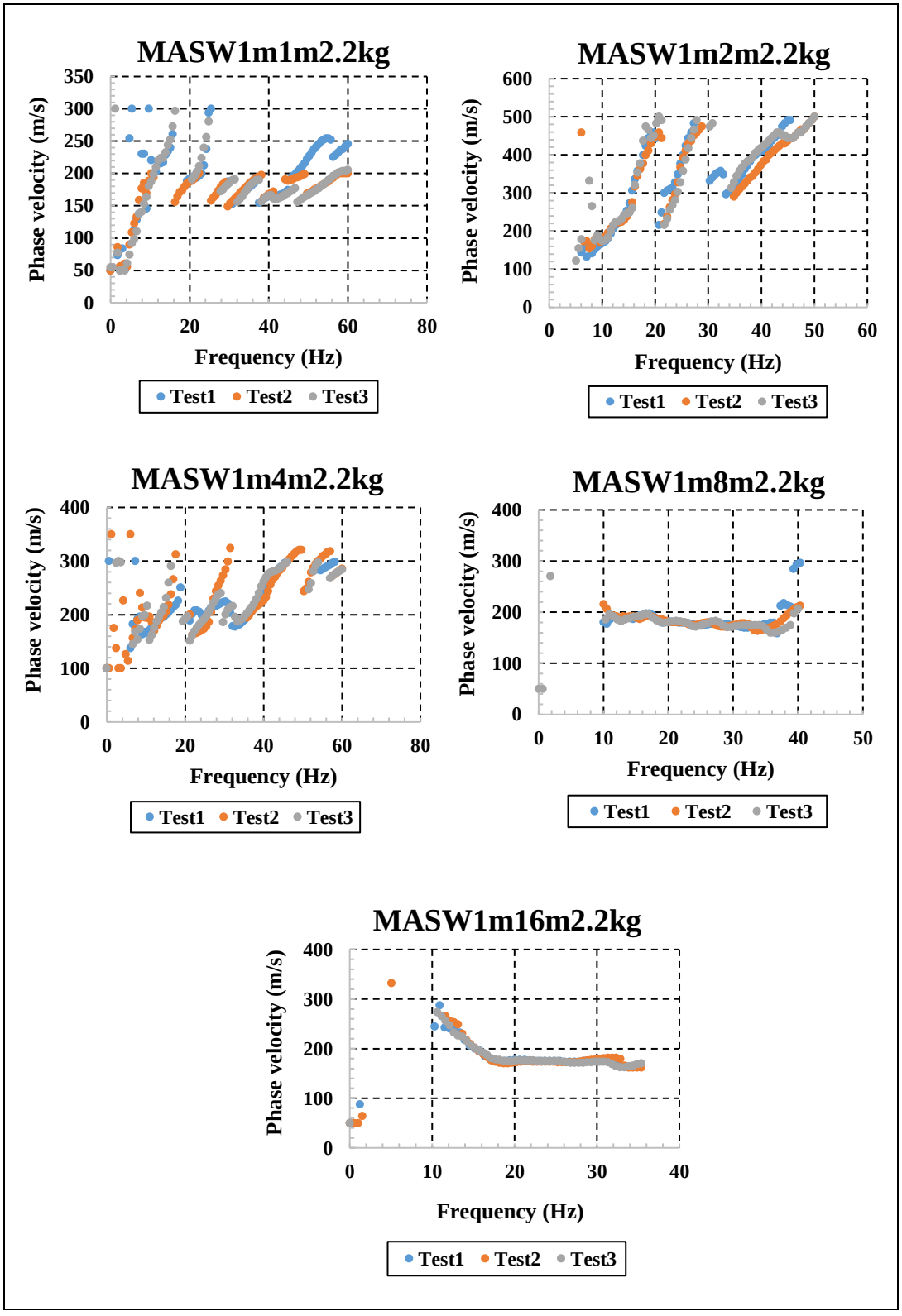

Figure 7.4: MASW1m repeatability dispersion curves for 2.2 kg sledgehammer at the shallow bedrock site

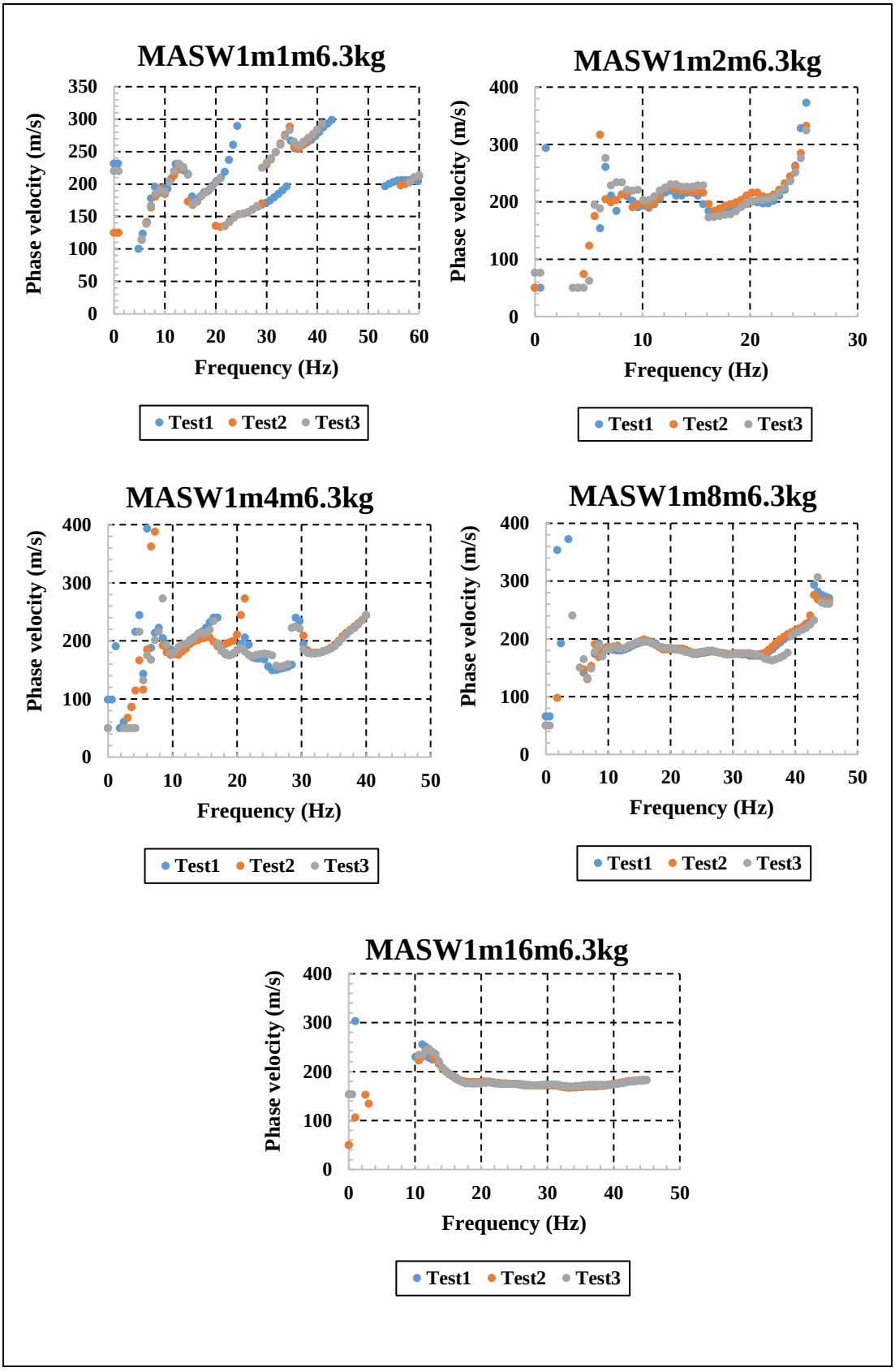

Figure 7.5: MASW1m repeatability dispersion curves for 6.3 kg sledgehammer at the shallow bedrock site

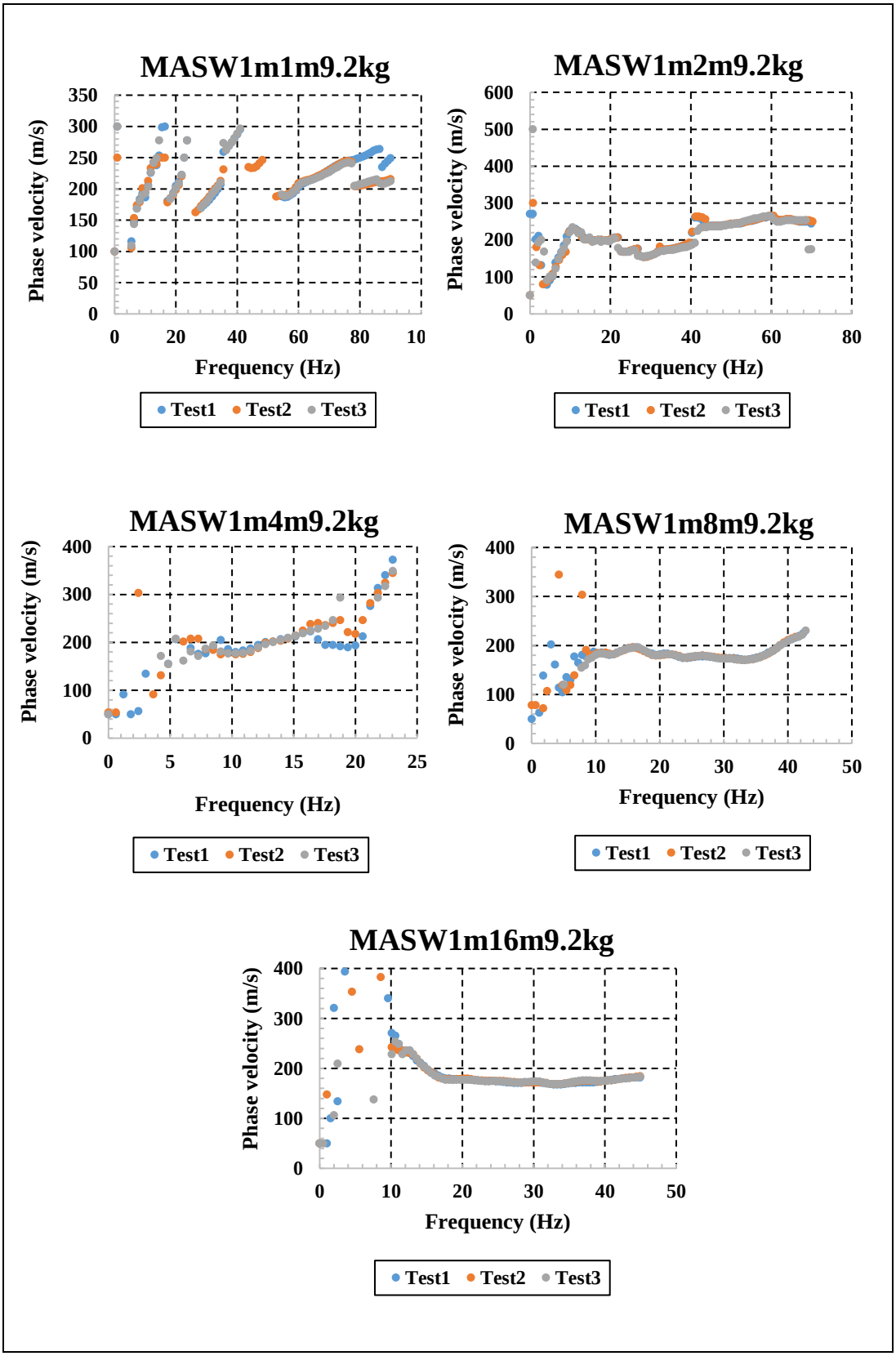

Figure 7.6: MASW1m repeatability dispersion curves for 9.2 kg sledgehammer at the shallow bedrock site

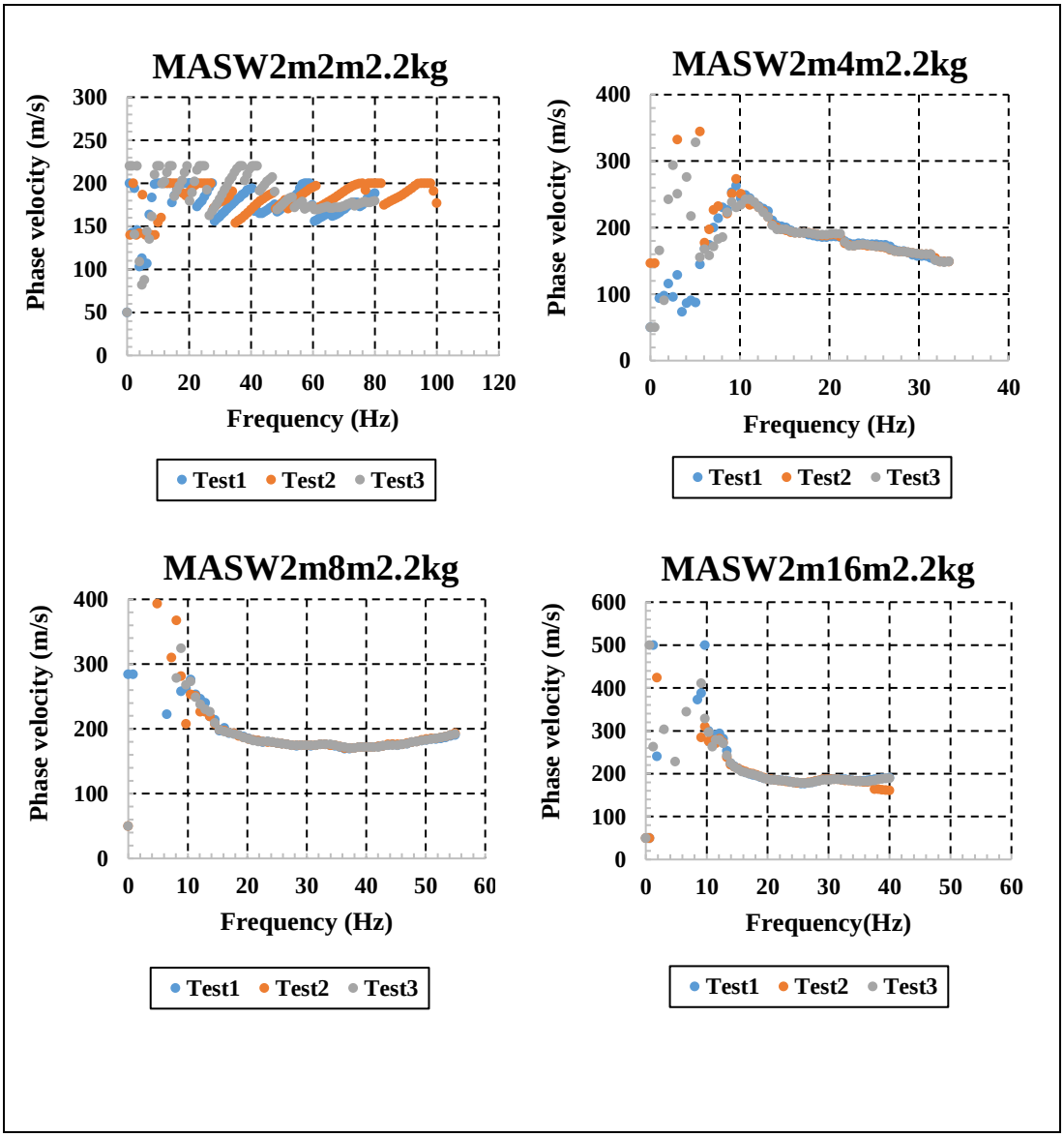

Figure 7.7: MASW2m repeatability dispersion curves for 2.2 kg sledgehammer at the shallow bedrock site

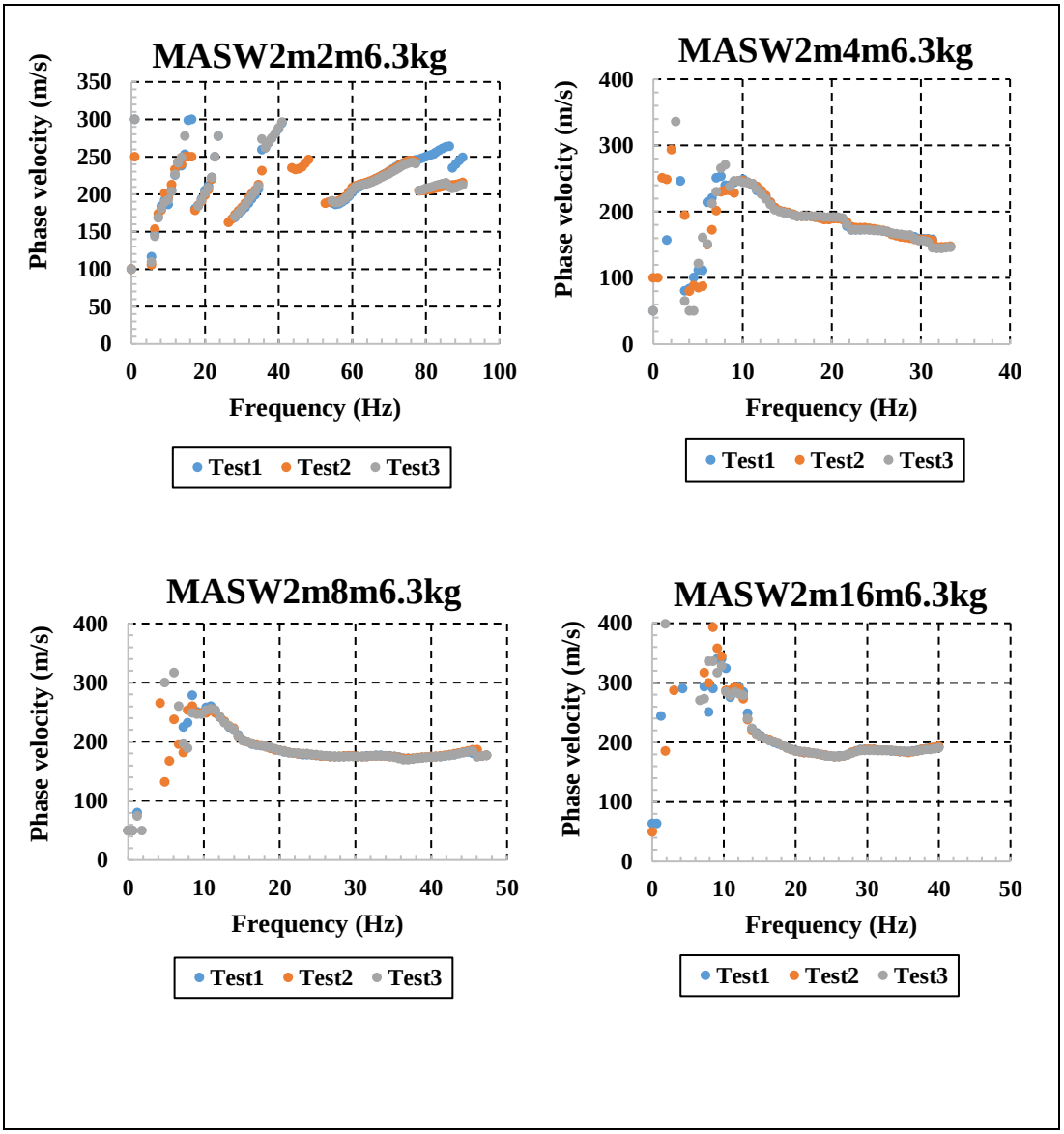

Figure 7.8: MASW2m repeatability dispersion curves for 6.3 kg sledgehammer at the shallow bedrock site

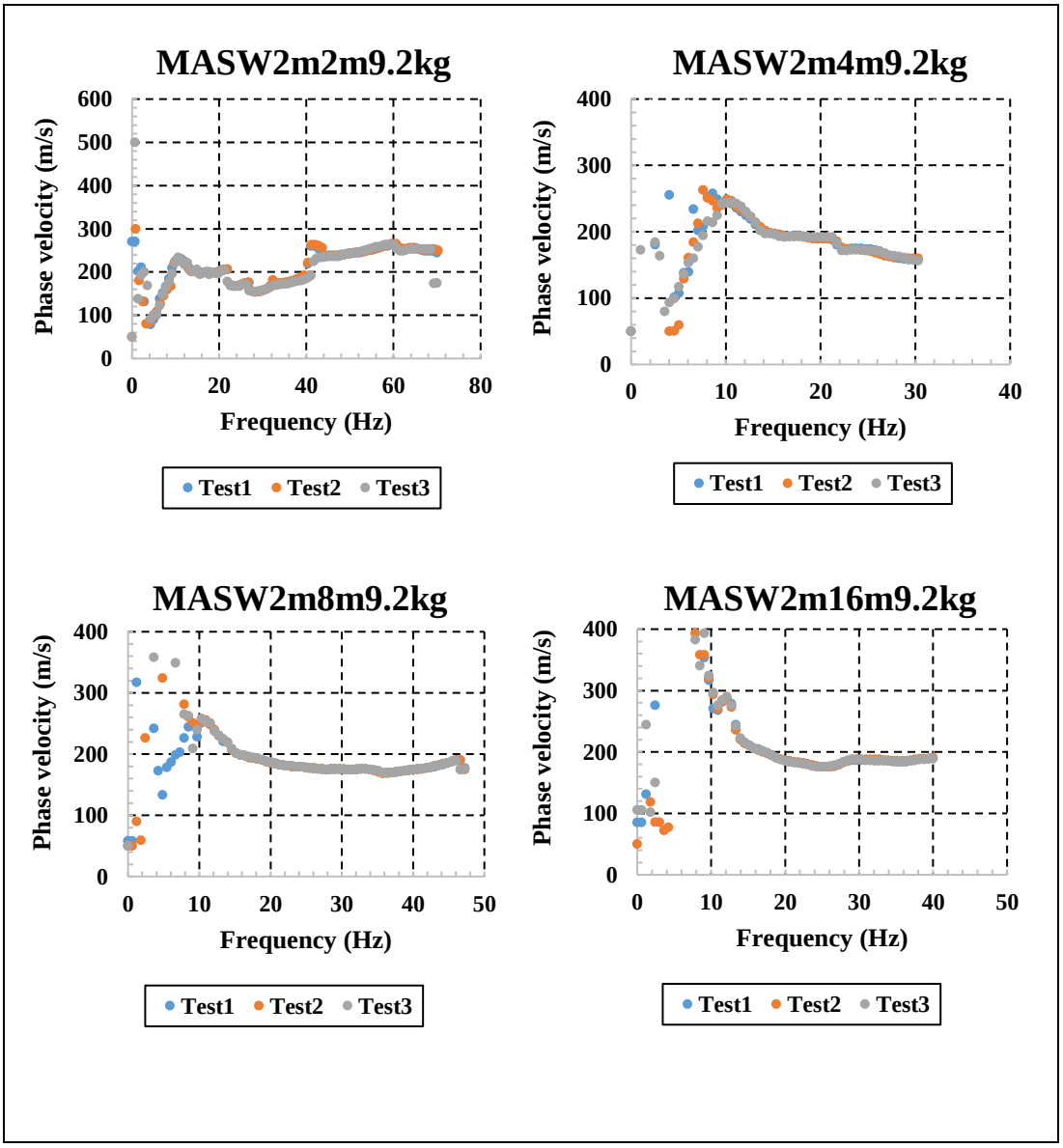

Figure 7.9: MASW2m repeatability dispersion curves for 9.2 kg sledgehammer at the shallow bedrock site

Table 7.1: SASW sampling depths at the shallow bedrock site

Test number	Sampling depth (m)	
	minimum	maximum
1	0.55	29.5
2	0.52	29.0
3	0.57	28.0
-	Average minimum depth (m)	Average maximum depth (m)
	0.55	28.8

Table 7.2: MASW1m sampling depths at the shallow bedrock site with 2.2 kg sledgehammer

Source type	Source offset (m)	Sampling depth (m)					
		Test1		Test2		Test3	
		min	max	min	max	min	max
2.2 kg Sledge hammer	1.00	-	-	-	-	-	-
	2.00	-	-	-	-	-	-
	4.00	-	-	-	-	-	-
	8.00	2.5	10.8	2.4	9.0	2.3	9.0
	16.00	2.4	13.2	2.3	11.4	2.4	12.9
	offset (m)	Average min depth (m)			Average max depth (m)		
	8.00	2.4			9.6		
	16.00	2.4			12.5		

Table 7.3: MASW1m sampling depths at the shallow bedrock site with 6.3 kg sledgehammer

Source type	Source offset (m)	Sampling depth (m)					
		Test1		Test2		Test3	
		min	max	min	max	min	max
6.3 kg Sledge hammer	1.00	5.1	9.1	5.9	9.1	5.9	9.1
	2.00	5.4	14.9	5.6	15.6	5.6	15.5
	4.00	2.9	13.7	5.3	13.7	2.9	13.7
	8.00	2.7	11.1	2.7	11.1	2.7	11.1
	16.00	2.0	11.5	2.0	10.5	2.0	10.2
	offset (m)	Average min depth (m)			Average max depth (m)		
	1.00	5.6			9.1		
	2.00	5.5			15.3		
	4.00	3.7			13.7		
	8.00	2.7			11.1		
	16.00	2.0			10.7		

Table 7.4: MASW1m sampling depths at the shallow bedrock site with 9.2 kg sledgehammer

Source type	Source offset (m)	Sampling depth (m)					
		Test1		Test2		Test3	
		min	max	min	max	min	max
9.2 kg Sledge hammer	1.00	-	-	-	-	-	-
	2.00	5.5	13.2	5.5	13.2	5.5	13.2
	4.00	5.2	14.1	5.4	16.6	6.8	11.4
	8.00	2.7	11.5	2.6	9.9	2.7	8.2
	16.00	2.0	13.4	2.0	12.1	2.0	12.0
	offset (m)	**Average min depth (m)**			**Average max depth (m)**		
	2.00	5.5			13.2		
	4.00	5.8			14.0		
	8.00	2.7			9.9		
	16.00	2.0			12.5		

Table 7.5: MASW2m sampling depths at the shallow bedrock site with 2.2 kg sledgehammer

Source type	Source offset (m)	Sampling depth (m)					
		Test1		Test2		Test3	
		min	max	min	max	min	max
2.2 kg Sledge hammer	2.00	-	-	-	-	-	-
	4.00	2.2	15.6	2.2	14.2	2.2	10.9
	8.00	1.8	13.7	1.8	12.1	1.8	13.8
	16.00	1.7	14.6	1.7	16.0	1.7	12.1
	32.00	-	-	-	-	-	-
	offset (m)	**Average min depth (m)**			**Average max depth (m)**		
	4.00	2.2			13.6		
	8.00	1.8			13.2		
	16.00	1.7			14.2		

Table 7.6: MASW2m sampling depths at the shallow bedrock site with 6.3 kg sledgehammer

Source type	Source offset (m)	Sampling depth (m)					
		Test1		Test2		Test3	
		min	max	min	max	min	max
6.3 kg Sledge hammer	2.00	4.7	10.9	4.7	10.9	4.7	10.9
	4.00	4.4	12.9	4.4	12.9	4.4	13.5
	8.00	1.9	16.4	1.9	16.1	1.9	14.7
	16.00	2.4	18.7	2.4	19.7	2.4	21.3
	32.00	-	-	-	-	-	-
	offset (m)	**Average min depth (m)**			**Average max depth (m)**		
	2.00	4.7			10.9		
	4.00	4.4			13.1		
	8.00	1.9			15.7		
	16.00	2.4			19.9		

Table 7.7: MASW2m sampling depths at the shallow bedrock site with 9.2 kg sledgehammer

Source type	Source offset (m)	Sampling depth (m)					
		Test1		Test2		Test3	
		min	max	min	max	min	max
9.2 kg Sledge hammer	2.00	4.7	11.0	4.7	11.0	4.7	11.0
	4.00	5.3	15.7	5.3	17.4	5.3	12.6
	8.00	4.1	17.9	4.1	15.4	4.1	16.8
	16.00	2.4	25.7	2.4	25.0	2.4	24.3
	32.00	-	-	-	-	-	-
	offset (m)	**Average min depth (m)**			**Average max depth (m)**		
	2.00	4.7			11.0		
	4.00	5.3			15.2		
	8.00	4.1			16.7		
	16.00	2.4			25.0		

Table 7.8: CSW sampling depths at the shallow bedrock site

Source offset (m)	Sampling depth (m)					
	Test1		Test2		Test3	
	min(m)	max(m)	min(m)	max(m)	min	max
1.00	1.2	13.0	1.2	13.0	1.2	13.0
2.00	1.1	13.3	1.1	13.6	1.1	13.6
4.00	1.3	14.3	1.2	14.1	1.2	14.0

offset (m)	Average min depth (m)	Average max depth (m)
1.00	1.2	13.0
2.00	1.1	13.5
4.00	1.2	14.1

8 APPENDIX B: DETAILED DATA FOR DEEP BEDROCK SITE

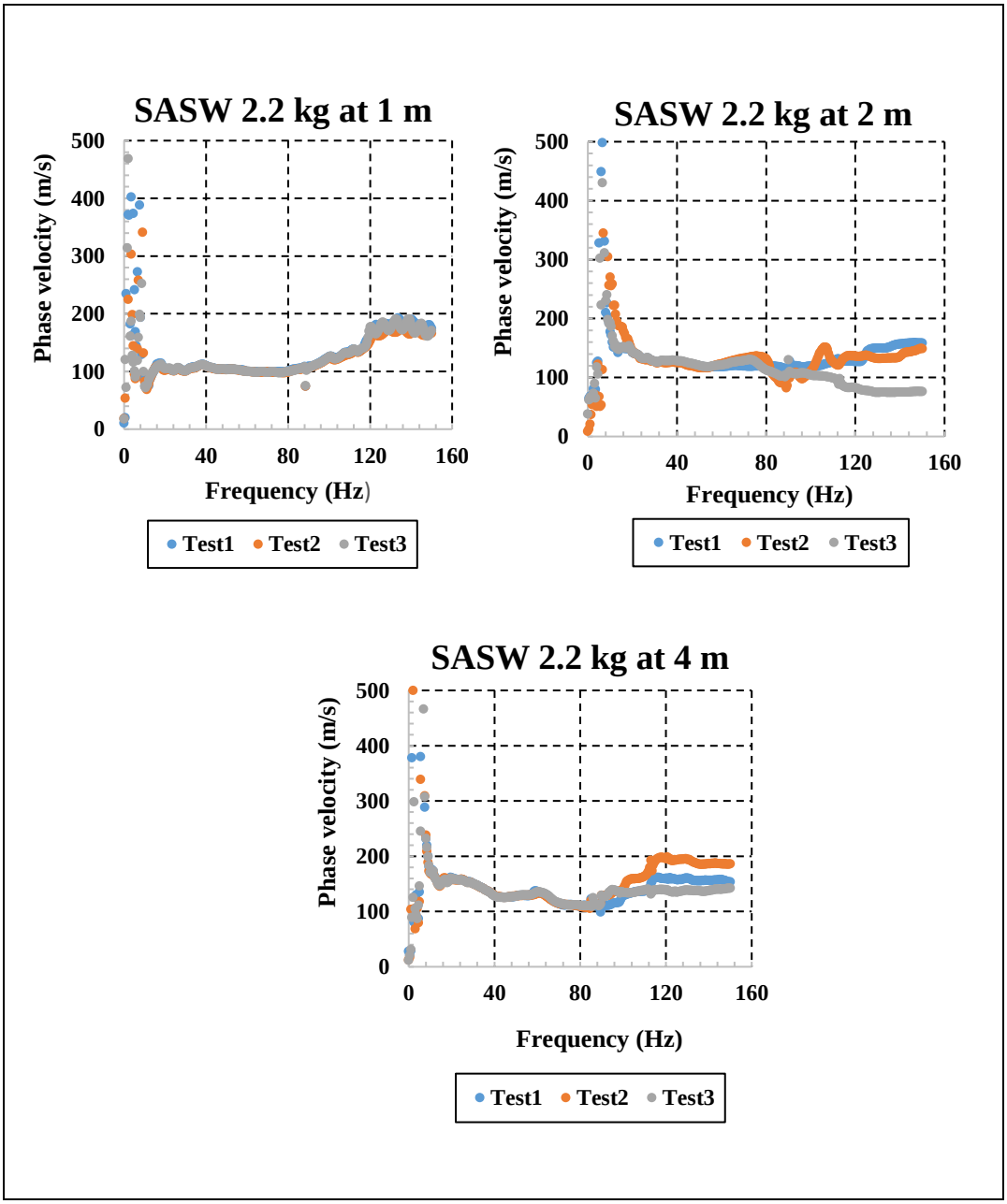

Figure 8.1: SASW repeatability dispersion curves for 2.2 kg sledgehammer at the deep bedrock site

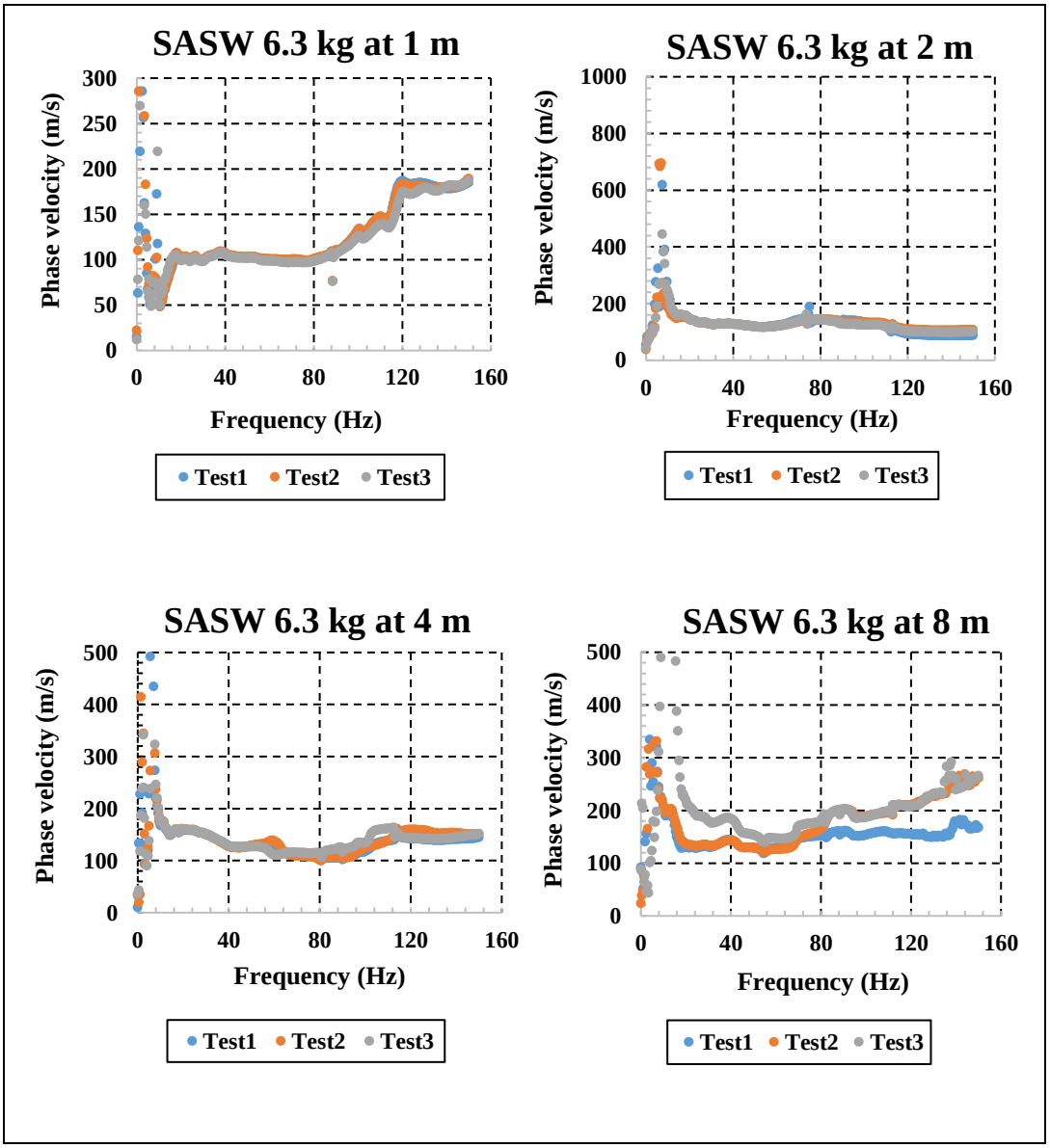

Figure 8.2: SASW repeatability dispersion curves for 6.3 kg sledgehammer at the deep bedrock site

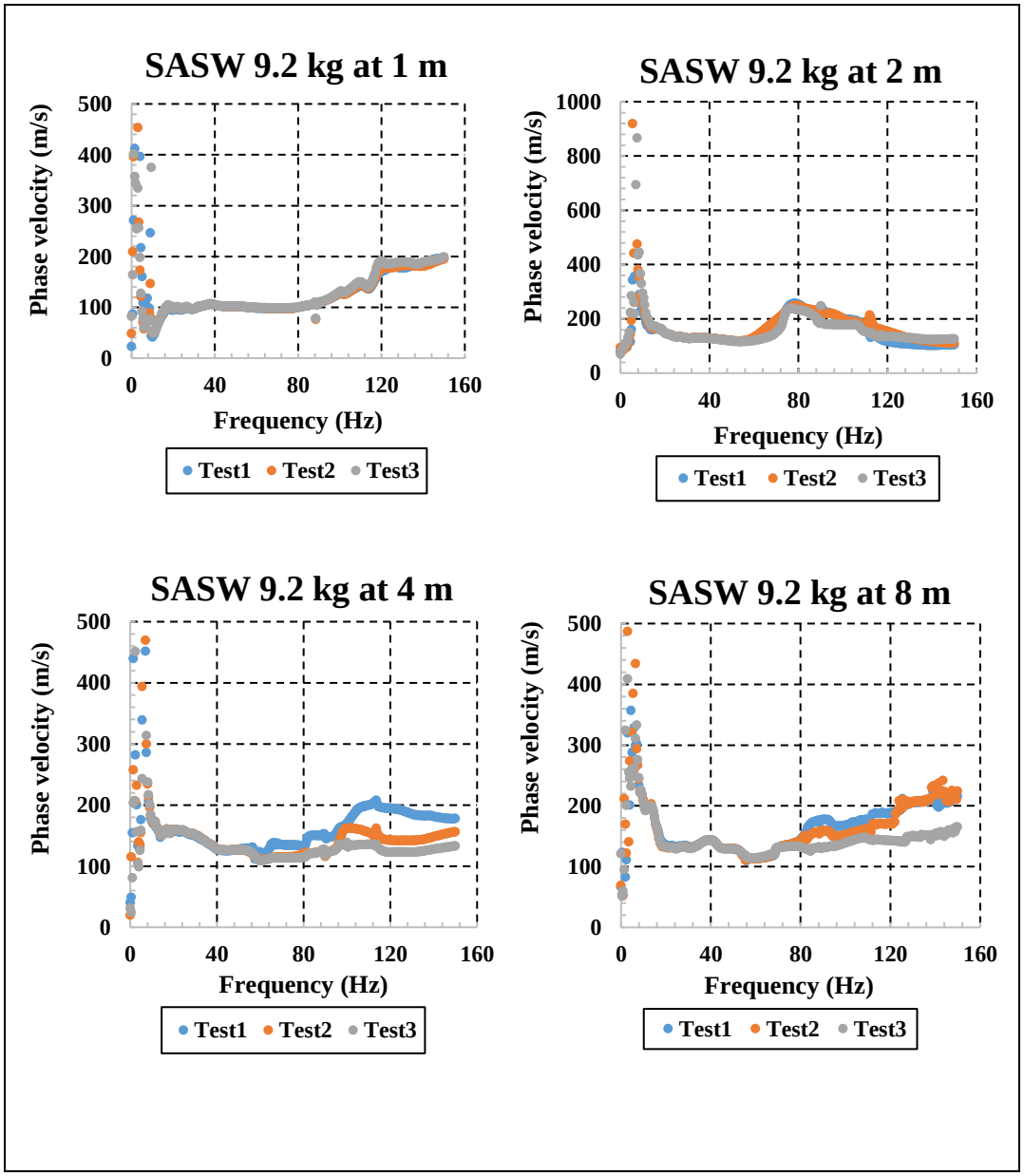

Figure 8.3: SASW repeatability dispersion curves for 9.2 kg sledgehammer at the deep bedrock site

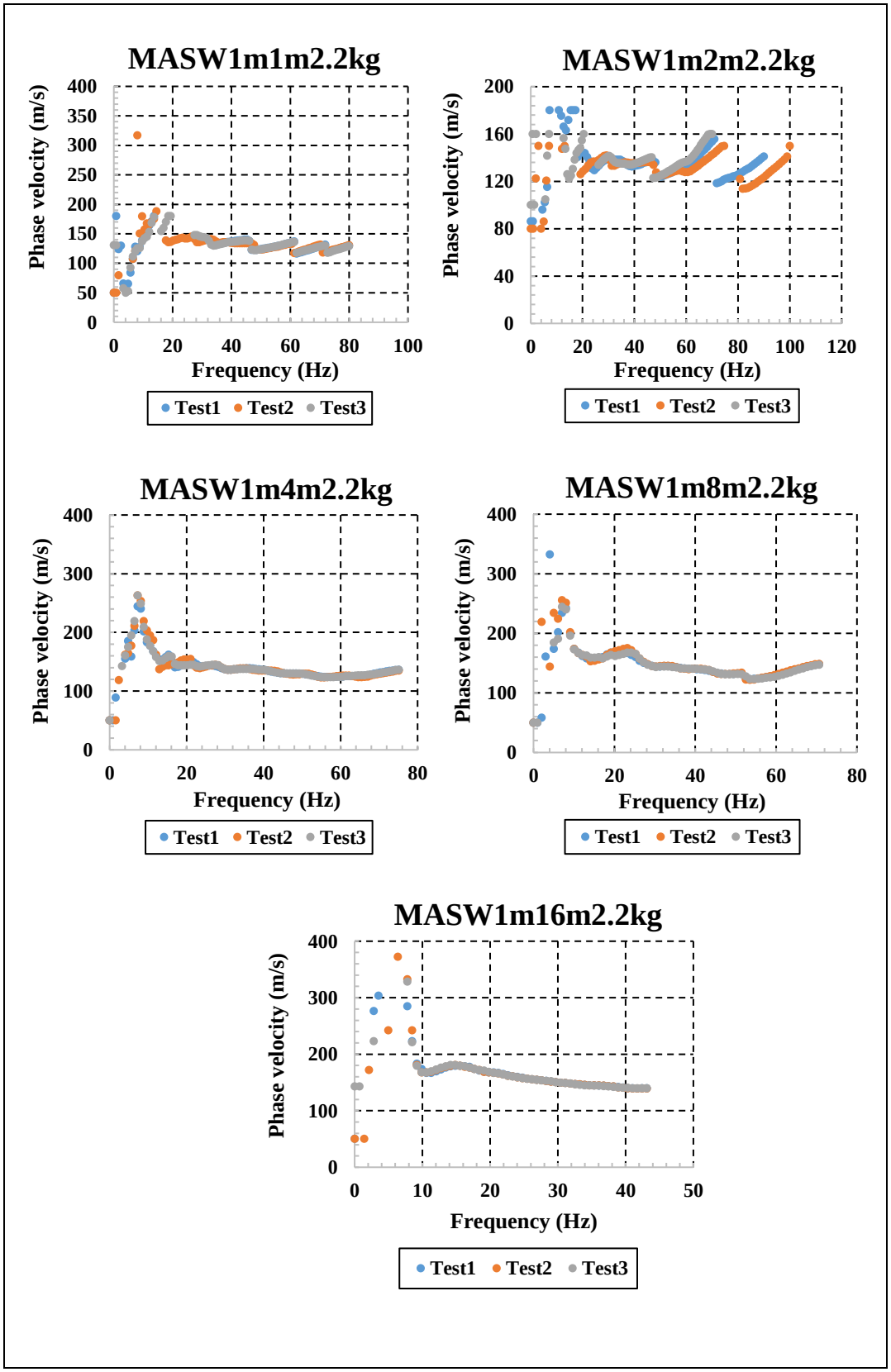

Figure 8.4: MASW1m repeatability dispersion curves for 2.2 kg sledgehammer at the deep bedrock site

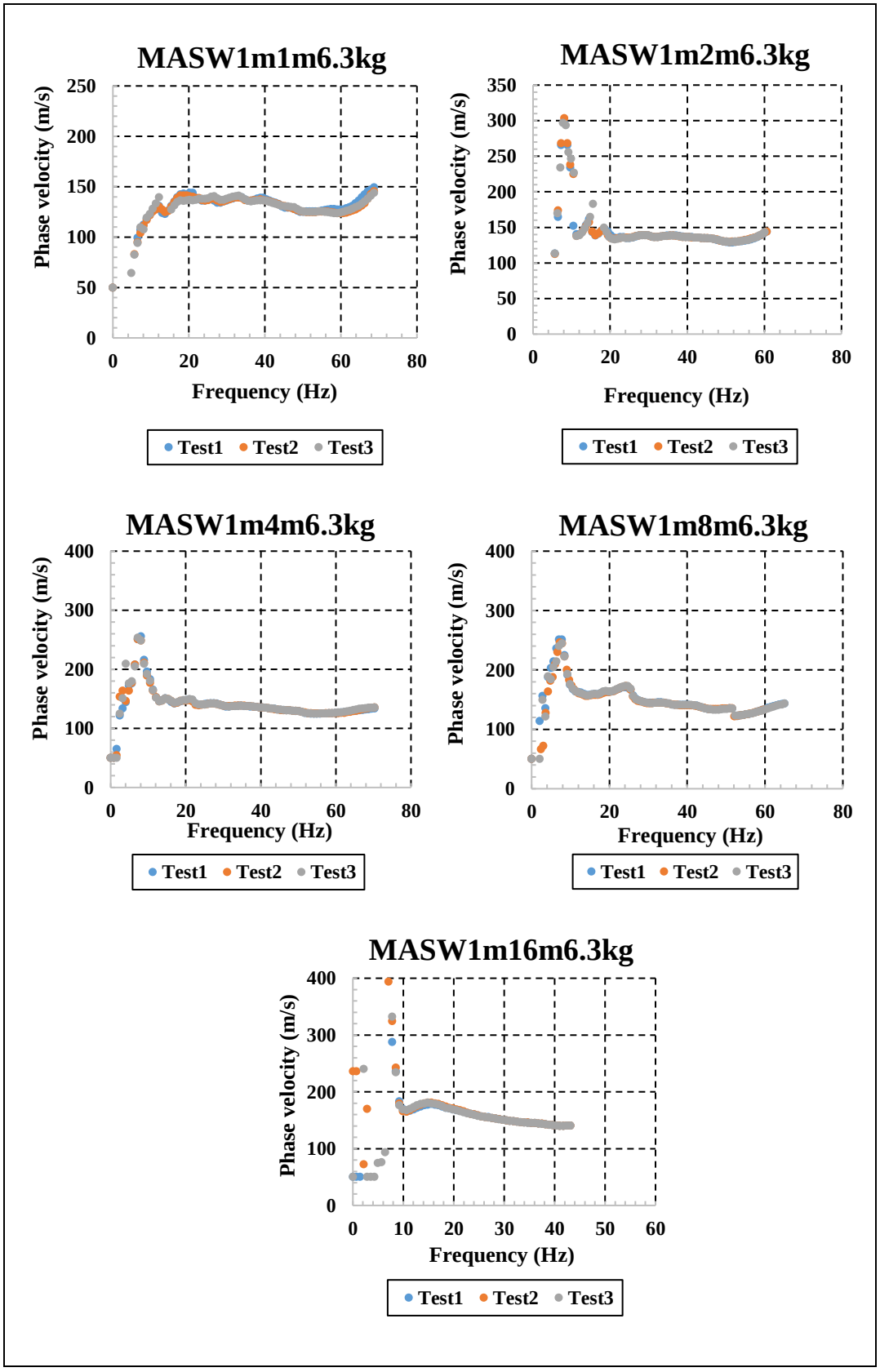

Figure 8.5: MASW1m repeatability dispersion curves for 6.3 kg sledgehammer at the deep bedrock site

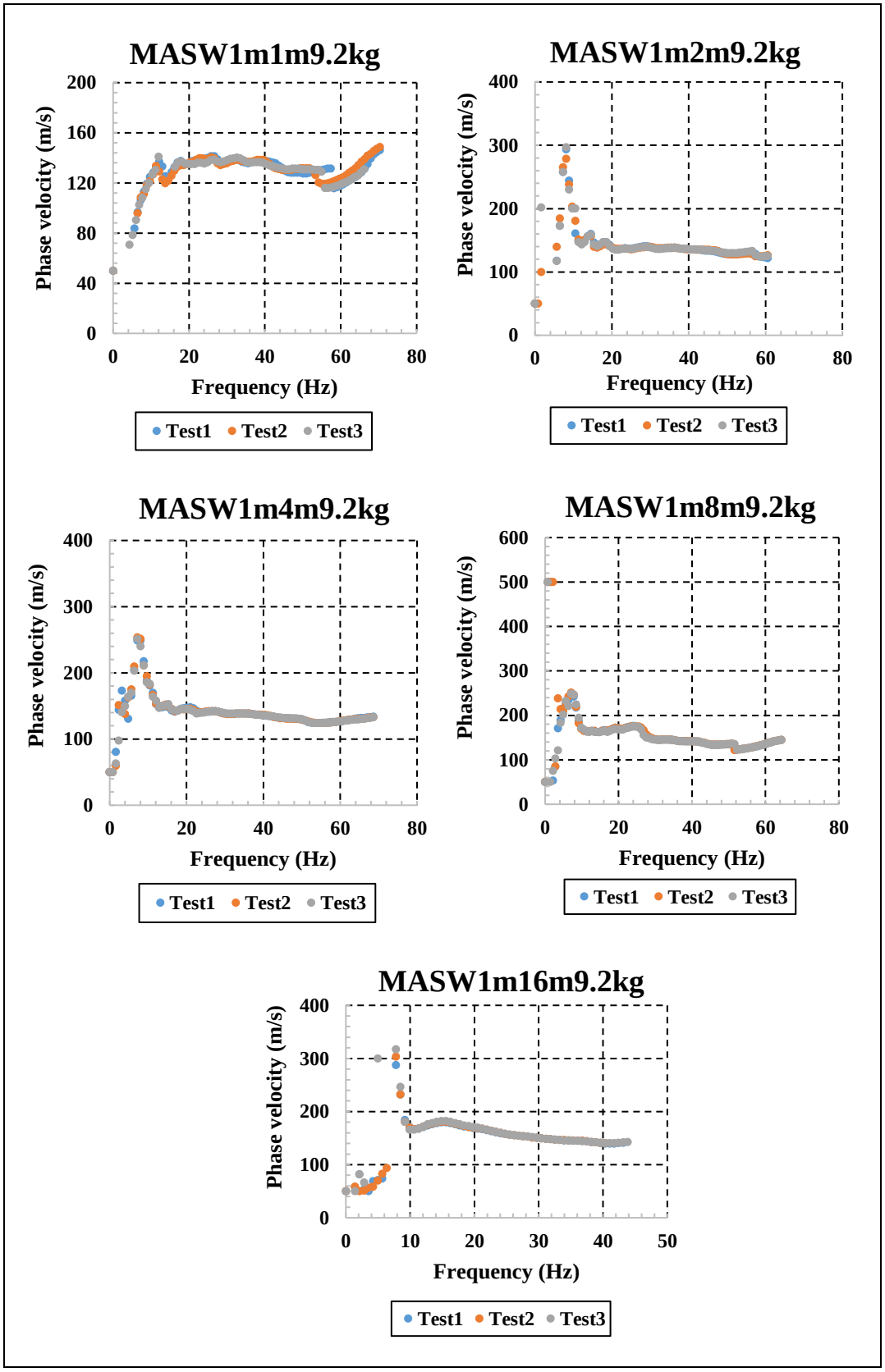

Figure 8.6: MASW1m repeatability dispersion curves for 9.2 kg sledgehammer at the deep bedrock site

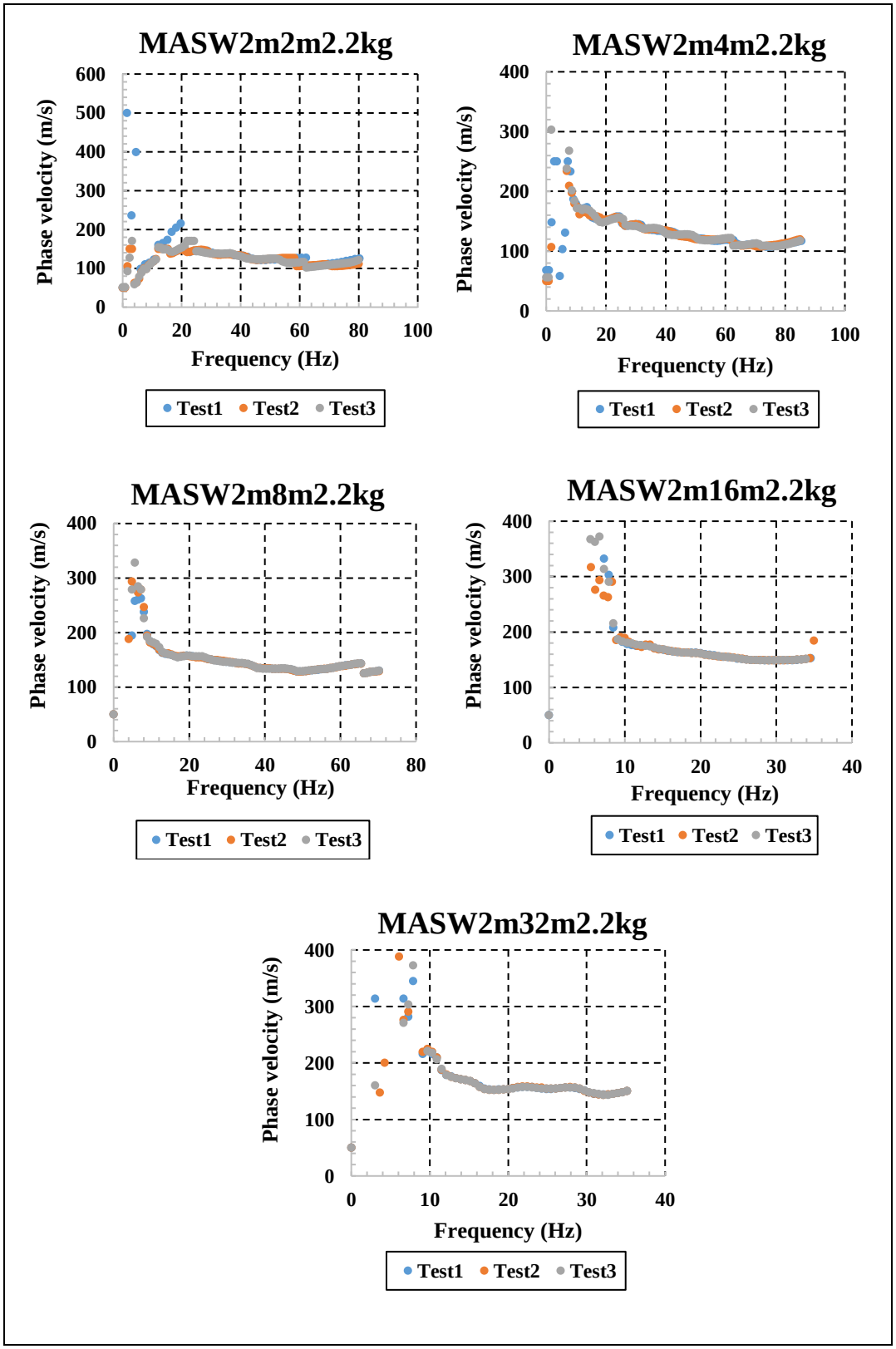

Figure 8.7: MASW2m repeatability dispersion curves for 2.2 kg sledgehammer at the deep bedrock site

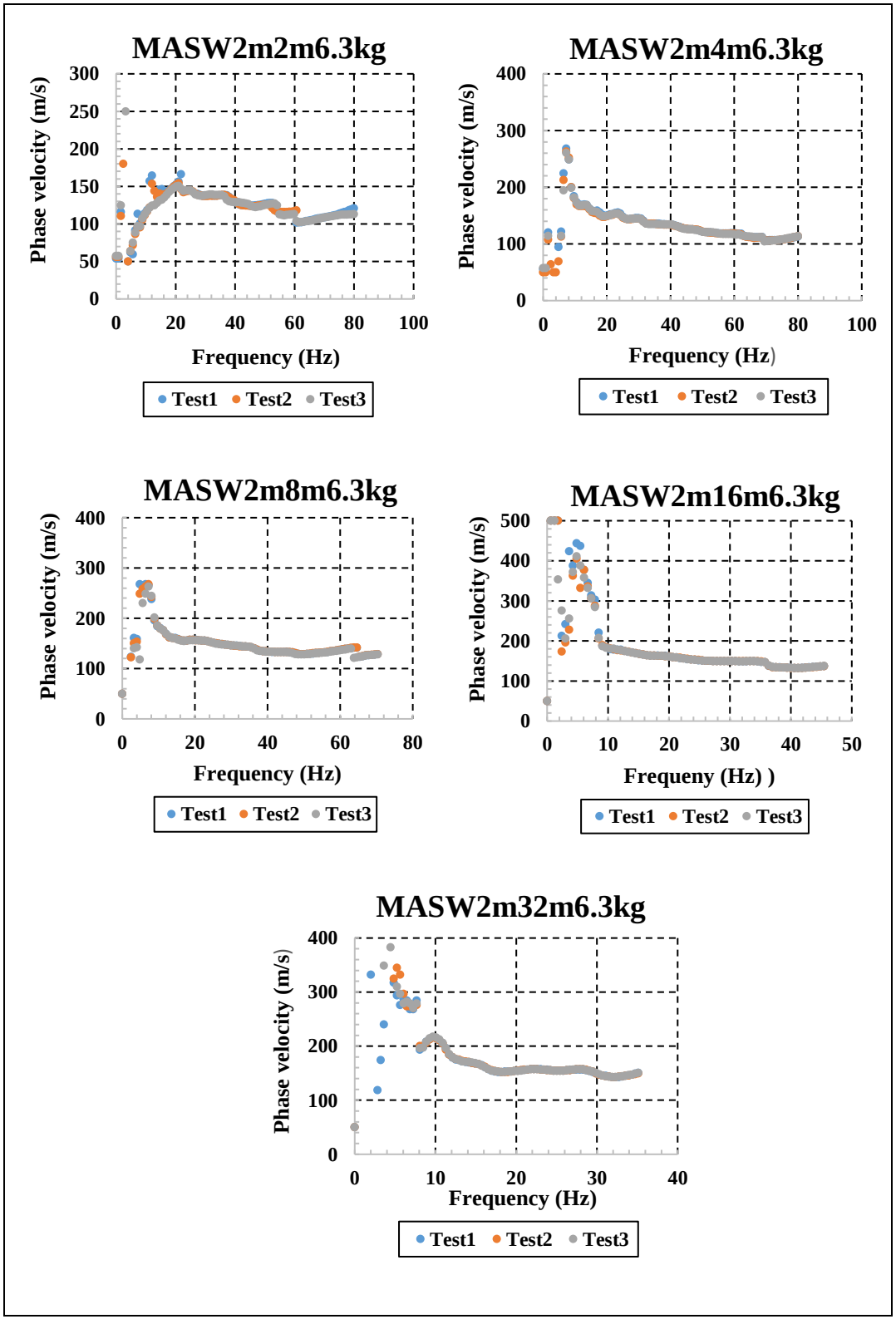

Figure 8.8: MASW2m repeatability dispersion curves for 6.3 kg sledgehammer at the deep bedrock site

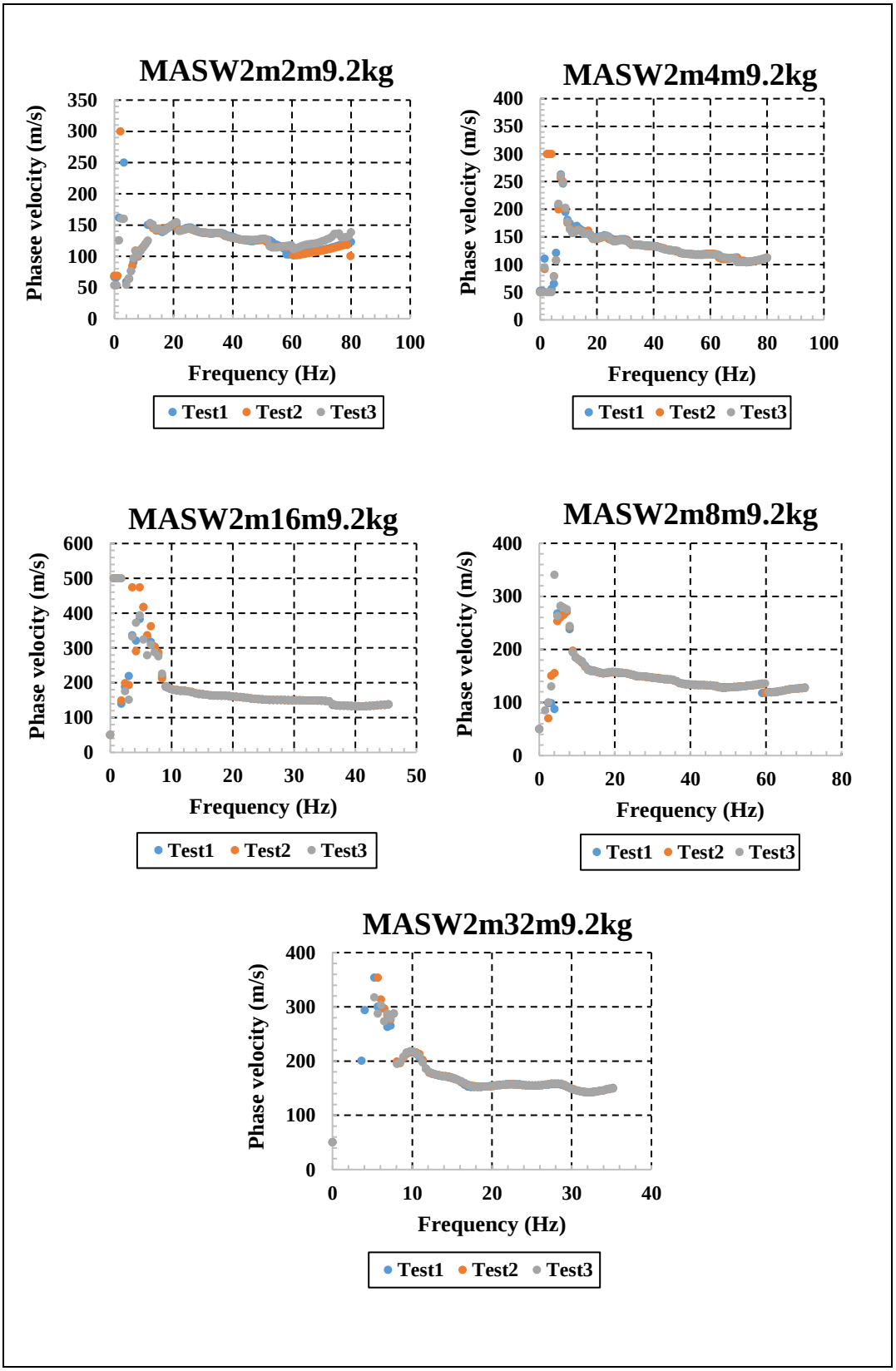

Figure 8.9: MASW2m repeatability dispersion curves for 9.2 kg sledgehammer at the deep bedrock site

Table 8.1: SASW sampling depths at the deep bedrock site

Test number	Sampling depth (m)	
	min	max
1	0.80	23.8
2	0.79	26.1
3	0.76	24.1
-	Average min depth (m)	Average max depth (m)
	0.78	24.7

Table 8.2: MASW1m sampling depths at the deep bedrock site with 2.2 kg sledgehammer

Source type	Source offset (m)	Sampling depth (m)					
		Test1		Test2		Test3	
		min	max	min	max	min	max
2.2 kg Sledge hammer	1.00	-	-	-	-	-	-
	2.00	3.3	16.9	3.3	15.8	3.3	16.7
	4.00	0.91	14.9	0.90	15.7	0.91	15.4
	8.00	1.1	15.0	1.1	14.9	1.1	15.5
	16.00	1.6	13.1	1.6	14.3	1.6	13.0
	offset (m)	Average min depth (m)			Average max depth (m)		
	2.00	3.3			16.5		
	4.00	0.91			15.3		
	8.00	1.1			15.1		
	16.00	1.6			13.5		

Table 8.3: MASW1m sampling depths at the deep bedrock site with 6.3 kg sledgehammer

Source type	Source offset (m)	Sampling depth (m)					
		Test1		Test2		Test3	
		min	max	min	max	min	max
6.3 kg Sledge hammer	1.00	1.1	4.0	1.1	3.8	1.1	3.8
	2.00	1.2	18.4	1.2	18.8	1.0	18.4
	4.00	0.95	15.8	0.96	15.4	0.96	15.4
	8.00	1.1	16.1	1.1	16.9	1.1	15.7
	16.00	1.6	18.5	1.6	20.9	1.6	20.9
	offset (m)	Average min depth (m)			Average max depth (m)		
	1.00	1.1			3.9		
	2.00	1.1			18.5		
	4.00	0.96			15.5		
	8.00	1.1			16.3		
	16.00	1.6			20.1		

Table 8.4: MASW1m sampling depths at the deep bedrock site with 9.2 kg sledgehammer

Source type	Source offset (m)	Sampling depth (m)					
		Test1		Test2		Test3	
		min	max	min	max	min	max
9.2 kg Sledge hammer	1.00	1.0	5.2	1.1	5.9	0.99	5.9
	2.00	1.0	18.2	1.0	17.3	1.0	18.4
	4.00	0.97	17.1	0.97	17.4	0.97	17.3
	8.00	1.1	17.4	1.1	17.7	1.1	17.6
	16.00	1.6	18.5	1.7	19.5	1.6	20.4
	offset (m)	Average min depth (m)			Average max depth (m)		
	1.00	1.0			5.7		
	2.00	1.0			17.9		
	4.00	0.97			17.3		
	8.00	1.1			17.6		
	16.00	1.7			19.5		

Table 8.5: MASW2m sampling depths at the deep bedrock site with 2.2 kg sledgehammer

Source type	Source offset (m)	Sampling depth (m)					
		Test1		Test2		Test3	
		min	max	min	max	min	max
2.2 kg Sledge hammer	2.00	0.78	3.5	0.70	6.2	0.75	6.3
	4.00	0.68	14.3	0.70	11.8	0.69	11.8
	8.00	0.92	14.7	0.92	15.3	0.92	14.0
	16.00	2.2	19.4	2.2	17.4	2.2	18.4
	32.00	2.1	11.9	2.1	12.1	2.1	11.4
	offset (m)	Average min depth (m)			Average max depth (m)		
	2.00	0.74			5.3		
	4.00	0.69			12.6		
	8.00	0.92			14.7		
	16.00	2.2			18.4		
	32.00	2.1			11.8		

Table 8.6: MASW2m sampling depths at the deep bedrock site with 6.3 kg sledgehammer

Source type	Source offset (m)	Sampling depth (m)					
		Test1		Test2		Test3	
		min	max	min	max	min	max
6.3 kg Sledge hammer	2.00	0.76	6.6	0.97	6.3	0.71	3.6
	4.00	0.71	15.4	0.71	15.4	0.71	15.4
	8.00	0.92	18.2	0.92	18.4	0.91	18.1
	16.00	1.5	21.6	1.5	21.1	1.5	21.1
	32.00	2.1	12.0	2.1	12.4	2.1	12.1
	offset (m)	**Average min depth (m)**			**Average max depth (m)**		
	2.00	0.81			5.5		
	4.00	0.71			15.4		
	8.00	0.92			18.2		
	16.00	1.5			21.2		
	32.00	2.1			12.2		

Table 8.7: MASW2m sampling depths at the deep bedrock site with 9.2 kg sledgehammer

Source type	Source offset (m)	Sampling depth (m)					
		Test1		Test2		Test3	
		min	max	min	max	min	max
9.2 kg Sledge hammer	2.00	0.77	6.6	0.75	6.2	0.77	5.8
	4.00	0.70	17.9	0.70	17.9	0.70	17.9
	8.00	0.91	18.8	0.91	18.6	0.91	19.0
	16.00	1.5	23.8	1.5	23.2	1.5	23.8
	32.00	2.1	11.2	2.1	12.3	2.1	12.1
	offset (m)	**Average min depth (m)**			**Average max depth (m)**		
	2.00	0.76			6.23		
	4.00	0.70			17.9		
	8.00	0.91			18.8		
	16.00	1.5			23.6		
	32.00	2.1			11.9		

Table 8.8: CSW sampling depths at the deep bedrock site

Source offset (m)	Sampling depth (m)					
	Test1		Test2		Test3	
	min	max	min	max	min	max
1.00	1.15	10.2	1.2	10.2	1.2	10.2
2.00	1.20	10.8	1.2	10.8	1.2	10.8
4.00	1.12	12.3	1.1	12.3	1.1	12.3
offset (m)	**Average min depth (m)**			**Average max depth (m)**		
1.00	1.2			10.2		
2.00	1.2			10.8		
4.00	1.1			12.3		

9 APPENDIX C: PYTHON CODE FOR ANALYSIS OF SASW DATA

```
# -*- coding: utf-8 -*-
"""
Created on Thu May  7 19:45:00 2020
@author: Mosito Ntaote
"""
#IMPORTING LIBRARIES AND MODULES
import numpy as np
from matplotlib import pyplot as plt
from scipy import signal as sg


#A FUNCTION THAT RETURNS THE COHERERENCE BETWEEN GEOPHONES AND
RESPECTIVE FREQUENCIES
def Coherene_and_frequencies(geo1,geo2,time):
    N=len(time)
    frequencies=[]
    df=1/time[-1]
    j=0
    i=0
    samp_f=1/(time[2]-time[1])

    while i<len(time):
        frequencies.append(j)
        j+=df
        i+=1

    fft1=np.fft.fft(geo1)
    fft2=np.fft.fft(geo2)
    spectAmp1=2*np.abs(fft1/N)
    spectAmp2=2*np.abs(fft2/N)

    Nseg=N/8

    f1,Cxy = sg.coherence(geo1,geo2,fs =
    samp_f,nperseg=Nseg,noverlap=0.1*Nseg)

    return (Cxy,f1,frequencies,spectAmp1,spectAmp2)


# A FUNCTION THAT RETURNS WRAPPED PHASE DIFFERENCE OF THE TWO
GEOPHONES
def Phase_differences(geo1,geo2,time,freq):

    jumpindex=[]
    phasediff=[]

    fft1=np.fft.fft(geo1)
    fft2=np.fft.fft(geo2)
    gspectr = fft2*np.conjugate(fft1)
```

```
    for l in range(0,len(fft1),1):
        phasediff.append(np.arctan(gspectr.imag[l]/gspectr.real[l]))

    half_array = int(len(phasediff)/2)+1
    x=0.5*np.pi # DEFINITION OF A JUMP
    for i in range(1,half_array):
        diff=phasediff[i]-phasediff[i-1]
        if diff>x or diff<-x:
            print("jump Frequency =",freq[i],"Index is =",i)
            jumpindex.append(i)

    return phasediff,jumpindex


# A FUNCTION THAT RETURNS UNWRAPPED PHASE DIFFERENCE OF THE TWO
GEOPHONES
def Unwrapping_phasedifference(angles,jumps):
    c=np.pi
    for i in jumps:
        diff=angles[i]-angles[i-1]
        if diff>0:
            for s in range(i,len(angles)):
                angles[s]=angles[s]-c
        elif diff<0:
            for s in range(i,len(angles)):
                angles[s]=angles[s]+c
    return angles


# A FUNCTION THAT CALCULATES AND RETURNS RALEIGH PHASE VELOCITY
def Raleigh_phase_velocity(vibfreq,unwrappedphasediff,spacing):
    Vr=[]
    n = len(vibfreq)
    for f in range(1,n):
     Vr.append((2*np.pi*spacing*vibfreq[f])/(np.absolute(unwrappedph
     asediff[f])))

    return Vr


# A FUNCTION THAT PLOTS THE COHERENCE WITH RESPECT TO FREQUENCY
def plot_coherence(cohere,freq1):
    plt.plot(freq1[:],cohere[:],"m.")
    plt.xlabel("Frequency(Hz)", fontsize=14)
    plt.ylabel("Coherence", fontsize=14)
    plt.title("Coherence curve", fontsize=16)
    plt.grid()
    plt.show()
```

```
# A FUNCTION THAT PLOTS THE WRAPPED PHASE DIFFERENCE WITH RESPECT TO
FREQUENCY
def plot_wrappedphasedifference(freq,phasedifference):
    N2 = len(freq)
   plt.plot(freq[:-(int(N2/2)+1)],phasedifference[:-
    (int(N2/2)+1)],"g.")
    plt.xlabel("Frequency(Hz)", fontsize=14)
    plt.ylabel("Wrapped Phase difference", fontsize=14)
    plt.title("Phase difference plot", fontsize=16)
    plt.grid()
    plt.show()


# A FUNCTION THAT PLOTS THE SPECTRAL AMPLITUDES OF THE TWO GEOPHONES
WITH RESPECT TO FREQUENCY
def plot_SpectralAmplitude(freq,amp1,amp2):
    N2 = len(freq)
   plt.plot(freq[:-(int(N2/2)+1)],amp1[:-(int(N2/2)+1)],"r-
   ",freq[:-(int(N2/2)+1)],amp2[:-(int(N2/2)+1)],"b-")
    plt.xlabel("Frequency(Hz)", fontsize=14)
    plt.ylabel("Spectral amplitude(volts)", fontsize=14)
    lengend_list=["geo1","geo2"]
    plt.title("Spectral amplitudes", fontsize=16)
    plt.grid()
    plt.legend(lengend_list,loc="upper right")
    plt.show()



#MAIN CODE
#REQUESTING THE USER TO ENTER GEOPHONE SPACING
spacing = float(input("enter geophone spacing in m:"))

#REQUESTING THE USER TO ENTER THE DIRECTORY OF THE DATA FOR FORWARD
SHOT
file_name=input("Enter the directory and file name for forward
shot:")

script=open(file_name,'r')#OPENING A TEXT FILE IN READ MODE
lines=script.readlines()[1:]# READING THE LINES OF THE FILE AND
SKIPPING THE FIRST LINE

time=[]
geo1f=[]
geo2f=[]


# A FOR LOOP THAT SPLITS THE COLUMNS OF THE READ LINES AND STORE
THEM INTO THEIR RESPECIVE GEOPHONES LISTS
for x in lines:
    time.append(float(x.split()[0]))
    geo1f.append(float(x.split()[1]))
    geo2f.append(float(x.split()[2]))
script.close()#TEXT FILE CLOSURE
```

```
rfile_name=input("Enter the directory,folder and files type for
reverse shot:")

 rscript=open(rfile_name,'r')#OPENING A TEXT FILE IN READ MODE
rlines=rscript.readlines()[1:]# READING THE LINES OF THE FILE AND
SKIPPING THE FIRST LINE

 geo1r=[]
 geo2r=[]

 for y in rlines:
     geo1r.append(float(y.split()[1]))
     geo2r.append(float(y.split()[2]))
 rscript.close()

 geo1 = (np.array(geo1f)+np.array(geo2r))/2
 geo2 = (np.array(geo2f)+np.array(geo1r))/2


cohere,freq1,freq,amp1,amp2=Coherene_and_frequencies(geo1,geo2,time)
phasedifference,jumpindexes=Phase_differences(geo1,geo2,time,freq)
plot_coherence(cohere,freq1)
plot_wrappedphasedifference(freq,phasedifference)
plot_SpectralAmplitude(freq,amp1,amp2)


#ASKING THE USER IF HE/SHE WOULD LIKE TO UNWRAPP MANUALLY OR
AUTOMATICALLY
unwrap_option = int(input("Do you want to unwrap manually? if yes
enter 1 else 0:"))
jumps=[]
if unwrap_option == 1:
    yes = 1
    while yes==1:
        index=int(input("Enter index of jump frequency:"))
        jumps.append(index)
         yes=int(input("Do you want to enter another index if yes
         type 1 else 0:"))
elif unwrap_option == 0:
    for v in jumpindexes:
        jumps.append(v)

unwrappedphasediff=Unwrapping_phasedifference(phasedifference,jumps)
velocity = Raleigh_phase_velocity(freq,unwrappedphasediff,spacing)


#OPENING A TEXT FILE IN WRITE MODE
wrt = open('E:\\seismics\\Freestate background noise.txt','w')
headings1 = ['frequency','Velocity','wrappedphasediff','S-
Amplitude1','S-Amplitude2']
heads1 =
str(headings1[0])+","+str(headings1[1])+","+str(headings1[2])+","+st
r(headings1[3])+","+str(headings1[4])+"\n"
wrt.write(heads1)
```

```
for s in range(0,len(velocity)):

    line1=str(freq[s])+","+str(velocity[s])+","+str(wrappedphases[s]
    )+","+str(amp1[s])+","+str(amp2[s])+"\n"
     wrt.write(line1)



headings2 = ['freq1','coherence']
heads2 = str(headings2[0])+","+str(headings2[1])+"\n"
wrt.write(heads2)
for y in range(0,len(freq1)):
     line2 = str(freq1[y])+","+str(cohere[y])+"\n"
     wrt.write(line2)
wrt.close()#TEXT FILE CLOSURE
```

10 APPENDIX D: PYTHON CODE FOR ANALYSIS OF CSW DATA

```
# -*- coding: utf-8 -*-
"""
Created on Tue Apr 21 14:01:29 2020
@author: Mosito Ntaote
"""

#IMPORTING LIBRARIES AND MODULES
import numpy as np
from matplotlib import pyplot as plt
import scipy as sp
from scipy import signal as sg
from math import*
import glob

#A FUNCTION THAT RETURNS WRAPPED ANGLES AND THE VIBRATION FREQUENCY
OF THE SHAKER
Defshaker_vibration_frequency_wrappedangles(geophones,n,minindex,max
index):
    time=geophones[0]
    wrapped_angles=[]
    frequencies=[]
    df=1/time[-1]
    j=0
    i=0
    while i<len(time):
        frequencies.append(j)
        j+=df
        i+=1

    N=len(geophones[1])

    for p in range(1,n+1,1):
        domint_freq=0
        geo_fft=np.fft.fft(np.array(geophones[p]))
        spectAmp=2*np.abs(geo_fft/N)
        x=spectAmp[minindex:maxindex].max()
        spectAmp_to_list=list(spectAmp[:-(int(N/2))])
        y=spectAmp_to_list.index(x)
        domint_freq=frequencies[:-(int(N/2))][y]

        if geo_fft.real[y]!= 0:
           wrapped_angles.append(atan(geo_fft.imag[y]/geo_fft.real[y
           ]))
        elif geo_fft.imag[y]<0 and geo_fft.real[y]== 0:
            wrapped_angles.append(-pi/2)
        elif geo_fft.imag[y]>0 and geo_fft.real[y]== 0:
            wrapped_angles.append(pi/2)

    return domint_freq,wrapped_angles
```

```
#A FUNCTION THAT CALCULATES RETURNS GEOPHONES SPECTRAL AMPLITUDES
AND CORRESPODING FREQUENCIES
def spectralamplitudes_and_frequencies(geophones,n):
    time1=geophones[0]
    frequencies=[]
    df=1/time1[-1]
    j=0
    i=0
    while i<len(time1):
        frequencies.append(j)
        j+=df
        i+=1

    spectral_amplitudes=[]

    N=len(geophones[1])

    for p in range(1,n+1,1):
        geo_fft=np.fft.fft(np.array(geophones[p]))
        spectAmp=2*np.abs(geo_fft/N)
        spectral_amplitudes.append(geo_fft)

    return spectral_amplitudes,frequencies

#A FUNCTION THATU UNWRAPS THE PHASE ANGLES RETURNS AND RETURNS THEM
def phase_angles_unwrapping(angles):
    i=0
    ua=np.pi
    while i<len(angles)-1:
        if angles[i+1]<angles[i]:
            i+=1
        else:
            i+=1
            while i<len(angles)-1:
                if angles[i+1]<=angles[i]:
                    angles[i]-=ua
                    i+=1
                else:
                    angles[i]=angles[i]-ua
                    ua+=np.pi
                    i+=1
            if angles[i]<=angles[i-1]:
                angles[i]-=ua
            else:
                angles[i]-=ua
    return angles

#A FUNCTION THAT RETURNS THE INVERSE OF THE SLPOE OF BEST FIT LINE
FOR THE GRAPH OF UNWRAPPED ANGLES VS GEOPHONE'S DISTANCE FROM THE
SHAKER
Def inverse_of_slope_of_best_fit_line(geo_dist,unwrapped_angles):
    fit=np.polyfit(geo_dist,unwrapped_angles,1)
    m=fit[0
    return 1/fit[0]
```

```
#A FUNCTION THAT CALCULATES AND RETURNS RALEIGH PHASE VELOCITY
def phase_velocities(inv_slope,dom_freq):
    wave_length=2*np.pi*inv_slope
    vels=np.abs(wave_length*dom_freq)
    return vels


#A FUNCTION THAT PLOTS SPECTRAL AMPLITUDES FOR GEOPHONES WITH
RESPECT TO FREQUENCY
def plotting_spectral_amplitude(spectral_amplitudes,frequency):

     plt.plot(frequency,spectral_amplitudes[0],"r.",frequency,spectr
     al_amplitudes[1],"y.",frequency,spectral_amplitudes[2],"m.",fre
     quency,spectral_amplitudes[3],"g.",frequency,spectral_amplitude
     s[4],"b.",)
     plt.xlabel("Frequency(Hz)", fontsize=14)
     plt.ylabel("Spectral amplitude (volts)", fontsize=14)
     plt.title("Spectral_amplitudes", fontsize=16)
     plt.grid()
     plt.show()


#A FUNTION THAT PLOTS THE DISPERSION CURVE
def plot_dispersion_curve(vibr_freq1,velocities1):
     plt.plot(vibr_freq1,velocities1,"m.")
     plt.xlabel("Frequency(Hz)", fontsize=14)
     plt.ylabel("Phase velocity (m/s)", fontsize=14)
     plt.title("Dispersion curve", fontsize=16)
     plt.grid()
     plt.show()




#MAIN CODE
geo_dist=[]
vibr_freq1=[]
inv_slope_fitline1=[]

n=int(input("enter the number of geophones:"))
b=float(input("enter geophone spacing in m:"))
c=float(input("enter source offset in m:"))

# A FOR LOOP THAT CALCULATES GEOPHONES POSITIONS RELATIVE TO THE
SHAKER
for g in range(0,n,1):
    k=c+g*b
    geo_dist.append(k)
```

```
directory=input("Enter files directory and files type:")


# A FORLOOP THAT READS SPECIFIC FILE TYPES IN THE SPECIFIED
DIRECTORY
for file_name in glob.glob(directory):
    script=open(file_name,'r') # OPENING A FILE IN A READ MODE
    lines=script.readlines()[1:] # READING THE LINES OF THE FILE

    geophones=[]
    time=[]
    geo1=[]
    geo2=[]
    geo3=[]
    geo4=[]
    geo5=[]

    # A FOR LOOP THAT SPLITS THE COLUMNS OF THE READ LINES AND
    STOREs THEM INTO THEIR RESPECIVE GEOPHONES LISTS
    for x in lines:
        time.append(float(x.split()[0]))
        geo1.append(float(x.split()[1]))
        geo2.append(float(x.split()[2]))
        geo3.append(float(x.split()[3]))
        geo4.append(float(x.split()[4]))
        geo5.append(float(x.split()[5]))
    script.close()# CLOSURE OF THE TEXT FILE

    geophones.append(time)
    geophones.append(geo1)
    geophones.append(geo2)
    geophones.append(geo3)
    geophones.append(geo4)
    geophones.append(geo5)


    spectral_amplitudes,frequencies=spectralamplitudes_and_frequenci
    es(geophones,n)
    plotting_spectral_amplitude(spectral_amplitudes,frequencies)


    # THE USER IS REQUESTED TO ENTER THE MAXIMUM OPERATING FREQUENCY
    OF THE SHAKER
    max_freq = float(input("Enter the maximum operating
    frequenncy of your shaker:"))

    # A FOR LOOP THAT PRINTS FREQUENCIES AND THEIR IDEXES
    for k in range(0,len(frequencies),1):
        if frequencies[k]<=max_freq:
         print("Frequency is:",frequencies[k],"and index is:",k)
        else:
             break
```

```
    #REQUESTING THE USER TO ENTER THE FREQUENCY RANGE IN WHICH THE
    SHAKER VIBRATION WILL BE EXTRACTED
    minindex = int(input("enter lower index:"))
    maxindex = int(input("enter upper index:"))



   freq,wrap_angles=shaker_vibration_frequency_wrappedangles(geophon
   es,n,minindex,maxindex)
   vibr_freq.append(freq)
   unwrap_angles=phase_angles_unwrapping(wrap_angles)
   inv_of_slope=inverse_of_slope_of_best_fit_line(geo_dist,unwrap_an
   gles)
    inv_slope_fitline.append(inv_of_slope)

velocities=phase_velocities(np.array(inv_slope_fitline),np.array(vib
r_freq))
plot_dispersion_curve(vibr_freq,velocities)

# OPENING A TEXT FILE IN WHICH THE PHASE VELOCITY AND FREQUECIES &
WILL BE WRITEN
wrt = open('E:\\seismics\\Freestate_CSW.txt','w')
headings1 = ['Shakerfrequency(Hz)','Phase Velocity(m/s)']
heads1=str(headings1[0])+","+str(headings1[1])+"\n"
wrt.write(heads1)


for f in range(0,len(vibr_freq1)):
   line1=str(vibr_freq1[f])+","+str(velocities1[f])+"\n"
   wrt.write(line1)
wrt.close() # CLOSURE OF THE TEXT FILE
```

11 APPENDIX E: BOREHOLE RESULTS

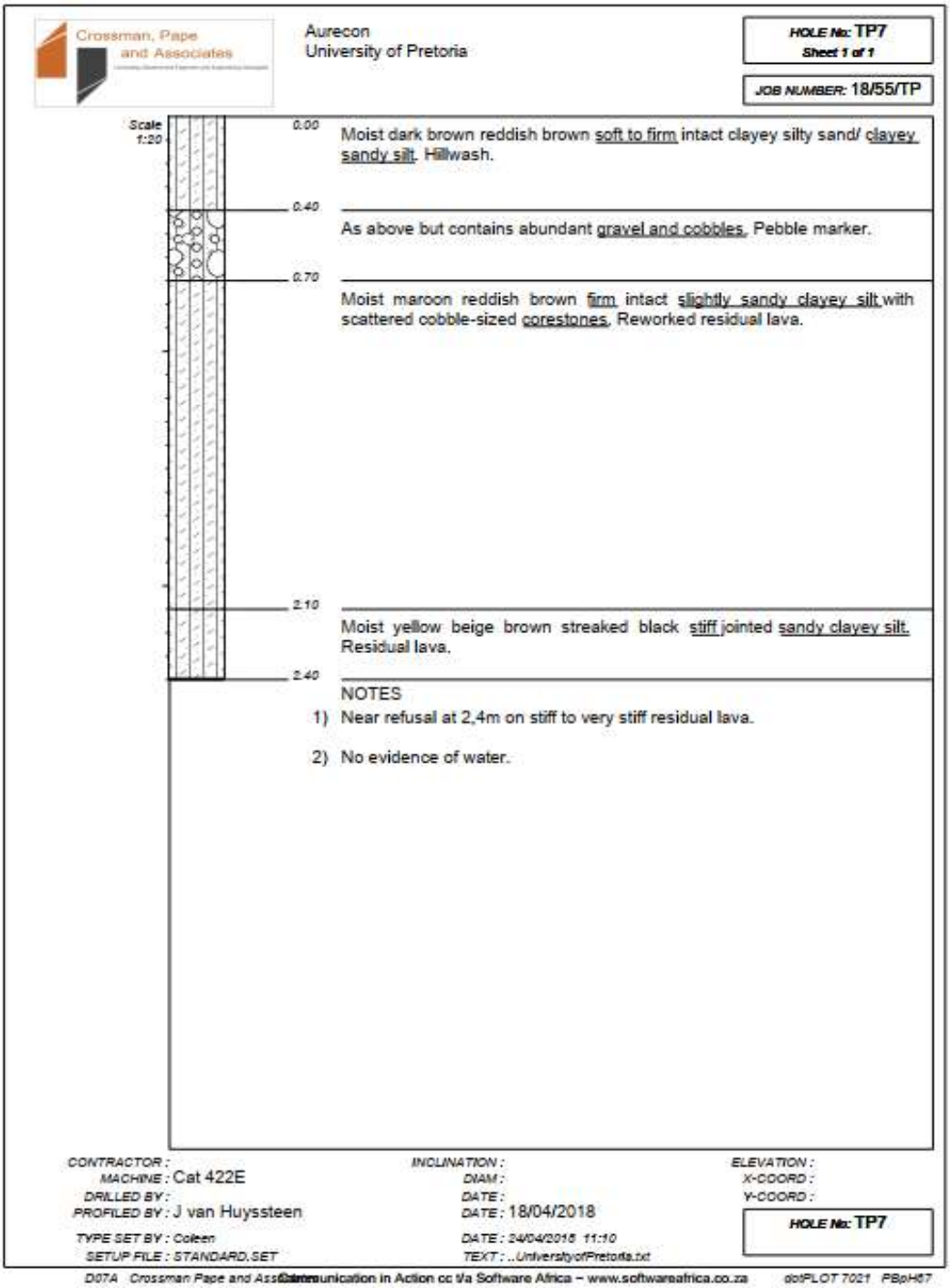

Figure 11.1: Borehole results for shallow bedrock site

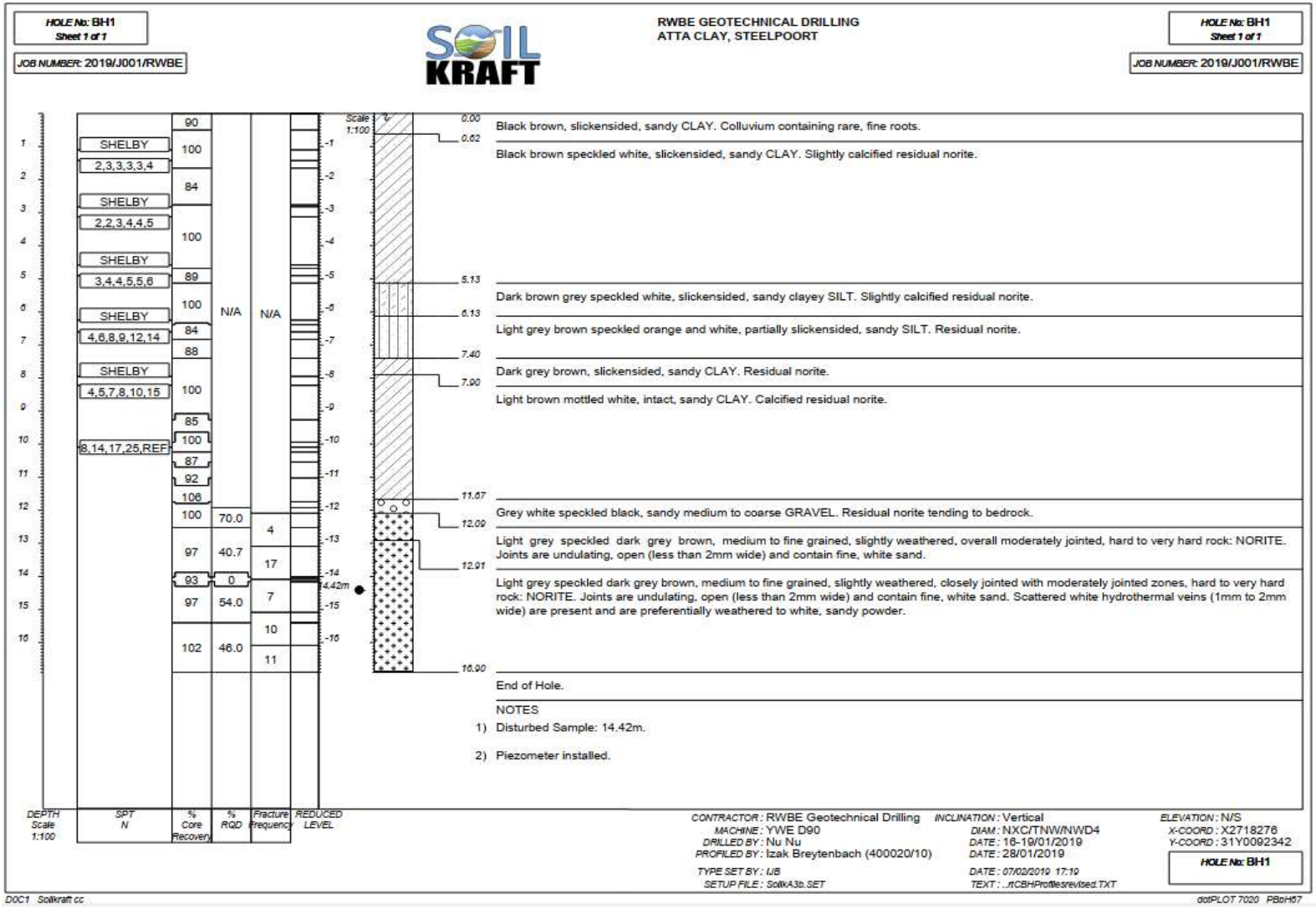

Figure 11.2: Borehole results for deep bedrock site